PERFORMANCES OF PASSIVE ELECTRIC NETWORKS AND PIEZOELECTRIC TRANSDUCERS FOR BEAM VIBRATION CONTROL

PORFIRI MAURIZIO

DOTTORATO DI RICERCA MECCANICA TEORICA E APPLICATA*
DIPARTIMENTO DI MECCANICA ED AERONAUTICA
UNIVERSITA' DI ROMA LA "SAPIENZA"

DIRETTORE DELLA SCUOLA: PROF. L. DE SOCIO
(Università degli studi di Roma "La Sapienza")

TUTORE SCIENTIFICO: PROF. UGO ANDREAUS
(Università degli studi di Roma "La Sapienza")

DIRETTORI DI TESI:
PROF. A. DI CARLO (Università degli studi Roma Tre)
PROF. SEPPECHER (Université de Toulon et du Var)

DOCENTI ESAMINATORI:
ING. A. FREGOLENT (Università degli studi di Roma "La Sapienza")
PROF. P. GAUDENZI (Università degli studi di Roma "La Sapienza")
PROF. S. PAGANO (Université Montpellier II)
PROF. J. POUGET (Université de Versailles/Saint-Quentin-en-Yvelines)
PROF. F. VESTRONI (Università degli studi di Roma "La Sapienza")

ABSTRACT

This thesis is focused on beam vibration control using piezoelectric transducers and passive electric networks.
The first part of this study deals with the modeling and the analysis of stepped piezoelectric beams. A refined one-dimensional model is derived and experimentally validated. The modal properties are determined with four numerical methods. A homogenized model of stepped periodic piezoelectric beams is derived by using two-scale convergence.
The second part deals with the performance analysis of three passive circuits in damping structural vibrations: the piezoelectric shunting, the second order transmission line and the fourth order transmission line. The effects of uncertainties of the electric parameters on the system performances are analyzed. Theoretical predictions are validated through different experimental setups.

Tesi di dottorato in co-tutela tra L'Università degli studi di Roma "La Sapienza" e L'Université de Toulon et du Var

"*Che triste sbaglio, pensò Drogo, forse è tutto così, crediamo che attorno ci siano creature simili a noi e invece non c'è che gelo, pietre che parlano una lingua straniera, stiamo per salutare l'amico ma il braccio ricade inerte, il sorriso si spegne, perché ci accorgiamo di essere completamente soli.*" D. Buzzati, Il deserto dei Tartari

Contents

Summary

The recent technological developments in the production of piezoelectric transducers, and the relevant consumers' attention towards the suppression of structural vibrations, increased the research efforts in their effective exploitation in control systems for actual engineering structures. An efficient control of structural vibrations leads to several benefits, such as the precision in mechanisms manoeuvres, the reduced fatigue loads, the reliability and durability of machineries. These are the main reasons to attract the interest of both mechanical and aerospace industries in this topic. This study is focused on beam vibration control using piezoelectric transducers and passive electric networks.

The first part of this study deals with the modeling and the analysis of stepped piezoelectric beams, i.e. beams hosting piezoelectric transducers. Classical beam theory and linear piezoelectricity are applied to derive a refined one-dimensional model of the stepped piezoelectric beam, which represents a reasonable trade-off between accuracy and complexity. An experimental setup assesses the accuracy of the model in describing the beam dynamics over a wide frequency range. The effects of piezoelectric transducers on the beam modal properties are investigated and the eigenvalue problem related to a system consisting of several one-dimensional continuous substructures is solved with four different numerical methods: last energy norm, assumed modes, enhanced assumed modes and finite-element. A homogenized model of stepped periodic piezoelectric beams is derived by using two-scale convergence and its accuracy is validated through numerical tests. The choice of the vibration control technique determines the most appropriate model for the stepped piezoelectric beam.

The second part deals with the performance analysis of three different passive circuits in damping structural vibrations: the resonant piezoelectric shunting, the second order transmission line and the fourth order transmission line.

In the first case, a single piezoelectric transducer is shunted with a resistor and an inductor. The presented refined model is used to derive a reduced-order model of the vibrating electromechanical system. The inductance and resistance are optimized in order to minimize the ∞-norm of the mechanical mobility. The effects of variations of the electric parameters on the system performances are analyzed. Closed-form expressions arising from the sensitivity analysis are validated with numerical tests. The results of the sensitivity analysis are used to model the effects of random variations of the electric parameters on the system norm. The application of this technique for the identification of piezoelectric capacitances and modal coupling is presented. The identification method is applied in an experimental setup.

In the second case, an array of piezoelectric transducers is positioned on the host beam and every element is connected to the adjacent one via a floating RL impedance. The homogenized model together with the results from the $\mathcal{H}_\infty$ control problem for the piezoelectric shunting are used for optimizing the electric boundary conditions and line impedances. Its forecasts are validated by the analysis of the transmission line when retaining the lumped nature of the circuit. The sensitivity of the electrical eigenproperties

with respect to the variations of the inductance is examined. The effects of uncertainties on the line inductances are studied and closed-form results are exhibited. An experimental prototype is realized for proving the transmission line effectiveness in abating the needed inductances and reducing the effects of electric uncertainties.

In the third case, an array of piezoelectric transducers is also used, but their electric terminals are interconnected via a more sophisticated network. The network is the circuit analog of a beam with structural damping endowed with dual boundary conditions with respect to the mechanical ones. The homogenized model is used for proving the effectiveness of the fourth order transmission line in damping multimodal vibrations. The concept of dual boundary conditions is presented and the relations between the spectral properties of the original and the dual problem are explained. The problem of synthesizing a lumped electric network approximating the distributed beam circuit analog is addressed by two different methods. In the first method the equilibrium and constitutive equations of the beam element are finite-difference approximated and a four port circuit analog to the beam element is conceived. In the second method the Lagrangian of the beam is discretized and by establishing an electromechanical analogy between the flux-linkages and the displacements, a lumped circuit governed by the discretized Lagrangian is assembled. The resulting circuit is constituted only by inductors, capacitors and two-port transformers. The problem of suitably inserting resistors for achieving the multimodal damping is tackled. A prototype is designed for proving the device effectiveness in simultaneously damping several structural modes and abating the needed inductances. The circuit analog is analyzed also as a lumped system and comparisons with the homogenized predictions are drawn.

Sommario

I recenti sviluppi tecnologici nella produzione di trasduttori e la crescente attenzione dei consumatori nei confronti della riduzione delle vibrazioni strutturali, hanno portato ad un aumento delle attività di ricerca nell'applicazione dell'effetto piezoelettrico al controllo delle vibrazioni meccaniche in strutture reali. Un efficiente controllo delle vibrazioni strutturali conduce a molti benefici, tra i quali annoveriamo: la precisione nei meccanismi, i ridotti carichi di fatica, l'affidabilità e la longevità dei macchinari. Queste sono le principali ragioni che attraggono gli interessi delle industrie aerospaziali e meccaniche in questo campo. Questo studio è finalizzato al controllo di vibrazione di travi usando trasduttori piezoelettrici e reti elettriche passive.

La prima parte di questo lavoro si occupa della modellazione e dell'analisi di travi piezoelettriche segmentate, vale a dire travi che ospitano trasduttori piezoelettrici. La teoria classica delle travi e la piezoelettricità lineare sono utilizzate nella derivazione di un raffinato modello unidimensionale della trave piezoelettrica segmentata, che rappresenta un ragionevole compromesso fra esattezza e complessità. Un apparato sperimentale dimostra l'accuratezza del modello nella descrizione del moto della trave in una ampia gamma di frequenze. Gli effetti dei trasduttori piezoelettrici sulle proprietà modali della trave sono studiati, e il problema agli autovalori relativo ad un sistema che consiste di diverse sottostrutture continue unidimensionali è risolto con quattro metodi numerici differenti: "last energy norm", "assumed modes", "enriched assumed modes" ed elementi-finiti. Un modello omogeneizzato di travi piezoelettriche segmentate periodiche è derivato sfruttando tecniche di convergenza a doppia scala, e la sua esattezza è dimostrata attraverso simulazioni numeriche. La scelta della tecnica di controllo determina il modello più consono alla trave piezoelettrica segmentata.

La seconda parte si occupa dell'analisi delle prestazioni di tre differenti circuiti passivi nella soppressione delle vibrazioni strutturali (il bipolo RL risonante, la linea di trasmissione del secondo ordine e la linea di trasmissione del quarto ordine). Nel primo caso, un singolo trasduttore piezoelettrico è connesso in parallelo ad un resistore e ad un induttore. Il modello raffinato è usato per derivare un modello ridotto del sistema elettromeccanico vibrante e l'induttanza e la resistenza sono ottimizzate per minimizzare la norma-∞ della mobilità meccanica. Gli effetti delle variazioni dei parametri elettrici sulle prestazioni del sistema sono analizzati. Le espressioni in forma chiusa dedotte dall'analisi di sensibilità sono validate da simulazioni numeriche. I risultati dell'analisi di sensibilità sono usati per modellare gli effetti delle variazioni aleatorie dei parametri elettrici sulla norma del sistema. Questa tecnica è applicata con successo anche all'identificazione delle capacità piezoelettriche e dell'accoppiamento modale in un prototipo sperimentale.

Nel secondo caso, una schiera di trasduttori piezoelettrici è posizionata sulla trave ospite ed ogni suo elemento è collegato all'adiacente da un'impedenza RL flottante. Il modello omogeneizzato e i risultati del problema di controllo $\mathcal{H}_\infty$ per il bipolo RL sono impiegati nell'ottimizzazione delle impedenze di bordo e di linea; le relative previsioni sono validate da una analisi della linea di trasmissione che tiene in conto della natura

discreta del circuito. La sensibilità delle proprietà spettrali elettriche rispetto alle variazioni dell'induttanza è esaminata. Gli effetti delle incertezze delle induttanze di linea sono studiati e risultati in forma chiusa sono esibiti. Un prototipo sperimentale è realizzato per dimostrare l'efficacia della linea di trasmissione nel ridurre le induttanze necessarie e nel mitigare gli effetti delle incertezze elettriche.

Nel terzo caso si utilizza ancora una schiera di trasduttori piezoelettrici, ma i loro terminali elettrici sono collegati da una rete più sofisticata. La rete elettrica è analoga ad una trave dotata di smorzamento strutturale e munita di condizioni al contorno duali a quelle meccaniche. Il modello omogeneizzato è sfruttato per dimostrare l'efficacia della linea di trasmissione del quarto ordine nello smorzamento di vibrazioni strutturali multimodali. Il concetto di condizioni al bordo duali è presentato e le relazioni fra le proprietà spettrali del problema originale e di quello duale sono analizzate. Il problema della sintesi di un circuito discreto che approssimi la rete distribuita analoga alla trave è risolto con due metodi differenti. Nel primo metodo le equazioni di equilibrio e le equazioni costitutive di un elemento di trave sono approssimate con uno schema a differenze finite e un circuito analogo ad un elemento di trave è concepito. Nel secondo metodo la Lagrangiana della trave è discretizzata e, stabilendo un'analogia elettromeccanica fra le tensioni elettriche e le velocità meccaniche, si sintetizza un circuito discreto che è governato da tale Lagrangiana. Il circuito risultante è costituito soltanto da induttori, condensatori e trasformatori a due porte. Il problema di inserire oculatamente resistori per smorzare vibrazioni multimodali è affrontato. La progettazione di un prototipo sperimentale dimostra l'efficacia del dispositivo nella soppressione di vibrazioni multimodali e nella riduzione delle induttanze necessarie. Inoltre, il circuito analogo è analizzato come un sistema discreto e sono effettuati confronti con le previsioni del modello omogeneizzato.

Résumé

Les récents développements technologiques dans les modalités de production des transducteurs piézoélectriques et l'augmenté intérêt général pour l'amortissement de vibrations structurales, sont des facteurs qui ont contribué à intensifier les recherches dans le domaine de l'exploitation des transducteurs piézoélectriques dans les systèmes de contrôle les structures réelles. Un contrôle efficace des vibrations structurales mène à beaucoup d'avantages comme plus de précision dans les manœuvres des mécanismes, des charges de fatigue réduites, des meilleures fiabilité et longévité des machineries. Ces raisons sont les principaux centres d'intérêt des industries mécaniques et aérospatiales dans cette matière. Cette étude est concentrée sur le contrôle de vibration des poutres par l'utilisation des transducteurs piézoélectriques et des circuits électriques passifs.

La première partie traite de la modélisation et de l'analyse des poutres piézoélectriques segmentées, i.e. les poutres équipées avec transducteurs piézoélectriques. La théorie classique des milieux unidimensionnels et de la piézoélectricité linéaire sont appliquées pour définir un modèle unidimensionnel raffiné de la poutre piézoélectrique segmentée, qui représente un compromis entre la précision et la complexité. Une installation expérimentale évalue l'exactitude du modèle en décrivant la dynamique de la poutre sur un grand intervalle de fréquences. Les effets des transducteurs piézoélectriques sur les propriétés modales de la poutre sont étudiés, et le problème de la détermination des valeurs principales pour un système se composant de plusieurs sous structures unidimensionnelles est résolu avec quatre méthodes numériques différentes: "last energy norm", "assumed modes", "enhanced assumed modes" et éléments finis. Un modèle homogénéisé des poutres piézoélectriques segmentées périodiques est dérivé en employant une convergence à deux échelles et est validé par des essais numériques. Le choix de la technique de contrôle de vibration détermine le modèle le plus approprié pour la poutre piézoélectrique.

La deuxième partie traite de l'analyse des performances de trois circuits passifs différents pour atténuer les vibrations structurales (le shuntage piézoélectrique résonant, la ligne de transmission du deuxième ordre et la ligne de transmission du quatrième ordre). Dans le premier cas, un seul transducteur piézoélectrique est shunté avec une résistance et un inducteur. Le modèle raffiné présenté est employé pour dériver un modèle d'ordre réduit du système électromécanique vibrant. L'inductance et la résistance sont optimisées afin de réduire au minimum la ∞-norme de la mobilité mécanique. Les effets des variations des paramètres électriques sur les performances de système sont analysés et les expressions analytiques dérivées de l'analyse de sensibilité sont validées avec des essais numériques. Les résultats de l'analyse de sensibilité sont employés pour modeler les effets des variations aléatoires des paramètres électriques sur la norme du système. L'application de cette technique pour l'identification des capacités piézoélectriques et du couplage modal est présentée. La méthode d'identification est appliquée dans une installation expérimentale.

Dans le deuxième cas, une rangée de transducteurs piézoélectriques est placée sur la poutre et chaque élément est connecté à l'adjacent par l'intermédiaire d'une impédance RL flottante. Le modèle homogénéisé, ainsi que les résultats du problème de contrôle $\mathcal{H}_\infty$ pour

le shuntage piézoélectrique, sont employés pour optimiser les conditions aux limites et les impédances électriques distribuées. Ces prévisions sont validées par l'analyse de la ligne de transmission, en retenant la nature discrète du circuit. La sensibilité des propriétés spectrales électriques en ce qui concerne les variations de l'inductance est examinée. Les effets des incertitudes sur les inductances sont étudiés et des résultats analytiques sont exhibés. Une installation expérimentale est réalisée pour prouver l'efficacité de la ligne de transmission en diminuant les inductances nécessaires et en réduisant les effets des incertitudes électriques.

Aussi, dans le troisième cas, une rangée de transducteurs piézoélectriques est utilisée, mais un réseau électrique passif plus sophistiqué est ici exploité. Le réseau électrique est analogue à une poutre avec l'atténuation structurale, dotée de conditions aux limites duales en ce qui concerne la mécanique. Le modèle homogénéisé est employé pour prouver l'efficacité de la ligne de transmission du quatrième ordre en atténuant des vibrations multimodales. Le concept de conditions aux limites duales est présenté et les relations entre les propriétés spectrales de l'original et du problème dual sont expliquées. Deux méthodes différentes sont présentées pour réaliser un circuit électrique discret analogue à la poutre. Dans la première méthode les équations d'équilibre et les lois de comportement de l'élément de la poutre sont approximées par la méthode des différences finies et un circuit analogue à l'élément de poutre est conçu. Dans la deuxième méthode le Lagrangien de la poutre est discrétisé et, en établissant une analogie électromécanique entre les voltages et les vitesses, un circuit discret régi par le Lagrangien discrétisé est réuni. Le circuit résultant est constitué seulement par des inducteurs, des condensateurs et des transformateurs. Le problème d'insérer convenablement des résistances pour réaliser l'atténuation multimodal est abordé. Un prototype est conçu pour prouver l'efficacité de dispositif en atténuant simultanément plusieurs modes structuraux et en diminuant les inductances nécessaires. Le circuit analogue est analysé comme un système discret et des comparaisons avec les prévisions du model homogénéisé sont dessinées.

Acknowledgements

I wish to first and foremost acknowledge my beloved girlfriend, Maria Grillo. Without her patience and encouragement this work would not have come to existence. I would like to express my deep gratitude to my parents, my sister and all my late grandparents who have always supported me, believed in me and covered me with love during all my studies. A special thank is due to my late grandmother Maria Brevetti and my uncle Roberto Carullo who have transmitted to me, with their great enthusiasm, the passion for books and reading since I was a kid.

Next, I would like to thank Prof. Andreaus for his invaluable advises on scientific, academic and human matters and for his endless support during my research. I sincerely hope that our deeply rooted professional relationship will continue to grow in future.

During these last years I have had the luck of co-working with several admirable scientists and I feel indebted to all of them. I want to thank Prof. R.C. Batra for having introduced me to computational mechanics, Prof. G. Martinelli for the invaluable talks on circuit theory, Dr. T. Lekszycki for the creative brainstormings on identification and optimization theory, Prof. D.K. Lindner for his experienced advises on control design, Prof. J. Pouget for the profitable discussions on piezoelectric transducers modeling, Prof. P. Seppecher for the precious directions on homogenization theory and functional analysis.

The experimental work could not have been done without the unconditional support of Prof. Sestieri. The numerical analyses would have not come to light without the attendance to the course on theory of structures by Prof. Ciampi.

This dissertation would not be complete without the intense collaboration during the past years with Silvio Alessandroni, Ugo Cacciotti, Corrado Maurini, Maurizio Paschero, Pier Mario Pollina, Giulio Sciarra, Davide Spinello, Domenico Vigilante and Stefano Vidoli. A special thank to Davide Spinello for his careful review of the manuscript and his help in preparing the french summary. I would be amiss to neglect to mention how much I appreciated Davide's help in overcoming all the melancholy moments and difficulties encountered since the last year. Another very special thank to Pier Mario Pollina, who showed to be not only the ideal officemate, but also a very good and sincere friend. We have had a unique chemistry in our office, and we have both had incredible fun. I will always look back on the time we shared with a smile.

Outside of my research environment, I have the obligation to extend my thanks to my Turkish friends Sibel Atasoy and Umut Balli for their therapy against depression based on smiles and friendship. Moreover, I cannot forget to thank the friends of She-Sha bar in Blacksburg for the nice office space that they offered me during the thesis preparation.

And finally, I want to thank Prof. E.G. Henneke and the entire department of Engineering Science and Mechanics of Virginia Tech for the warm hospitality and support during the last years.

CHAPTER 1

Introduction

1. Review of the vibration control literature

Extensive vibrations in mechanical systems can limit the performances of a structure, reduce its lifetime and affects its reliability. By using piezoelectric transducers in conjunction with appropriate electric networks (see e.g. [**Lesieutre (1998)**] and [**Wang (2001)**]), the mechanical vibrational energy can be dissipated, strengthening the performance and extending the lifetime of the structure.

Piezoelectricity was discovered by the Curie brothers (Pierre and Jacques Curie) in 1880, but it took several decades before this phenomenon could be exploited in real applications. It is reasonable to assess that the first use of piezoelectric materials dates back to the 1940s, during the second World War, as an ultrasonic detector for submarines. Piezoelectrics undergo deformation when an electric field is applied across their terminals (motor action, converse effect), and conversely produce voltage when strain is imposed (generator action, direct effect). For a concise description of the piezoelectric effect see e.g. [**IEEE (1987)**]. With the discovery of piezoceramics and the consequent development of sophisticated transducer architectures (for more details on the novel concepts used in the design of piezoelectric transducers see [**Niezreski et al. (2001)**]), the domain of the applications of piezoelectric materials has expanded considerably. Applications include space systems, aircraft, automotives, machine tools and medical systems (for more detailed information about new trends in the application of piezoelectric transducers for transportation vehicles, see e.g.[**Boller (1998)**]).

1.1. Electronic damping. The so-called electronic damping (see [**Olsen (1956)**], [**Forward and Swigert (1981)**], [**Hanagud (1985)**] and [**Hanagud et al. (1992)**]) was one of the first applications conceived for the developed family of transducers in the field of active vibration control. A set of piezoelectric devices is placed on a host structure to sense and control the mechanical vibrations. The deformation of the sensing elements results in electrical signals, which are conditioned by suitably-designed feedback electronics and then applied to actuating elements. The actuators convert the applied electrical energy into mechanical energy, transmitting mechanical control actions to the host structure. Such a concept proved to be effective, as the available actuators can exert forces of several hundred newtons as a response to voltage signals of several hundred volts without losing their dielectric properties or undergoing destructive strain deformations (see e.g. [**Chopra (2002)**]). Indeed, the most remarkable feature of the modern piezoelectric transducers is their capability to remain in the linear range in the presence of strains on the order of 0.1% (see again [**Niezreski et al. (2001)**]). When electronic damping is used, the piezoelectric transducers' driving requires complex power amplifiers and associated precise sensing electronics, resulting in the consumption of a significant amount of electrical power. Furthermore, the presence of an active controller can cause instability in the closed-loop system, the plant (vibrating structure) of which is naturally passive. Spillover phenomena can also be introduced, inducing dramatic oscillations of the structure at high frequencies.

An interesting development of the electronic damping is found in [**Canon and Lenczner (1999)**], [**Bernadou and Haenel (2000)**] and [**Kader (2001)**], where the design of optimal distributed electronic active controllers is addressed. This includes a distributed array of piezoelectric elements uniformly positioned over a host structure and a distributed interconnecting active electronic circuit. The piezoelectric layer is employed to measure the deformation of the flexible structure and to exert a control action at every point. The purpose of the distributed electronic circuit is to extract the complete state of the plant from the sensors, to optimally condition these signals, and to feed the actuators at high voltage. The resulting smart structure is able to efficiently suppress mechanical vibrations induced by broadband disturbances. Nevertheless, the intrinsic active nature of the controller and the complexity of the required circuitry may limit its technical feasibility and exploitation in industrial applications.

1.2. Piezoelectric shunting. In [**Hagood and von Flotow (1991)**] the possibility of damping mechanical vibrations by means of a single piezoelectric transducer positioned on a structural element and shunted with completely passive electric circuits is investigated. In particular two different shunting circuits are considered: a resistive (R) one and a resistive-inductive (RL) one. By placing such an electrical impedance across the terminals of the piezoelectric transducer, the passive network is capable of damping structural vibrations. If a simple resistor is placed across the terminals of the transducer, the piezoelectric element will act as a viscoelastic damper. If the network consists of an inductor-resistor circuit, the passive network combined with the inherent capacitance of the piezoelectric transducer creates damped electromechanical beating. The resonance can be tuned so that the piezoelectric element acts as a vibration absorber (paralleling the classical mechanical vibration absorber in [**Den Hartog (1934)**]). The piezoelectric shunting proposed in [**Hagood and von Flotow (1991)**] allows for an efficient single-mode control of structural vibrations whenever the resonant circuit is tuned to the mechanical mode to be suppressed. Nevertheless, the efficiency of the electromechanical coupling strongly depends on the position of the transducer over the host structure. Moreover, the technical feasibility of the passive piezoelectric controller proposed in [**Hagood and von Flotow (1991)**] is limited, since impossibly large inductances are required to produce low-frequency electrical resonance with the small inherent capacitance of the piezoelectric transducer. Indeed, for typical values of piezoelectric inherent capacitances ($10 \div 100$ nF), very high inductances ($10 \div 1000$ H) are needed to tune the electrical resonance frequency to the structural one. Furthermore, the large internal parasitic dissipation of such a large inductor may exceed the optimal design dissipation for low frequency vibration suppression. Many efforts have been devoted to simulating huge inductors by means of active electronic circuits. In particular, in [**Fleming et al. (2000)**], an implementation method using a digital signal processor is presented, while in [**Keun-Ho and In (2001)**] an analog realization exploiting operational amplifiers and multipliers is addressed. Nevertheless, when considerable structural vibrations are taken into account, several drawbacks can appear in these synthetic inductors due to saturation and nonlinearities. In order to decrease the needed inductance, some authors proposed (see e.g. [**Park and Inman (2003)**] and [**Fleming et al. (2003)**]) to place an additional capacitance across the transducer terminals thus reducing the optimal shunting inductance. Nevertheless, as underlined also by [**Fleming et al. (2003)**], an increase of the overall capacitance (with respect of the inherent piezoelectric capacitance) induces a performance loss (see e.g. the experimental results in Figures 7 and 8 of [**Park and Inman (2003)**]).

The comparison between this approach and the classical constrained layer damping has been presented in [**Hollkamp (1994)**]. In [**Corr and Clark (2002)**] its performances are compared with those of switching shunt circuit. In [**Tang and Wang (2001)**] different active-passive control methodologies based on the classical piezoelectric shunting are addressed and in [**Tsai1 and Wang (2002)**] their robustness is examined. In [**Caruso (2001)**] the inherent mechanical damping is accounted for in the circuit tuning. In [**Park (2003)**] a clear presentation of the technique is provided. In [**Kim et al. (2000)**] an alternative approach for optimizing the shunt circuit parameters is discussed.

The principles of the piezoelectric shunting have been applied to the multimodal control of vibrations (as done in [**Wu (1996)**], [**Hollkamp (1994)**] and [**Fleming et al. (2002)**]), by using intricate shunting and block impedances. These control methodologies seem to present severe inconveniences: the used inductances are still very high and the damping efficiency, even for few modes, may be reduced.

1.3. Piezo-ElectroMechanical (PEM) beams.

In [**dell'Isola and Vidoli (1998, 1)**], the possibility of damping the structural vibrations of a truss modular beam by means of an array of piezoelectric transducers embedded in the truss and interconnected by a distributed circuit is investigated. Every truss module is endowed with a piezoelectric bar; each transducer is shunted with a grounded RL impedance and the transducers of two adjacent modules are interconnected by a floating RL impedance. This attempt represents the first realization of what is known as a Piezo-ElectroMechanical (PEM) beams (see [**dell'Isola et al. (2003, 1)**] for a survey). A PEM beam is constituted by a beam on which an array of uniformly distributed piezoelectric elements is positioned, and a passive electric network which interconnects the transducers' terminals. In this way one provides a synthetic support for low-speed electrical signals, to be effectively coupled to mechanical waves (a precursory work of the aforementioned technique can be found in [**Valis et al. (1991)**]).

In [**dell'Isola et al. (2004)**], a PEM beam prototype obtained by interconnecting distributed piezoelectric elements either by RL impedances (second order transmission line or RL network) is presented. The main advantage of this strategy, shown in [**dell'Isola et al. (2004)**], is the drastic reduction of employed optimal inductances with an increasing number of transducers, thus making conceivable the realization of a truly passive control network. Nevertheless, in this framework a multimodal resonant control is not achievable, but an acceptable viscous-like damping is added at higher frequencies.

The optimization problem of finding the best distributed passive electric network (piezoelectrically coupled to the vibrating host structure) for achieving the most effective multimodal energy transduction has been partially addressed in [**Vidoli and dell'Isola (2000)**]. There, it is heuristically proven that in order to guarantee the maximum energy transfer between the mechanical and electric systems, they should be governed by the same partial differential equations. This property is often summarized by stating that the sought optimal distributed network should be the electric analog of the host structure. Therefore, the analog electrical circuit exhibits the same modal characteristics as those defining the host structure, so that a multiresonance electromechanical coupling can be established. Nevertheless, in [**Vidoli and dell'Isola (2000)**], no attention is paid to the suppression of structural vibrations and boundary conditions are only marginally examined. In [**dell'Isola et al. (2003, 2)**] the problem of finding an optimal distributed electric controller, within a rather wide class of local controllers, to attenuate propagating waves over any frequency range is tackled. The results presented in [**dell'Isola et al. (2003, 2)**] expand those shown in [**Vidoli and dell'Isola (2000)**],

assessing that for infinite beams the optimal continuous network for beam vibration damping should be governed by the same partial differential equations as the vibrating structure (i.e. the beam equation). But, at the same time, the network should be endowed with an internal dissipation proportional to the rate of change of the electric curvature (i.e. the second spatial derivative of the electric potential). Nevertheless both the works ignored the problems related to the boundary conditions. Some efforts in understanding the effects of boundary conditions may be found in [**Porfiri et al. (accepted)**] where simply supported beams are examined.

In [**dell'Isola and Vidoli (1998, 2)**], an active lumped electric circuit governed by a discrete approximation of the beam equation is proposed. The problem of synthesizing a completely passive circuit analog of the Euler-Bernoulli beam has been extensively analyzed in [**Alessandroni et al. (2002)**] and in [**dell'Isola et al. (2001)**]. Nevertheless, the proposed circuits have stern practical inconveniences, either due to negative inductors or multiport transformers. The former are typical active elements needing to be electronically simulated, and the latter are, in general, very heavy and their weights can represent a significant part of the mass of the overall smart structure. For a critical analysis of this control technique and comparisons among the electric controllers proposed in [**dell'Isola and Vidoli (1998, 1)**] and [**Alessandroni et al. (2002)**], see [**Maurini et al. (2004, 1)**].

The synthesis of a passive electric analog of an Euler-Bernoulli beam by using inductances, capacitors and two-port transformers has been presented in
[**Andreaus et al. (2004)**] and [**Porfiri et al. (2004)**]. In these works different synthesis techniques are exploited to achieve a satisfactory electric analog. In
[**Andreaus et al. (2004)**], a Lagrangian based approach is used: the Lagrangian of a Timoshenko beam is discretized and by establishing an electromechanical analogy between the flux-linkages (currents) and the displacements (forces) a discrete circuit governed by the discretized beam Lagrangian is assembled. In [**Porfiri et al. (2004)**], on the other hand, the equilibrium and constitutive equations of a Timoshenko beam element are finite-difference approximated and following two distinct analogies a four port circuit analog to the beam element is conceived.

2. Objectives

The focus of this work is the vibration suppression of beams via piezoelectric transducers and passive electric networks. The detailed objectives are as follows:

- Present the basic tools for modeling a stepped piezoelectric beam, i.e. a beam hosting piezoelectric transducers;
- Develop different and reliable algorithms for computing the modal characteristics of a stepped piezoelectric beam;
- Develop a homogenized model suitable for distributed control applications;
- Develop some identification methods for estimating the key modal parameters of a stepped piezoelectric beam;
- Present the basic concepts of the piezoelectric shunting technique;
- Demonstrate the use of RL distributed circuits for damping narrow-band structural vibrations;
- Analyze the effects of uncertainties of the electric parameters on the passive damping performances;
- Prove the effectiveness of the concept of electric analogs in the design of distributed passive controllers.

3. Overview

The Chapters constituting the dissertation can be basically organized into two groups. The first one (Chapters 2, 3 and 4) is focused on the modeling and analysis of stepped piezoelectric beams. The main results obtained in this part include a refined one-dimensional model of the stepped piezoelectric beam which accounts for the discontinuities introduced by the transducers, and a homogenized model which averages the periodically varying electromechanical constitutive properties. The choice of the vibration control technique (piezoelectric shunting/PEM) naturally determines the most suitable model for the stepped piezoelectric beam (refined/homogenized). The second group (Chapters 5, 6 and 7) deals with the analysis of three different passive circuits in damping structural vibrations. The classical piezoelectric shunting is used to present a general discussion about resonantly coupled systems and to introduce a novel modal identification technique. This knowledge together with the results stemming from the homogenized model are applied to the design of the second order transmission line for narrow band vibration suppression, and the fourth order transmission line for multimodal control.

The detailed organization of the work is:

- In Chapter 2, we develop a one dimensional model of stepped piezoelectric beams. We start by briefly covering the fundamental concepts of linear piezoelectricity. By the use of those concepts and elementary beam theory, we derive a simple and valuable model of a stepped piezoelectric beam and we indicate possible ameliorations. We provide the governing equations of the resulting electromechanical system both in the strong and weak formulations.
- In Chapter 3, we study the modal properties of a stepped piezoelectric beam. The computation of the exact modal frequencies and mode shapes of a stepped piezoelectric beam is not a trivial task, since piezoelectric elements introduce several material discontinuities to the initially homogeneous beam. The modal analysis is tackled by the exploitation of four different techniques relying on either classical (assumed modes, finite-element analysis) or recent methods (least energy norm method, special jump functions). The numerical results are also compared with those arising from an experimental setup, which is aimed at the validation of the proposed model.
- In Chapter 4, we present the homogenization of a beam clamped on both ends excited by voltages applied at the periodically distributed piezoelectric elements. Homogenization techniques allows for the transformation of differential equations with rapidly oscillating coefficients into simpler ones (homogenized) characterized by effective coefficients which are calculated from the solution of so-called unit cell problem. The adopted technique is the classical two-scale convergence, which enables to simultaneously obtain homogenized equations and prove convergences. Numerical tests are performed and the homogenized model is validated with, even, different boundary conditions.
- In Chapter 5, we review the basic concepts of the resonant piezoelectric shunting technique. In addition to presenting the basic knowledge from the wide literature in the field, we address some unexplored related topics. Indeed, we show a detailed sensitivity analysis aimed at evaluating the effects of changes in the electrical elements on the damping performances, conveyed in the system ∞-norm. We treat the effects of large variations and provide closed-form expressions for small perturbations. The results are used to model the effects of electrical parameters' uncertainties on the damping effectiveness. Finally we mention a

possible application of piezoelectric shunting in identification processes and test the method on an experimental prototype.

- In Chapter 6, we consider a PEM beam, whose electric control circuit is comprised of a simple second order transmission line. Every piezoelectric element of the array is connected to the adjacent one via a floating RL impedance. We initially analyze the resulting PEM structure as a continuous medium by the usage of its homogenized model and draw general considerations. Then, we resort to the treatment of the electric circuit as a finite degrees of freedom system. The $\mathcal{H}_\infty$ control problem is solved and optimal values of the line inductance and the line resistance are found for both the homogenized and the discrete cases, and comparisons are made. We consider the effects of uncertainties of the inductances on the system performances. The theoretical results are validated through an experimental prototype. The resulting network is capable of effectively damp narrow-band structural vibrations, moderate the required optimal inductances and abate the influence of the uncertainties of the electric parameters on the system performance.
- In Chapter 7, we consider a PEM beam, whose electric controller is the electric analog of a beam endowed with structural damping (fourth order transmission line) and constrained with dual boundary conditions. We study the vibrations of the resulting PEM beam as continuous medium and prove that, by the use of this network, multimodal vibrations can be suppressed and the damping efficiency is mode independent. The treatment of the resulting system makes use of fundamental features of the fourth order derivative operator which are reviewed. A realization of a finite-difference approximation of the fourth order transmission line is presented and two distinct synthesis methods are indicated (multiport synthesis and Lagrangian based synthesis). A PEM beam prototype is designed, its technical feasibility and its damping effectiveness are confirmed. Finally, the homogenized model of the electric circuit is questioned and the modal analysis of its lumped realization is sketched.
- Chapter 8 is left for conclusions.

CHAPTER 2

Modeling stepped piezoelectric beams

Layers of electroded piezoelectric ceramics are integrated in structural elements, by either surface bonding or direct embedding, resulting into piezocomposite structures. The sensing and actuation capability of piezoelectric layers is used for designing vibration control systems. To realize reliable devices, many research efforts have been devoted to develop accurate structural models of piezoelectric composites and efficient numerical tools for solving the associated governing equations. Complete review of the works about beam and plate models of piezoelectric composites can be found in [**Saravanos and Heyliger (1999)**], [**Gopinathan et al. (2000)**] and [**Chopra (2002)**]; for finite-element formulations one can refer to [**Gaudenzi and Bathe (1995)**], [**Mackerle (1998)**], [**Benjeddou (2000)**] and [**Mackerle (2003)**].

The objective of the present Chapter is to present a simple 1D model of beams hosting piezoelectric elements, which represents a reasonable trade-off between accuracy and complexity. We start by reviewing the basic concepts of linear piezoelectricity, focusing on piezoceramics, which are very common in vibration control. Next, we present a simple model of a piezoelectric transducer adhesively bonded on a host beam. The classical Euler-Bernoulli beam theory is used for modeling the host beam and rude hypotheses are made on the piezoelectric laminae behavior. The stepped piezoelectric beam constitutive coefficients are computed by using simple formulas similar to those found in [**Crawley and de Luis (1987)**], [**Strambi et al. (1995)**]and [**Chopra (2002)**]. From a short review of the technical literature, possible ameliorations of the needed constitutive parameters are suggested. The governing equations of the stepped piezoelectric beam are presented in both the strong and the weak formulations.

1. Linear piezoelectricity

We consider a solid body $\mathfrak{B}$ which is composed of an anisotropic non homogeneous linear piezoelectric medium, i.e. a non-magnetizable linear elastic dielectric that is not heat and electric conducting. We assume that the body has a natural configuration B, which will be used as reference. B is assumed to be a subset of the three-dimensional Euclidean point space $\mathbb{E}^3$, which is referred to a Cartesian inertial frame of reference consisting of an origin $\mathfrak{o}$ and an orthonormal basis $\{\mathbf{e}_1, \mathbf{e}_2, \mathbf{e}_3\}$. Moreover, we refer only to small electric fields and small deformation fields superimposed on the reference configuration, so that the linear theory of piezoelectricity is adequate. In linear piezoelectricity, the piezoelectric effect couples the equations of linear elasticity to the equations of electrostatics. However, the electric variables are not purely static; because of their coupling to the dynamic mechanical equations they vary in time and they are usually named quasistatic. The governing equations are (see e.g. [**Tiersten (1969)**], [**IEEE (1987)**], [**Parton and Kudryavtev (1988)**] and [**Ikeda (1990)**])

$$\mathrm{Div}\mathbf{T} = \rho\,\ddot{\mathbf{u}}, \qquad \mathbf{S} = \mathrm{Sym}\boldsymbol{\nabla}\mathbf{u}, \qquad \mathrm{Div}\mathbf{D} = 0, \qquad \mathrm{Rot}\mathbf{E} = 0,$$
$$\mathbf{T} = \mathbf{c}^E\mathbf{S} - \mathbf{e}^{\mathrm{T}}\mathbf{E}, \qquad \mathbf{D} = \boldsymbol{\epsilon}^S\mathbf{E} + \mathbf{e}\mathbf{S}$$

where $\mathbf{T}$ is the stress tensor, $\mathbf{D}$ is the electric displacement vector, $\mathbf{E}$ is the electric field vector, $\mathbf{u}$ is the displacement vector. $\mathbf{c}^E$, $\mathbf{e}$ and $\boldsymbol{\varepsilon}^S$ are the elastic, piezoelectric, and electric permittivity tensors, respectively, whose Cartesian components satisfy the symmetry properties:

$$c^E_{ijkl} = c^E_{ijlk} = c^E_{jikl} = c^E_{klij}, \qquad \epsilon^S_{ij} = \epsilon^S_{ji}, \qquad e_{ijk} = e_{ikj}.$$

Usually, in technical literature, the compressed matrix notation is used to study the material symmetry of piezoelectric materials and the following indices correspondence arises:

ij or kl	p or q
11	1
22	2
33	3
23 or 32	4
31 or 13	5
12 or 21	6

The constitutive behavior becomes:

$$T_p = c^E_{pq} S_q - e_{kp} E_k, \qquad D_i = e_{iq} S_q + \epsilon^S_{ik} E_k,$$

where S_q indicates the engineering strains and repeated indices denote summation. By the use of this notation the elastic and piezoelectric constants as well as the dielectric constants can be written as matrices:

$$\mathbf{c}^E = \begin{bmatrix} c^E_{11} & c^E_{12} & c^E_{13} & c^E_{14} & c^E_{15} & c^E_{16} \\ c^E_{12} & c^E_{22} & c^E_{23} & c^E_{24} & c^E_{25} & c^E_{26} \\ c^E_{13} & c^E_{23} & c^E_{33} & c^E_{34} & c^E_{35} & c^E_{36} \\ c^E_{14} & c^E_{24} & c^E_{34} & c^E_{44} & c^E_{45} & c^E_{46} \\ c^E_{15} & c^E_{25} & c^E_{35} & c^E_{45} & c^E_{55} & c^E_{56} \\ c^E_{16} & c^E_{26} & c^E_{36} & c^E_{46} & c^E_{56} & c^E_{66} \end{bmatrix},$$

$$\mathbf{e} = \begin{bmatrix} e_{11} & e_{21} & e_{31} \\ e_{12} & e_{22} & e_{32} \\ e_{13} & e_{23} & e_{33} \\ e_{14} & e_{24} & e_{34} \\ e_{15} & e_{25} & e_{35} \\ e_{16} & e_{26} & e_{36} \end{bmatrix}, \quad \boldsymbol{\epsilon}^S = \begin{bmatrix} \epsilon^S_{11} & \epsilon^S_{12} & \epsilon^S_{13} \\ \epsilon^S_{12} & \epsilon^S_{22} & \epsilon^S_{23} \\ \epsilon^S_{12} & \epsilon^S_{23} & \epsilon^S_{33} \end{bmatrix}.$$

Therefore, the number of constitutive constants is in general $21 + 18 + 6 = 45$.

In control applications, usually piezoceramics are used (see e.g. [**Chopra (2002)**]). The ceramic is initially isotropic and, being composed of the random orientation of piezoelectric crystallites, is inactive, i.e., the effects from the individual crystals cancel each other and no discernible piezoelectricity is present. Poling is a commonly used method to orient the domains (regions of equally oriented polarization vectors are known as domains), by polarizing the ceramic through the application of a static electric field, say in the 3 direction. Appropriate electrodes are applied to the ceramic and a sufficiently high electric field is applied such that the domains rotate and switch in the direction of the electric field. Hence, the isotropy is destroyed in the poling direction (see e.g. [**Jordan and Ounaies (2001)**]). The material is transversely isotropic, with the axis of transverse isotropy in the poling direction. The symmetry elements are an axis of rotation of infinite order in the direction of poling and an infinite set of planes parallel to the polar axis as reflection planes. In crystallographic notation (Hermann-Mauguin), this symmetry is described as ∞mm and is equivalent to the hexagonal polar crystal class

6mm (see e.g. [**IEEE (1987)**]). The elastic, dielectric and piezoelectric matrices for the cylindrical symmetry of poled PZT are shown in the equations below.

$$\mathbf{c}^E = \begin{bmatrix} c_{11}^E & c_{12}^E & c_{13}^E & 0 & 0 & 0 \\ c_{12}^E & c_{11}^E & c_{13}^E & 0 & 0 & 0 \\ c_{13}^E & c_{13}^E & c_{33}^E & 0 & 0 & 0 \\ 0 & 0 & 0 & c_{44}^E & 0 & 0 \\ 0 & 0 & 0 & 0 & c_{44}^E & 0 \\ 0 & 0 & 0 & 0 & 0 & \frac{1}{2}\left(c_{11}^E - c_{12}^E\right) \end{bmatrix},$$

$$\mathbf{e} = \begin{bmatrix} 0 & 0 & e_{31} \\ 0 & 0 & e_{31} \\ 0 & 0 & e_{33} \\ 0 & e_{15} & 0 \\ e_{15} & 0 & 0 \\ 0 & 0 & 0 \end{bmatrix}, \quad \boldsymbol{\epsilon}^S = \begin{bmatrix} \epsilon_{11}^S & 0 & 0 \\ 0 & \epsilon_{11}^S & 0 \\ 0 & 0 & \epsilon_{33}^S \end{bmatrix},$$

and the number of constitutive coefficients reduces to $5 + 3 + 2 = 10$. Sometimes it is convenient to express the constitutive behavior in a different form, i.e.

$$S_p = s_{pq}^E T_q + d_{kp} E_k, \qquad D_i = d_{iq} T_q + \epsilon_{ik}^T E_k,$$

where, for piezoceramics polarized in the 3 direction:

$$\mathbf{s}^E = \begin{bmatrix} s_{11}^E & s_{12}^E & s_{13}^E & 0 & 0 & 0 \\ s_{12}^E & s_{11}^E & s_{13}^E & 0 & 0 & 0 \\ s_{13}^E & s_{13}^E & s_{33}^E & 0 & 0 & 0 \\ 0 & 0 & 0 & s_{44}^E & 0 & 0 \\ 0 & 0 & 0 & 0 & s_{44}^E & 0 \\ 0 & 0 & 0 & 0 & 0 & 2\left(s_{11}^E - s_{12}^E\right) \end{bmatrix}, \tag{1.1}$$

$$\mathbf{d} = \begin{bmatrix} 0 & 0 & d_{31} \\ 0 & 0 & d_{31} \\ 0 & 0 & d_{33} \\ 0 & d_{15} & 0 \\ d_{15} & 0 & 0 \\ 0 & 0 & 0 \end{bmatrix}, \quad \boldsymbol{\epsilon}^T = \begin{bmatrix} \epsilon_{11}^T & 0 & 0 \\ 0 & \epsilon_{11}^T & 0 \\ 0 & 0 & \epsilon_{33}^T \end{bmatrix}.$$

2. Modeling a piezoelectric transducer

A bimorph pair of piezoceramics elements adhesively bonded on a host beam is shown in Figure 1. A beam of rectangular cross section is considered, the origin of the frame is located at the centroid of an arbitrary cross section, the coordinates x_2 and x_3 are principal, and $x_1 = x$ is on the beam axis. The piezoelectric elements are poled in the same direction, symmetrically positioned on the beam surfaces and their electrodes are parallel connected in the so-called bender configuration (in this way pure bending occurs see e.g. [**Chopra (2002)**]). The beam material is homogeneous and isotropic. Furthermore, the beam behaves as a perfect conductor which short-circuit two electrodes of the laminae to ground.

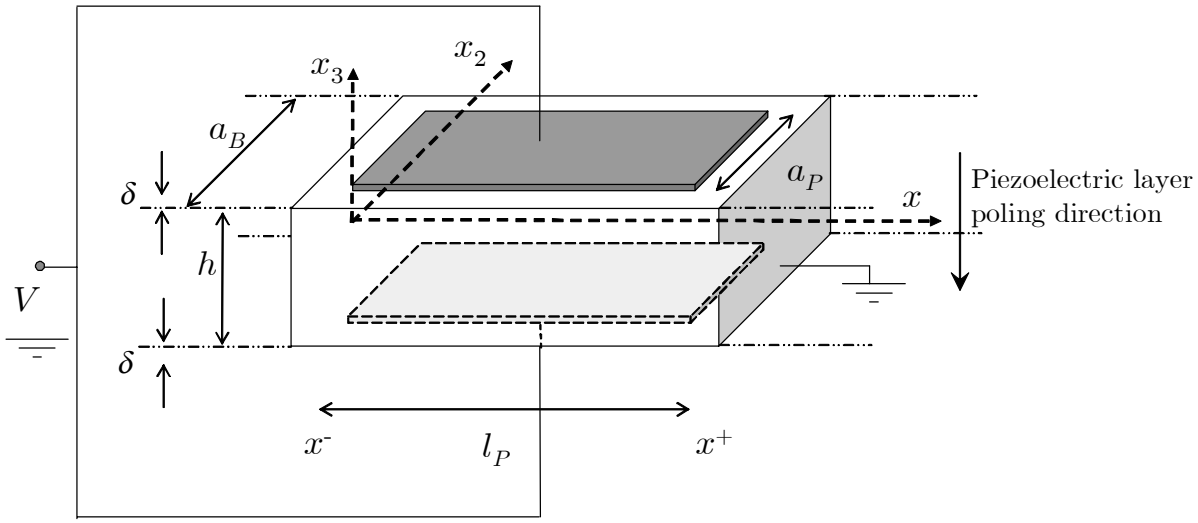

FIGURE 1. Sketch of a bimorph pair bonded on a host beam.

We model the piezoelectric beam by using the classical Euler-Bernoulli beam theory. Many interesting and rigorous works have been dedicated to increase the model accuracy by introducing more and more state variables to describe higher order shear effects. However, the associated corrections have been shown to be relevant only for relatively thick beams
[**Maxwell and Asokanthan (2004)**] and, especially for control applications, the Euler-Bernoulli model is still the most popular because of its simplicity.

We assume that the thickness δ of the piezoelectric transducers is negligible compared to the thickness h of the beam and that a perfect adhesive bonding between the beam and the actuators is realized (for analysis of the effects of finite bonding see [**de Faria (2003)**]). Moreover we assume that in each patch the stress and the electric field are of the following form (for more details see [**Crawley and de Luis (1987)**], [**Hagood and von Flotow (1991)**] and [**Hanagud et al. (1992)**]):

$$\mathbf{T} = \begin{bmatrix} T_{11}(x) \\ 0 \\ 0 \\ 0 \\ T_{13}(x, x_3) \\ 0 \end{bmatrix}, \qquad \mathbf{E} = \begin{bmatrix} 0 \\ 0 \\ E_3 \end{bmatrix}.$$

In particular. the electric field is assumed to be constant and to lie in the 3 direction. Plane stress in the 13 plane is assumed, where the only nonvanishing stresses are the traction in the beam direction (depending only on x) and the 13 shear. These assumptions are physically well-grounded when $\delta << h$ (see [**Krommer (2001)**]).

Once the constitutive equations in (1.1) are assumed, the one-dimensional constitutive equations for the piezoelectric patches reduce to

$$\begin{bmatrix} S_{11} \\ D_3 \end{bmatrix} = \begin{bmatrix} s_{11}^E & -d_{31} \\ -d_{31} & \epsilon_{33}^T \end{bmatrix} \begin{bmatrix} T_{11} \\ E_3 \end{bmatrix}. \tag{2.1}$$

We assume that the variation of the strain along the thickness of the actuators is negligible, so that

$$S_{11}^u = -\frac{h}{2}w''(x), \quad S_{11}^l = +\frac{h}{2}w''(x),$$

where the superscripts u and l indicate respectively the upper and lower lamina, w indicates the beam deflection field (i.e. the component of the displacement along $\mathbf{e}_3$ evaluated on the beam axis), prime indicates strong differentiation with respect to the abscissa x, and the Euler-Bernoulli beam hypotheses have been used.

Furthermore, we assume that also the electrical displacement field is constant over the thickness of the patch. As the flux of D_3 over the two patches electrodes is equal to the charge stored in each actuator, then integrating the electric displacement field over the surface of the piezo-layer it is easy to obtain:

$$Q = 2\frac{a_P l_P \left(s_{11}^E \epsilon_{33}^T - d_{31}^2\right)}{s_{11}^E \delta} V - \frac{h a_P d_{31}}{s_{11}^E}\left(w'\left(x^+\right) - w'\left(x^-\right)\right),$$

where Q is the charge stored in the bimorph pair, a_P and l_P are respectively the width and length of each lamina, $w'(x^\pm)$ are the rotations of the cross sections of the beam at the edges of the patches and V is the voltage drop measured with respect to the ground. Sometimes the electromechanical coupling coefficient k_{31} (see e.g. [**IEEE (1987)**]) is used and the previous expression takes the form:

$$Q = 2\frac{a_P l_P \epsilon_{33}^T}{\delta}\left(1 - k_{31}^2\right) V - \frac{h a_P d_{31}}{s_{11}^E}\left(w'\left(x^+\right) - w'\left(x^-\right)\right),$$

with:

$$k_{31} = d_{31}\sqrt{\frac{1}{s_{11}^E \epsilon_{33}^T}}.$$

The bending moment along $\mathbf{e}_2$ at a generic cross section between x^+ and x^- is equal to:

$$M(x) = -\int_{-a_B/2}^{a_B/2}\int_{-h/2-\delta}^{h/2+\delta} T_{11} x_3 dx_2 dx_3,$$

where a_B is the beam width. By considering the constitutive relation in (2.1) and neglecting higher order terms, the above equation gives:

$$M(x) = \left(EI + \frac{h^2 a_P \delta}{2 s_{11}^E}\right) w''(x) + \frac{h a_P d_{31}}{s_{11}^E} V,$$

where I is the moment of inertia of the cross section ($I = a_B h^3/12$) and E is the Young modulus of the beam. Hence, the constitutive equations for the stepped beam element in Figure 1 can be written as:

$$M(x) = k_P w''(x) - gV, \tag{2.2a}$$

$$Q = CV + g\left(w'\left(x^+\right) - w'\left(x^-\right)\right), \tag{2.2b}$$

with:

$$k_P = k_B + \frac{h^2 a_P \delta}{2 s_{11}^E}, \quad k_B = EI, \tag{2.3a}$$

$$C = 2\frac{a_P\left(s_{11}^E \epsilon_{33}^T - d_{31}^2\right)}{s_{11}^E \delta} l_P = 2\frac{a_P l_P \epsilon_{33}^T}{\delta}\left(1 - k_{31}^2\right), \tag{2.3b}$$

$$g = -\frac{h a_P d_{31}}{s_{11}^E}. \tag{2.3c}$$

The constant k_P is the bending stiffness of the three-layers piezocomposite beam for short-circuited transducers ($V = 0$) and it is made of two summands, namely the beam bending stiffness k_B and the piezoelectrics' stiffnesses. The constant C measures the piezoelectric capacitance when the relative rotation at the laminae ends is zero ($w'(x^+) = w'(x^-)$). The constant g measures the piezoelectric coupling, i.e. the additional bending moment due to a unitary negative applied voltage and, simultaneously, the additional stored charge due to a unitary relative rotation at the laminae ends[1]. From an electric point of view the piezoelectric transducer can be viewed as a capacitor in parallel connection with a charge source driven by the mechanical deformation; while, from the mechanical point of view it adds stiffness to the host beam and it introduces a constant amount of bending moment dependent only the applied voltage.

We emphasize that equations (2.3) provide the estimations of the constitutive parameters of a three layers composite beam modelled as an Euler-Bernoulli beam. Within the same Euler-Bernoulli modeling of the composite beam, different techniques, see e.g. [**Maurini et al. (2004, 2)**], can be used to estimate the above constitutive parameters.

REMARK 1. *For a single piezoelectric lamina bonded on the given structure, the transducer capacitance C, the added bending stiffness and the coupling coefficient g are half of the bimorph value reported above.*[2]

When one wants to consider more refined model of piezoelectric transducers, dispensing with the hypothesis of negligible piezoelectric thickness, the problem of consistent electromechanical modeling arises. Only recently beam models fully accounting for the two-fold electromechanical coupling have been proposed (see e.g. [**Kapuria et al. (2003)**]) and consistent distributions of the electromechanical fields have been established (see e.g.[**Sze et al. (2004)**]). A careful electromechanical modeling is required especially for passive vibration control applications, where besides mechanical and coupling parameters, also the purely electrical properties, such as the piezoelectric capacitance, can strongly influence the controller design (see e.g. [**Hagood and von Flotow (1991)**] and [**Andreaus et al. (2004)**] for single-mode and multimodal passive vibration control, respectively).

In the present work the stepped beam is assumed to be under plane stress conditions in the 13 plane. Recent works (see [**Beckert and Pfundtner (2002)**] and [**Maurini et al. (2004, 2)**]) have investigated the validity of this hypothesis by studying the the effect of transversal (along the width) interactions between different layers. In particular, in [**Maurini et al. (2004, 2)**] it has been shown that it can lead to errors in the estimation of the electromechanical constitutive parameters (especially for the equivalent piezoelectric capacitance) and corrected constitutive equations have been proposed.

3. Modeling the whole stepped beam

In the present Section, we establish the equations of motion for the generic beam segment (distinguishing between purely elastic and piezocomposite ones) and the continuity conditions between adjacent segments. Moreover, an alternative global weak formulation of the problem, suitable for numerical analysis, is proposed.

[1] If the poling direction is reversed, the sign of g should be changed.

[2] When a single piezoelectric element is used, the host beam bends and extends (see e.g. [**Strambi et al. (1995)**]).

3.1. Geometry. We consider a beam of length l with N_P adhesively bonded piezoelectric transducers. The resulting stepped piezoelectric beam consists of N regular segments, each one of them being a beam with constant constitutive properties. Purely elastic segments alternate with multi-layered segments composed of one elastic core and one or two piezoelectric laminae, as that described in Section 2. The generic material point of the beam axis is labelled by the abscissa x. The generic beam node is indicated by X_h and the generic beam segment of length l_h between X_h and X_{h+1} is indicated by S_h (see Figure 2). For the sake of convenience, we introduce the subsets of indices I_B and I_P associated, respectively, to elastic and piezocomposite segments.

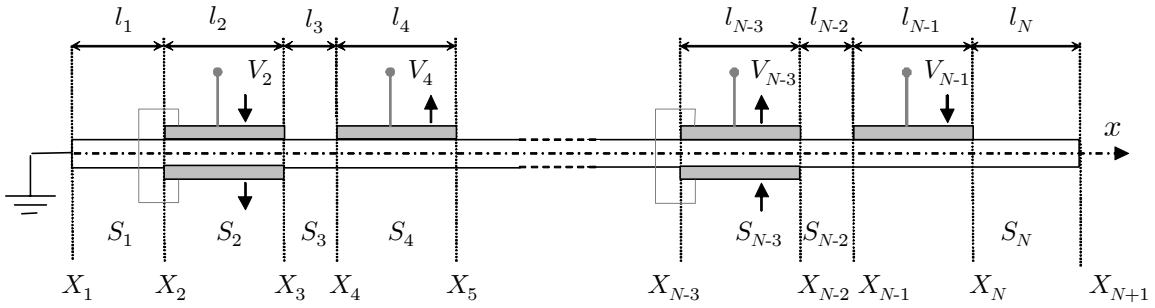

FIGURE 2. Sketch of a stepped piezoelectric beam.

3.2. Equations of motion. The generic segment of stepped beam S_h is modelled as an Euler-Bernoulli beam and, for plane motions, its kinematical state is described by the beam axis deflection field w_h and the voltage V_h across the terminals of the transducer (which is defined only if S_h is a piezocomposite segment).

3.2.1. *Strong Formulation.*

Elastic segment. For a purely elastic segment S_h ($h \in \mathrm{I}_B$), the mechanical equilibrium equation is (here and henceforth rotational inertia is neglected):

$$M_h(x,t)'' + \rho_B \ddot{w}_h(x,t) - b_h(x,t) = 0, \tag{3.4}$$

where M_h is the bending moment, b_h the external transversal load, t the time variable, ρ_B is the linear mass density and the superimposed dot denotes the time-derivative. The constitutive relation for the bending moment is

$$M_h(x,t) = k_B w_h''(x,t), \tag{3.5}$$

where k_B denotes the bending stiffness[3]. Hence, the mechanical equation of motion in the generic elastic segment is given by

$$k_B w_h^{IV}(x,t) + \rho_B \ddot{w}_h(x,t) = b_h(x,t).$$

Piezocomposite segment. For a piezocomposite segment S_h ($h \in \mathrm{I}_P$), the mechanical equilibrium equation is completed by the charge equilibrium at the electric terminals of the bimorph pair, namely:

$$M_h(x,t)'' + \rho_h \ddot{w}_h(x,t) - b_h(x,t) = 0, \tag{3.6a}$$

$$Q_h(t) = \hat{Q}_h(t), \tag{3.6b}$$

[3]The stiffnesses of all the elastic segments and their linear mass densities do not vary.

where Q_h is the stored charge and $\hat{Q}_h$ is the overall prescribed charge. That charge may be externally blocked, either by open circuiting the piezoelectric terminal or by using a charge source, or it may be related to the time evolution of an auxiliary control circuit, either passive or active, coupled to the vibrating stepped beam. The electrical and mechanical fields are coupled by constitutive equations of the type (2.2):

$$M_h(x,t) = k_h w_h''(x,t) - g_h V_h(t), \tag{3.7a}$$

$$Q_h(t) = g_h\left[w_h'(X_{h+1},t) - w_h'(X_h,t)\right] + C_h V_h(t), \tag{3.7b}$$

where g_h is the piezoelectric coupling coefficient and C_h the piezoelectric capacitance[4]. The inertial forces are taken into account as for (3.4), with properly modified linear mass density. Hence, the electromechanical equations of motion for the generic piezocomposite segment are

$$k_h w_h^{IV}(x,t) + \rho_h \ddot{w}_h(x,t) - b_h(x,t) = 0 \tag{3.8a}$$

$$g_h\left[w_h'(X_{h+1},t) - w_h'(X_h,t)\right] + C_h V_h(t) = \hat{Q}_h(t). \tag{3.8b}$$

Continuity conditions. The continuity conditions between the h-th and the $(h+1)$-th segments are assured by imposing the continuity of deflections, rotations, bending moment and shear forces, i.e.:

$$w_h(X_{h+1},t) = w_{h+1}(X_{h+1},t), \tag{3.9a}$$

$$w_h'(X_{h+1},t) = w_{h+1}'(X_{h+1},t), \tag{3.9b}$$

$$M_h(X_{h+1},t) = M_{h+1}(X_{h+1},t) \Rightarrow k_h w_h''(X_{h+1},t) - g_h V_h(t) = k_B w_{h+1}''(X_{h+1},t), \tag{3.9c}$$

$$T_h(X_{h+1},t) = T_{h+1}(X_{h+1},t) \Rightarrow k_h w_h'''(X_{h+1},t) = k_B w_{h+1}'''(X_{h+1},t), \tag{3.9d}$$

where, without loss of generality, we assume that the $(h+1)$-th element is elastic and the h-th is piezocomposite. In the above expression $T_h = -M_h'(x,t)$ indicates the shear force in the h-th segment.

3.2.2. *Weak formulation.* The function defining the deflection of the entire beam axis is defined in terms of the local deflections w_h satisfying the kinematic continuity conditions (3.9a) and (3.9b), and the prescribed kinematic boundary conditions by:

$$w(x,t) = \sum_{h=1}^{N} w_h(x,t)\left(\mathrm{H}(x - X_h) - \mathrm{H}(x - X_{h+1})\right), \tag{3.10}$$

where H is the Heaviside function. Whenever it is convenient we drop the distinction between the mechanical properties of the elastic and piezocomposite segments, by writing simply ρ_h and k_h for the linear mass density and stiffness of the h-th segment.

A weak formulation for the mechanical equilibrium equations (3.4) (accounting for the natural continuity conditions (3.9c), (3.9d), and homogeneous natural boundary conditions) is obtained by imposing that for all the admissible (i.e. regular and satisfying the kinematic boundary conditions) test fields $\tilde{w}$, the following equality holds:

$$\sum_{h=1}^{N}\int_{S_h} M_h(x,t)\tilde{w}''(x)dx = \sum_{h=1}^{N}\int_{S_h} b_h(x,t)\tilde{w}(x)dx - \sum_{h=1}^{N}\int_{S_h}\rho_h\ddot{w}(x,t)\tilde{w}(x)dx. \tag{3.11}$$

[4]The stiffness, linear mass density, coupling coefficient and capacitance of the piezoelectric segments are in general different for each active segment.

By substituting the constitutive equations for the bending moment and the inertial actions, (3.11) becomes:

$$\sum_{h=1}^{N}\int_{S_h} k_h w''(x,t)\tilde{w}''(x)dx - \sum_{h\in \mathrm{I}_P} g_h V_h(t)\left(\tilde{w}'(X_{h+1}) - \tilde{w}'(X_h)\right) = \\ -\sum_{h=1}^{N}\int_{S_h}\rho_h \ddot{w}(x,t)\tilde{w}(x)dx + \sum_{h=1}^{N}\int_{S_h} b_h(x,t)\tilde{w}(x)dx. \tag{3.12}$$

We leave to Chapter 4 more mathematical details on the choices of suitable spaces for the strong and weak formulations. The weak formulation above is the starting point to derive approximate solutions to the coupled electromechanical problem by Galerkin-type discretizations of the stepped beam.

CHAPTER 3

Modal analysis of stepped piezoelectric beams

Piezoelectric elements, besides providing the electromechanical coupling that can be used for sensing and actuating, modify also the structural properties by adding mass and stiffness and consequently material discontinuities. It has been shown that, especially for lightweight structures, neglecting these additional contributions can result in significant errors in estimating the modal properties of the overall structure. On the other hand, the precise knowledge of the stepped beam modal properties represents the starting point for the design of reduced-order controllers (see e.g. [**Hagood and von Flotow (1991)**]). Therefore, accurate tools for the theoretical prediction of the modal properties of stepped beams are needed. In literature, modal analysis is usually performed either by the assumed modes methods (i.e. by expanding the solution of the stepped beam on a finite number of mode shapes of the homogeneous beam, see e.g. [**Hagood and von Flotow (1991)**] and [**Park (2003)**]), or by finite-element methods [**Kusculuoglu et al. (2004)**]. The problem of finding exact modal properties of a stepped piezoelectric beam has been formulated in [**Yang and Lee (1994, 1)**], [**Yang and Lee (1994, 2)**] and [**Maxwell and Asokanthan (2004)**]. The main problem in this contest is to solve a trascendental eigenvalue problem. The method applied in the cited papers is the natural extension of that used for uniform beams and requires the inversion of usually ill-conditioned matrices for finding mode shapes. Consequently, it implies numerical problems that become quickly unsolvable when increasing the number of piezoelectric elements.

In this Chapter, different methods for finding mode shapes and natural frequencies of a stepped piezoelectric beam are described. The starting point is the frequency domain formulation of the system equations of motion. Aiming at deriving modal models to be used in control applications, we study the modal characteristics of the stepped beam with the piezocomposite segments simultaneously short-circuited to ground. Therefore, no distinction occurs between elastic and piezocomposite segments. The analysis of stepped beam including passive electric circuits may be directly tackled by following similar procedures.

We propose four different methodologies (see [**Maurini et al. (submitted)**] for details). The first one is based on a reliable and efficient method recently proposed in [**Zhaohui et al. (2004)**] to solve the exact trascendental eigenvalue problem, once formulated in terms of the dynamic stiffness matrix, and it will be denoted as Last Energy Norm (LEN) method. Hence, three different Galerkin methods for obtaining a discretized finite-dimensional version of the systems are proposed and compared, by assessing their accuracies with respect to results from the LEN method. Namely, besides the standard and popular Assumed Modes (AM) method and Finite-Element (FE) method, we test a novel enhanced version of the assumed modes method, where special jump functions are introduced to enrich the standard basis functions (Enhanced Assumed Modes, EAM). Finally an experimental set up is described (see [**Maurini et al. (submitted)**] for details) , aiming at the validation of the model proposed in Chapter 2. The numerical techniques are tested on the considered prototype and general considerations are presented.

1. Problem formulation

The eigenvalue problem for the stepped piezoelectric beam can be posed by looking for harmonic solutions in the form

$$w_h(x,t) = \mathsf{w}_h(x)e^{i\omega t}, \tag{1.1}$$

where w_h is the spectral component of the mechanical displacement. Hence, the N governing equations obtained from the beam equation by discarding external loads and setting the piezoelectric voltages to zero, can be rewritten as

$$\mathsf{w}_h^{IV}(\xi_h) - \eta_h^4 \mathsf{w}_h(\xi_h) = 0, \tag{1.2}$$

where

$$\eta_h = l_h\sqrt{\omega}\sqrt[4]{\frac{\rho_h}{k_h}}, \quad \xi_h = \frac{x - X_h}{l_h}, \tag{1.3}$$

ξ_h being the normalized local coordinate of the h-th segment. The corresponding continuity conditions (3.9) of Chapter 2 become:

$$\mathsf{w}_h(1) = \mathsf{w}_{h+1}(0), \tag{1.4a}$$
$$\mathsf{w}_h'(1) = \mathsf{w}_{h+1}'(0), \tag{1.4b}$$
$$k_h\mathsf{w}_h''(1) = k_{h+1}\mathsf{w}_{h+1}''(0), \tag{1.4c}$$
$$k_h\mathsf{w}_h'''(1) = k_{h+1}\mathsf{w}_{h+1}'''(0), \tag{1.4d}$$

In addition, let us assume that N_w constraints (including at least 4 boundary conditions at the beam ends) are imposed on the deflection fields. Finally, the eigenvalue problem for the stepped piezoelectric beam is posed by looking for

(1) the angular frequencies ω (modal frequencies),
(2) the sets of N deflection fields w_h (mode shapes),

satisfying the N beam equations equations (1.2) with the continuity conditions (1.4) and the N_w mechanical boundary conditions. We explicitly remark that the whole modal shape w is found by the use of (3.10) of Chapter 2, upon substituting w_h with w_h.

The corresponding weak formulation of the eigenvalue problem is obtained by substituting the harmonic type solution (1.1) into (3.12) of Chapter 2 and assuming vanishing voltages.

2. Last Energy Norm method

The general solution of equation (1.2) is

$$\mathsf{w}_h(\xi_h) = A_{1h}\cos(\eta_h\xi_h) + A_{2h}\sin(\eta_h\xi_h) + A_{3h}\cosh(\eta_h\xi_h) + A_{4h}\sinh(\eta_h\xi_h), \tag{2.5}$$

where A_{1h}, A_{2h}, A_{3h} and A_{4h} are arbitrary real constants. For each segment, we introduce the nodal displacement vector $\mathbf{w}_h$

$$\mathbf{w}_h = \left[\ \mathsf{w}_h(0) \quad \mathsf{w}_h'(0) \quad \mathsf{w}_h(1) \quad \mathsf{w}_h'(1)\ \right]^{\mathrm{T}}, \tag{2.6}$$

and the nodal force vector $\mathbf{f}_h$ defined by:

$$\mathbf{f}_h = \left[\ -\mathsf{T}_h(0) \quad -\mathsf{M}_h(0) \quad \mathsf{T}_h(1) \quad \mathsf{M}_h(1)\ \right]^{\mathrm{T}},$$

where

$$\mathsf{M}_h(0) = k_h\mathsf{w}_h''(0), \quad \mathsf{M}_h(1) = k_h\mathsf{w}_h''(1), \quad \mathsf{T}_h(0) = -\mathsf{M}_h'(0), \quad \mathsf{T}_h(1) = -\mathsf{M}_h'(1),$$

and superscripted T indicates matrix transposition.

For a generic segment the nodal forces are related to nodal displacement by

$$\mathbf{f}_h = \mathbf{K}_h \mathbf{w}_h,$$

where the so-called segment dynamic stiffness $\mathbf{K}_h$ is given by:

$$\mathbf{K}_h = \frac{k_h}{r} \begin{bmatrix} a & -c & f & -d \\ -c & b & d & g \\ f & d & a & c \\ -d & g & c & b \end{bmatrix},$$

with a, b, c, d, f, g, r functions of η_h and l_h, defined by by

$$\begin{aligned} a &= -\eta_h^3 \left(\cosh\left(\eta_h\right)\sin\left(\eta_h\right) + \cos\left(\eta_h\right)\sinh\left(\eta_h\right)\right), \\ b &= l_h^2\eta_h \left(-\cosh\left(\eta_h\right)\sin\left(\eta_h\right) + \cos\left(\eta_h\right)\sinh\left(\eta_h\right)\right), \\ c &= l_h\eta_h^2 \sin\left(\eta_h\right)\sinh\left(\eta_h\right), \\ d &= l_h^2\eta_h \left(\cosh\left(\eta_h\right) - \cos\left(\eta_h\right)\right), \\ f &= \eta_h^3 \left(\sin\left(\eta_h\right) + \sinh\left(\eta_h\right)\right), \\ g &= l_h^2\eta_h \left(\sin\left(\eta_h\right) - \sinh\left(\eta_h\right)\right), \\ r &= l_h^3 \left(-1 + \cos\left(\eta_h\right)\cosh\left(\eta_h\right)\right). \end{aligned}$$

Next, by introducing the global $2\left(N+1\right)$ displacement-vector $\hat{\mathbf{w}}$ and imposing the continuity conditions (1.4) one obtains the following equation

$$\hat{\mathbf{K}}\,\hat{\mathbf{w}} = \mathbf{0}, \tag{2.7}$$

where the global $2\left(N+1\right) \times 2\left(N+1\right)$ stiffness matrix, $\hat{\mathbf{K}}$ is found by assembling the segment matrices with standard procedures (completely analogous to those used in FE analysis). When accounting for the N_w mechanical boundary conditions the dynamic stiffness is modified by deleting respective rows and columns[1]. For instance, for a cantilever beam with the left side clamped one has to delete the first two rows and column and remove the first two mechanical nodal displacements. Hence the following constrained version of (2.7) is obtained

$$\mathbf{K}_D(\omega)\mathbf{w} = \mathbf{0}, \tag{2.8}$$

in terms of the free $n = (2N + 2 - N_w)$ displacement-vector $\mathbf{w}$. From the nodal vectors $\mathbf{w}$ the deflection fields at each beam segment are found by using (2.6). The $n \times n$ dynamic stiffness matrix $\mathbf{K}_D(\omega)$ is real symmetric, non-negative definite and its entries are trascendental functions of ω.

The problem of finding the eigenvalues of the stepped beam requires to find the roots of the characteristic equation associated to equations (2.8). Due to the distributed nature of the mechanical system the characteristic equation is trascendental in ω and finding is roots is not trivial. Moreover, whenever a modal frequency is found, standard algorithms generally fail in finding associated mode shapes since the inversion of usually ill-conditioned matrices is required. In what follows we apply the accurate algorithm developed in [**Zhaohui et al. (2004)**] as an improvement of the well-known Wittrick-Williams algorithm (see [**Williams and Wittrick (1970)**] and [**Wittrick and Williams (1971)**]) for the solution of trascendental eigenvalue problem. By means of this technique one can find simultaneously the eigenvalues and the corresponding mode shapes without any matrix inversion. In particular, the natural frequencies are found as the roots of the last

[1]More general linear mechanical constraints may be considered by properly reducing the appearing matrices and degrees of freedom.

energy norm, defined in equation (2.11), and the corresponding modal nodal displacement vectors by the recursive relations (2.13). Once modal nodal displacement vectors are found, the corresponding mode shape $\mathsf{w}^{(i)}(x)$ at the given modal radian frequency $\omega^{(i)}$ is easily found from (2.5), (2.6) and the harmonic version of (3.10). Here and henceforth, we will assume that the mode shape $\mathsf{w}^{(i)}(x)$ is normalized so as to satisfy

$$\sum_{h=1}^{N} \int_{S_h} \rho_h \left(\mathsf{w}^{(i)}(x)\right)^2 dx = m,$$

where m is the total mass of the stepped piezoelectric beam. Therefore the normalized mode shape $\mathsf{w}^{(i)}(x)$ is dimensionless.

2.1. Algorithm. In this Section, we briefly review the procedure presented in [**Zhaohui et al. (2004)**] (and called in the present work LEN method) for solving the trascendental eigenvalue problem (2.8).

At any trial frequency $\bar{\omega}$ the symmetric matrix $\mathbf{K}_D$ can be decomposed in terms of a non singular lower triangular matrix $\mathbf{L}$ with unit diagonal elements and a diagonal matrix $\mathbf{D}$:

$$\mathbf{K}_D = \mathbf{L}\mathbf{D}\mathbf{L}^{\mathrm{T}}. \tag{2.9}$$

Or equivalently,

$$\mathbf{P}^{\mathrm{T}}\mathbf{K}_D\mathbf{P} = \mathbf{D},$$

where the upper triangular matrix $\mathbf{P}$, satisfying

$$\mathbf{P} = \mathbf{L}^{-\mathrm{T}}, \tag{2.10}$$

has been introduced. The last entry of $\mathbf{D}$ is called last energy norm and is given by

$$d_n = \mathbf{P}_n^{\mathrm{T}}\mathbf{K}_D\mathbf{P}_n, \tag{2.11}$$

where the matrix subscript k indicates the k-th column, i.e. $\mathbf{P}_k$ is the last column vector of $\mathbf{P}$. From equations (2.9) and (2.10) we find:

$$\mathbf{K}_D\mathbf{P}_n = (\mathbf{K}_D\mathbf{P})_n = (\mathbf{L}\mathbf{D})_n,$$

and by noticing that $\mathbf{L}$ is lower triangular with unit diagonal elements and $\mathbf{D}$ is diagonal we obtain

$$\mathbf{K}_D\mathbf{P}_n = d_n\mathbf{I}_n, \tag{2.12}$$

where $\mathbf{I}$ is the n dimensional identity matrix. Therefore, if d_n vanishes at $\bar{\omega}$, then $\bar{\omega}$ is a natural frequency and $\mathbf{P}_n$ is the corresponding eigenvector. For every trial frequency $\bar{\omega}$, the vector $\mathbf{P}_n$my be found without any matrix inversion, by using the following recursive relations:

$$\mathbf{P}_1 = \mathbf{I}_1, \tag{2.13a}$$

$$\mathbf{F}_1 = (\mathbf{K}_D)_1, \tag{2.13b}$$

$$\mathbf{P}_k = \mathbf{I}_k - \sum_{i=1}^{k-1} \frac{(\mathbf{F}_k)_i}{(\mathbf{F}_i)_i}\mathbf{P}_i, \tag{2.13c}$$

$$\mathbf{F}_k = (\mathbf{K}_D)_k - \sum_{i=1}^{k-1} \frac{(\mathbf{F}_k)_i}{(\mathbf{F}_i)_i}\mathbf{F}_i, \tag{2.13d}$$

where $\mathbf{F}$ is a lower triangular matrix defined by

$$\mathbf{F} = \mathbf{P}^{-\mathrm{T}}\mathbf{D} = \mathbf{K}_D\mathbf{P}. \tag{2.14}$$

In this way, the eigenvalues can be found as the root of the last energy norm d_n computed from (2.12) where $\mathbf{P}_n$ is evaluated from the above recursive relations. Therefore, the natural frequencies and the corresponding eigenvectors are simultaneously found. Moreover, it is possible to show [**Zhaohui et al. (2004)**] that d_n is a monotonically decreasing function of the frequency ω and its graph is composed of infinite branches separated by singular points, where the function is approaching $-\infty$ from the left and $+\infty$ from the right. Therefore, for each branch there is a unique root of d_n which can be easily found by applying standard root-searching algorithms (e.g. bisection [**Press (1992)**]).

The problem of properly locating each eigenvalue, i.e. giving suitable upper and lower bounds on any specific eigenvalue, can be solved by using the Wittrick-Williams mode count function ([**Wittrick and Williams (1971)**])

$$J\left(\bar{\omega}\right) = \sum_{k=1}^{n} J_k\left(\bar{\omega}\right) + s\left(\mathbf{K}_D\left(\bar{\omega}\right)\right),$$

giving the number J of natural frequencies lying below a trial frequency $\bar{\omega}$. The term J_k is the number of natural frequencies of the k-th substructure which would be exceeded by $\bar{\omega}$ if its ends were to be clamped (i.e. the nodal displacements set to zero). For Euler-Bernoulli beams a simple formula for J_k may be derived (see [**Williams and Wittrick (1970)**]):

$$J_k = j - \frac{1}{2}\left(1 - (-1)^j \,\mathrm{SIGN}\left(1 - \cosh\eta_k \cos\eta_k\right)\right),$$

where η_k is defined in (1.3), where the trial frequency $\bar{\omega}$ replaces ω, j is the largest integer $< \eta_k/\pi$ and $\mathrm{SIGN}(\cdot)$ gives the argument sign. The term $s\left(\mathbf{K}_D\left(\bar{\omega}\right)\right)$ is the so-called sign count of the symmetric matrix $\mathbf{K}_D$, which can be calculated as the number of negative elements along the diagonal of $\mathbf{D}$ appearing in (2.9). From (2.14) and (2.10) we notice that the elements of the diagonal matrix $\mathbf{D}$ equal the elements on the diagonal of the lower triangular matrix $\mathbf{F}$, which is found from the set of recursive relations.

With this procedure only the eigenvalues related to eigenvectors having zero displacement for the last node are missed [**Zhaohui et al. (2004)**]. Indeed, by assuming that $\bar{\mathbf{v}}$ is the eigenvector associated to $\bar{\omega}$ and that $d_n\left(\bar{\omega}\right) \neq 0$, from decomposition (2.9), one can straightforwardly see that

$$0 = \left(\mathbf{K}_D\bar{\mathbf{v}}\right)_n = d_n\left(\bar{\mathbf{v}}\right)_n;$$

therefore, the nodal displacement $\left(\bar{\mathbf{v}}\right)_n$ vanishes. In [**Zhaohui et al. (2004)**] it is shown how to determine these particular eigenvalues by re-numbering the nodes or, for modes characterized by zero displacement at each node, by introducing some additional node.

3. Galerkin methods

Approximate solutions for the natural frequencies and mode shapes of the considered stepped beam can be found starting from the weak formulation (3.12) in Chapter 2, by using standard Galerkin methods.

In this framework, one looks for approximate harmonic solution for the mechanical displacement of the form

$$w(x,t) = \left(\boldsymbol{\phi}^{\mathrm{T}}(x)\mathbf{W}\right)e^{i\omega t}, \tag{3.1}$$

where $\mathbf{W}$ and $\boldsymbol{\phi}(x)$ are N_G dimensional vectors, N_G being the number of basis functions for the Galerkin expansion of the mechanical displacement. The vector $\boldsymbol{\phi}(x)$ collects the N_G basis functions, satisfying the kinematical boundary conditions, and $\mathbf{W}$ is composed of the respective weighting coefficients.

Hence, from the harmonic version of the weak formulation in (3.1) and by choosing the test functions from the same space of the basis functions, one gets

$$-\omega^2 \mathbf{M}_G \mathbf{W} + \mathbf{K}_G \mathbf{W} = 0,$$

where

$$\begin{aligned} \mathbf{K}_{G\,ij} &= \sum_{h=1}^{N} k_h \int_{S_h} \left(\phi^{(i)}(x)\right)'' \left(\phi^{(j)}(x)\right)'' dx, \\ \mathbf{M}_{G\,ij} &= \sum_{h=1}^{N} \rho_h \int_{S_h} \phi^{(i)}(x)\phi^{(j)}(x) dx, \end{aligned}$$

and i, j vary in $\{1, ..., N_G\}$. In this case, the eigenvalue problem is linear in ω^2 and can be easily solved with standard techniques (see e.g. [**Press (1992)**]).

As the number N_G of basis functions increases, the solution becomes more accurate. Nevertheless, ad-hoc choices of basis functions may lead to fast convergence of the approximate solutions to the exact one. In the following work we compare three different methods for generating the basis functions. The first method is very common and relies on the mode shapes of the homogeneous beam, i.e. the beam without the piezoelectric elements (assumed modes). In the second method we propose to enrich the simple beam basis function with special jump functions, which allow to grasp the curvature discontinuities at the end of each segment. The third method is the standard Finite-Element method for Euler-Bernoulli Beams, and is based on Hermitian basis functions.

3.1. Assumed Modes method. Very often, approximate solutions are found by considering as basis functions the mode shapes of the continuous beam without the array of piezoelectric elements, i.e. as the solutions of:

$$\phi^{IV}(\xi) - \eta^4 \phi(\xi) = 0, \quad \eta = l\sqrt{\omega}\sqrt[4]{\frac{\rho_B}{k_B}}, \quad \xi = \frac{x}{l},$$

with given purely mechanical boundary conditions. The resulting approximate mode shapes are smooth functions which are not describing the curvature discontinuities at the interphase between elastic and piezocomposite segments.

For a cantilever beam the eigenvalues are the roots of the following trascendental equation:

$$1 + \cosh\eta \cos\eta = 0.$$

The numerical values for the eigenvalues $\eta^{(i)}$ and the corresponding mode shapes $\phi^{(i)}$ can be found in several handbooks (see e.g. [**Meirovitch (2000)**]). The ϕ's are normalized to satisfy

$$\sum_{h=1}^{N} \int_{S_h} \rho_h \left(\phi(x)\right)^2 dx = m. \tag{3.3}$$

3.2. Enhanced Assumed Modes method. A more refined approximate solution can be found by completing the homogeneous beam mode shapes with suitable discontinuity functions (see e.g. [**Krongauz and Belytschko (1998)**] and [**Batra et al. (2004)**]) aiming at introducing in the mode shapes the effects of material discontinuities. Here we propose to introduce N_E discontinuity functions $\left\{\chi^{(h)}\right\}_{h=1}^{N_E}$; each one of them is generated as the static deflection of the homogeneous beam when a concentrated moment is applied in correspondence of the h-th interface between elastic and piezocomposite segments in the stepped beam.

For a left cantilevered beam, with the first and the last elastic segments $N_E = 2N_P$, the solution of the simple static problem of a concentrated moment applied at X_{h+1} is

$$\chi^{(h)} = \begin{cases} \alpha_h \dfrac{x^2}{2l}, & x \in [0, X_{h+1}] \\ \alpha_h \dfrac{X_{h+1}}{2l} \left(2x - X_{h+1}\right), & x \in [X_{h+1}, l] \end{cases} . \tag{3.4}$$

The constant α_h can be chosen in order to normalize the special jump functions as in (3.3). The introduced function $\chi^{(h)}$ (3.4) is continuous with its first derivative, satisfy the boundary conditions and its second derivative jumps at X_{h+1} from α_h to 0.

3.3. Finite-Element method. In the Finite-Element work each beam segment is divided into a number of disjoint elements. The trial solution in the generic element is constructed from the values of the deflection and rotation at the element nodes (nodal displacements) by using classical Hermite polynomials. Therefore $\mathbf{W}$ is comprised of the amplitudes of the nodal displacements at all the beam nodes and the mass and stiffness matrices of the e-th element are (see e.g. [**Juang and Phan (2001)**]):

$$\mathbf{M}_e = \rho_e \begin{bmatrix} \frac{13}{35} l_e & \frac{11}{210} l_e^2 & \frac{9}{70} l_e & -\frac{13}{420} l_e^2 \\ \frac{11}{210} l_e^2 & \frac{1}{105} l_e^3 & \frac{13}{420} l_e^2 & -\frac{1}{140} l_e^3 \\ \frac{9}{70} l_e & \frac{13}{420} l_e^2 & \frac{13}{35} l_e & -\frac{11}{210} l_e^2 \\ -\frac{13}{420} l_e^2 & -\frac{1}{140} l_e^3 & -\frac{11}{210} l_e^2 & \frac{1}{105} l_e^3 \end{bmatrix} \tag{3.5a}$$

$$\mathbf{K}_e = k_e \begin{bmatrix} \frac{12}{l_e^3} & \frac{6}{l_e^2} & -\frac{12}{l_e^3} & -\frac{13}{420} l_e^2 \\ \frac{6}{l_e^2} & \frac{1}{105} l_e^3 & -\frac{6}{l_e^2} & \frac{2}{l_e} \\ -\frac{12}{l_e^3} & -\frac{6}{l_e^2} & \frac{12}{l_e^3} & -\frac{6}{l_e^2} \\ -\frac{13}{420} l_e^2 & \frac{2}{l_e} & -\frac{6}{l_e^2} & \frac{4}{l_e} \end{bmatrix} , \tag{3.5b}$$

where l_e is the element size, and the values of the mass density ρ_e and stiffness k_e are those of the segment including the e-th element. The global stiffness, mass and coupling matrices are computed by assembling the element matrices and by imposing the kinematical constraints.

4. Experimental setup

A cantilever aluminum beam (Al6061-T6) hosting two surface bonded bimorph pairs of piezoelectric transducers (Piezo-System T110-H4E-602) has been realized[2], so as to form a stepped piezoelectric beam composed of 5 regular segments, three elastic and two piezoelectric (see Figure 1 and 2).

[2]All the experimental tests have been performed in the Laboratory of "Meccanica delle Vibrazioni" of the University of Rome "La Sapienza" directed by Prof. Sestieri.

TABLE 1. Dimensions of the stepped piezoelectric beam.

Dimensions (mm)				
$l_1 = 5.0$	$l_2 = 35.65$	$l_3 = 6.0$	$l_4 = 36.5$	$l_5 = 117.0$
$l = 201.0$	$a_P = 17.6$	$a_B = 20$	$\delta = 0.267$	$h = 2.85$

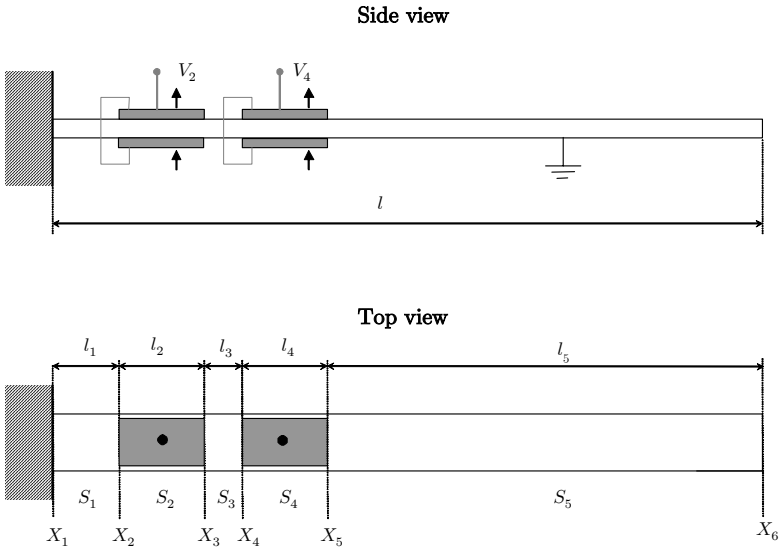

FIGURE 1. Sketch of the stepped beam under experimental investigations.

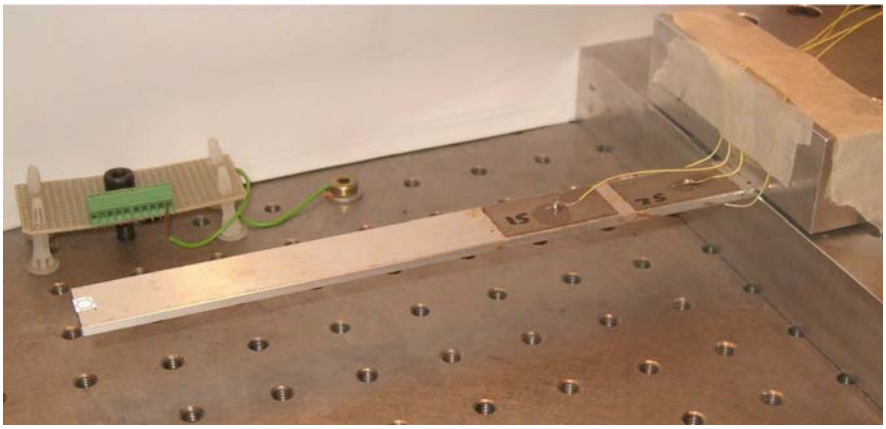

FIGURE 2. Picture of the stepped prototype.

Its frequency response has been measured and its relevant modal properties have been identified. The corresponding geometric and material properties are reported in Tables 1 and 2. In particular $\rho^V_{B,P}$ represent the volumetric mass densities and the linear mass densities are easily computed from the volumetric ones with

$$\rho_B = \rho^V_B a_B h, \quad \rho_P = \rho_B + 2\delta a_P \rho^V_P$$

where ρ_P is denoting the common linear mass density in the piezocomposite segments and the factor of 2 is due to the presence of 2 active laminae. The piezoelectric patches have been adhesively bonded on the beam by a thin-layer of non-conductive epoxy resin and each bimorph pair has been electric interconnected as shown in Figure 1 of Chapter

TABLE 2. Material data for aluminum and piezoelectric ceramics.

Aluminum (Al6061-T6)		Piezoelectric ceramics (PZT-5H-S4-ENH)	
ρ_B^V	$2700\ \mathrm{kg/m^3}$	ρ_P^V	$7800\ \mathrm{kg/m^3}$
E	$69 \times 10^9\ \mathrm{N/m^2}$	$\left(s_{11}^E\right)^{-1}$	$62 \times 10^9\ \mathrm{N/m^2}$
		d_{31}	$-320 \times 10^{-12}\ \mathrm{m/V}$
		ϵ_{33}^T	$3800\varepsilon_0$

2, in the so-called bender configuration. The single piezoelectric transducer is made of a layer of thickness-polarized piezoelectric ceramic (PZT-5H) having the upper and lower surfaces electroded by a nickel film. The electric contact between the lower electrode of each transducer and the grounded beam has been achieved by applying a small spot of electrically conductive adhesive at the central region of the piezoelectric transducer, where interfacial stresses are low (see [**Crawley and de Luis (1987)**]).

The beam frequency response has been determined by exciting the structure with a frequency sweep signal at one of the two piezoelectric pairs and measuring the beam tip velocity by a laser velocimeter (Polytec OFV 350) (see Figure 3 for the experimental setup).

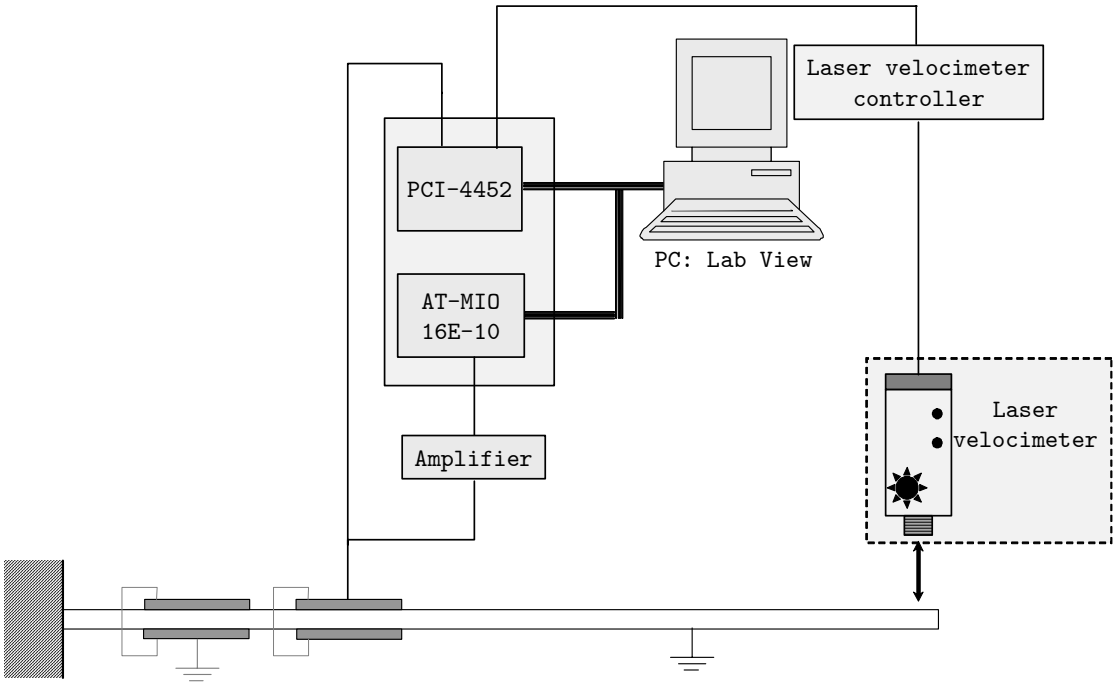

FIGURE 3. Experimental Setup.

The input signal has been generated digitally in Labview, converted by the D/A converter National Instruments AT-MIO-16E-10, and amplified by ad-hoc designed voltage amplifier. The analog output of the laser and the voltage applied at the exciting transducer have been measured by the A/D converter National Instruments PCI-4452 and a personal computer was used for digital signal processing. The entire experimental set up was designed in order to do not alter the stepped beam modal properties. Noninvasive measurements have been performed by exciting the beam with one of the surface-bonded

TABLE 3. First four natural frequencies of the stepped beam with short-circuited piezoelectric transducers. Comparisons between experimental values and numerical values obtained with the different methods. The percentage errors with respect to the values found with the LEN method are reported.

	$f^{(1)}$ (Hz)	$f^{(2)}$ (Hz)	$f^{(3)}$ (Hz)	$f^{(4)}$ (Hz)
Experimental	66.25 (−1.56%)	360.2 (−1.54%)	990 (−1.79%)	1943 (−1.37%)
LEN	65.3662	360.596	991.088	1941.85
AM	65.7985 (+0.66%)	362.174 (+0.44%)	995.802 (+0.48%)	1952.54 (+0.55%)
EAM	65.3666 ($+5.04E^{-4}$%)	360.604 ($+2.13E^{-3}$%)	991.148 ($+6.01E^{-3}$%)	1941.99 ($+7.18E^{-3}$%)
FE	65.3664 ($+2.05E^{-4}$%)	360.611 ($+4.15E^{-3}$%)	991.325 (+0.0238%)	1943.88 (+0.104%)
Uniform beam	57.61 (−11.9%)	361.02 (−0.117%)	1010.86 (+1.99%)	1980.88 (+2.01%)

transducers (included in the model, being part of the stepped beam itself), and by measuring the tip velocity with the laser-vibrometer (which does not introduce any additional mass to the structure).

In the first line of Table 3 the measured natural frequencies of the first four structural modes $f^{(1)}, f^{(2)}, f^{(3)}$ and $f^{(4)}$ are reported.

5. Numerical comparisons

The constitutive properties of the considered stepped beam resulting from formulas (2) are:

$$k_1 = k_3 = k_5 = k_B = 2.66215\,\mathrm{N\,m^2}, \tag{5.1a}$$

$$g_2 = g_4 = g = 1.006 \times 10^{-3}\,\mathrm{N\,m\,V^{-1}}, \tag{5.1b}$$

$$k_2 = k_4 = k_P = 3.85884\,\mathrm{N\,m^2}, \tag{5.1c}$$

while the linear mass densities are:

$$\rho_1 = \rho_3 = \rho_5 = \rho_B = 0.1539\,\mathrm{kg\,m^{-1}},$$
$$\rho_2 = \rho_4 = \rho_P = 0.228041\,\mathrm{kg\,m^{-1}}.$$

The numerically computed first four natural frequencies for short-circuited piezoelectric elements are listed in Table 3 and the results obtained with the proposed numerical methods are compared. The values computed with the LEN method are chosen as a reference for the approximate methods and the errors are tabulated in brackets. Indeed, the LEN methods is based on the exact formulation of the trascendental eigenvalue problem for the infinite dimensional stepped piezoelectric beam and errors are limited to those implied by the numerical accuracy used for computing the roots of the last energy norm and can be easily controlled. On the other hand, the results obtained by the other methods, in addition to the numerical errors implied by the numerical computation of the solution of the associated (linear) eigenvalue problems, are affected by the errors due to the approximation of the infinite dimensional system with a finite dimensional one. In particular, the numerical results computed through the assumed modes method relies on the first

TABLE 4. Comparison between the four numerical methods for modal analysis

	LEN	AM	EAM	FE
Accuracy on frequencies	—	Good	High	High
Accuracy on mode shapes	—	Poor	High	Acceptable
Basis functions	—	Mode shapes of the homogeneous beam	Mode shapes oft he homogeneous beam and special jump functions	Hermite polynomials
Stiffness matrix	Trascendental function of the frequency, symmetric, banded	Symmetric, not-banded	Symmetric, not-banded	Symmetric, banded
Assembly of matrices	Easy	Not needed	Not needed	Easy
Accuracy on modal curvatures	—	Very poor	High	Poor, without post-processing

eight mode shapes of the homogeneous cantilever beam (8 d.o.f.); in the enhanced assumed modes method four special jump functions of the type (3.4) are used to enrich the assumed modes basis functions (12 d.o.f.); in the finite-element formulation each beam segment is divided into elements of the same length and the first segment is discretized with one element, the second with three, the third with one, the fourth with three, and the fifth with five (13 nodes and 26 d.o.f.).

In Figure 4, the first four mode shapes and modal curvatures are plotted by using all of the four proposed numerical methods. In the Finite-Element work, only the average element curvatures, calculated as the mean value of the nodal rotations, are reported.

Table 4 summarizes the characteristic features of the presented numerical methods, based on the analyses of the achieved results and on the efforts required to get the numerical solutions. Although the assumed modes method is the most popular, it exhibits several drawbacks. Indeed, due to the excessive smoothness of the assumed basis functions, it is not capable to capture the curvature jumps at the material discontinuities and does not lead to very accurate estimations of the beam natural frequencies. On the other hand, the special jump functions introduced in its enhanced version allow to simultaneously increase the frequencies accuracies and account for the effects of the beam segmentation. The finite-element method provides accurate estimates of the lowest natural frequencies. However, the mode shapes are not accurately computed, due to the lack of continuity of the curvatures at the element junctions. It is remarkable that, while the errors implied by the finite-element estimations is rapidly increasing with the mode number, the enhanced assumed modes method provide good estimates for even higher natural frequencies.

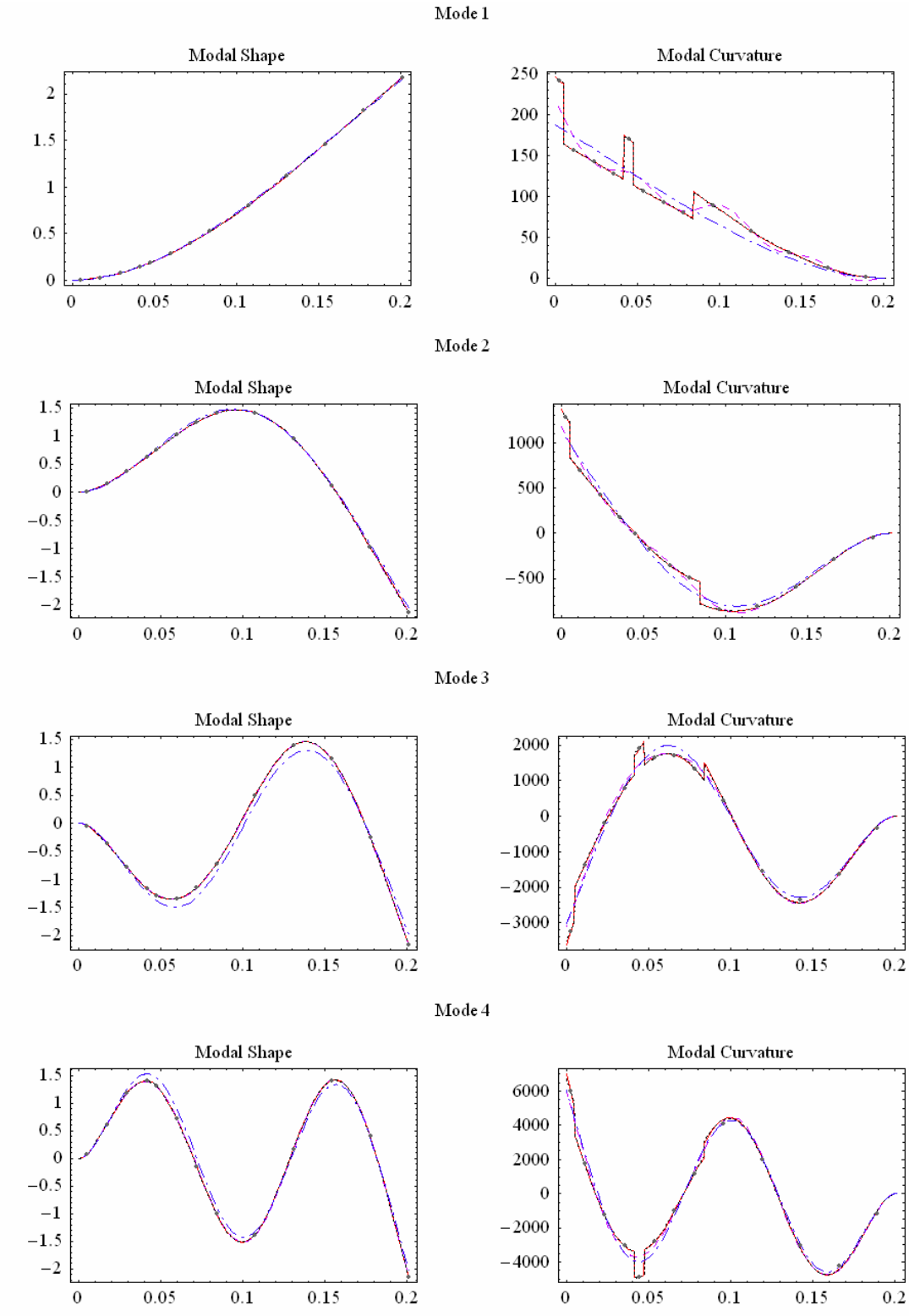

FIGURE 4. Mode shapes of the stepped beam computed by the use of the presented algorithm (dashed blu: homogeneous beam; dashed orange: LEN; dotted grey: FE; dashed black: EAM; dashed purple: AM). The abscissa is in meters.

CHAPTER 4

Homogenized model of periodic stepped piezoelectric beams

When studying stepped piezoelectric beams with a considerable number of periodically distributed piezoelectric transducers, it is advisable to adopt homogenized models. In this way differential equations with rapidly oscillating coefficients (density, stiffness and coupling) are transformed into simpler ones (homogenized) characterized by effective coefficients which are calculated from the solution of the so-called unit cell problem. In the present chapter, we present the homogenization of a beam clamped on both ends excited by constant voltages applied at the periodically distributed piezoelectric elements. The used technique is the classical two-scale convergence (see e.g. [**Allaire (1992)**]). The main advantage of this technique lies in its self-containedness, since it enables to simultaneously obtain the homogenized equations and prove the convergence. Similar results may be obtained by the application of the method of asymptotic formal expansion (see e.g. [**Sanchez-Palencia (1980)**]), but a subsequent proof is required. The presented model is validated through some numerical tests and also different boundary conditions are treated.

The study of more complicated problems involving geometric nonlinearities [**Hoffman and Botkin (1998)**], transient problems [**Hoffman and Botkin (2000)**], reinforcements [**Kalamkarov and Georgiades (2002)**] and electric circuits [**Canon and Lenczner (1999)**], [**Kader (2001)**], [**Lenczner and Mercier (2004)**] may be worked out similarly. The notation is slightly different from the previous Chapters, since spatial derivatives are performed with respect of two distinct space variables (two scales) and it is convenient to account for the structure periodicity.

1. Problem setting

1.1. Geometry. In this instance, we assume that the N_P equal piezoelectric transducers are periodically bonded on the beam of length l (as shown in Figure 1). The resulting stepped piezoelectric beam is a periodic structure. Purely elastic segments alternate with piezocomposite segments. The length of each piezocomposite segment is denoted by l_P, the length of each elastic segment is called d. Therefore the period of the structure, say ε, is equal to $l_P + d$. The region of the stepped beam domain $S = [0, l]$ occupied by the i-th piezoelectric element is denoted by S_{P_i}, the overall piezoelectric domain by $S_P = \bigcup_{i=1}^{N_P} S_{P_i}$ and the overall elastic domain by $S_B = S \backslash S_P$. It is also convenient to introduce the unit cell $Y = [0, 1]$ and its subset $Y_P = \left[\frac{d}{2\varepsilon}, 1 - \frac{d}{2\varepsilon}\right]$, representing the piezoelectric covering on the unit cell.

1.2. Governing equations. The stepped beam is modelled as an Euler-Bernoulli beam and, for plane motions, its kinematical state is simply described by the beam axis deflection field w^ε, where the superscript ε emphasizes the dependence of the solution on

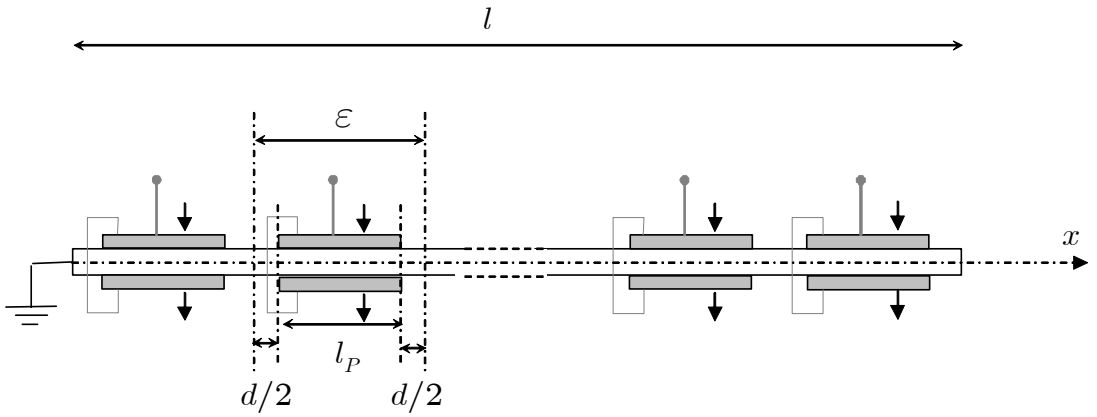

FIGURE 1. Sketch of the periodic stepped piezoelectric beam.

the period of the structure. The governing equation reads

$$D^2\left(k\,D^2\left(w^\varepsilon\right)\right) = g\sum_{i=1}^{N_P} V_i D^2\left(\mathfrak{C}_i\right) + b, \tag{1.1}$$

where $\mathfrak{C}_i$ is the characteristic function of S_{P_i}, k is the bending stiffness, g the piezoelectric coupling coefficient, D is the weak space-derivative and b the external applied load. The stiffness is varying along the beam abscissa x according to

$$k\left(x\right) = \left\{\begin{array}{ll} k_P, & x \in S_P \\ k_B, & x \in S_B \end{array}\right. .$$

The continuity of the deflection, the slope, the bending moment and the shear are ensured by the following additional interface conditions, which are equivalent to (3.9) in Chapter 2:

$$\left[\!\left[w^\varepsilon\right]\!\right] = 0, \quad \left[\!\left[D\left(w^\varepsilon\right)\right]\!\right] = 0, \quad \left[\!\left[kD^2\left(w^\varepsilon\right) - g\sum_{i=1}^{N_P} V_i\mathfrak{C}_i\right]\!\right] = 0, \quad \left[\!\left[D\left(kD^2\left(w^\varepsilon\right)\right)\right]\!\right] = 0, \tag{1.2}$$

where $[\![(\cdot)]\!]$ indicates the jump of $(\cdot)$ at the generic discontinuity (interphase between different segments) in the stepped beam. For the sake of simplicity we consider clamping boundary conditions:

$$w^\varepsilon|_{x=0} = 0, \quad D\left(w^\varepsilon\right)|_{x=0} = 0, \quad w^\varepsilon|_{x=l} = 0, \quad D\left(w^\varepsilon\right)|_{x=l} = 0. \tag{1.3}$$

We assume that the applied control voltages are chosen in order to sample and hold the average of a voltage distribution, $v \in L^2\left(S\right)$, prescribed over the whole beam, i.e.

$$V_i = \langle v\rangle_{S_{P_i}} = \frac{1}{l_P}\int_{S_{P_i}} v\left(x\right)dx, \tag{1.4}$$

where the brackets$\langle\cdot\rangle$ indicate mean values. Furthermore we assume that also the distributed load b is in $L^2\left(S\right)$. Next, we define the voltage distribution v^ε being equal to v on the elastic segment and to the averaged constant voltages on the piezocomposite segments. We emphasize that as ε goes to zero v^ε converges to v in $L^2\left(S\right)$.

The periodicity of the stepped beam constitutive behavior, may be accounted for by introducing the Y-periodic function $k_\#$ defined by:

$$k_\#\left(y\right) = k_P\mathfrak{C}\left(y\right) + k_B\left(1 - \mathfrak{C}\left(y\right)\right),$$

where $\mathfrak{C}$ is the characteristic function of Y_P on Y. Therefore (1.1) becomes

$$D^2\left(k_{\#}\left(\frac{x}{\varepsilon}\right)\, D^2 w^{\varepsilon}\right) = gD^2\left(v^{\varepsilon}\mathfrak{C}\left(\frac{x}{\varepsilon}\right)\right) + b. \tag{1.5}$$

2. Two-scale convergence

2.1. Weak Formulation. A weak formulation for the considered problem may be found by multiplying equation (1.5) by a smooth test function $\tilde{w}$ (satisfying the boundary conditions (1.3)), integrating twice in space, accounting for the boundary conditions (1.3), and the continuity conditions (1.2). Therefore, we obtain the integral equation:

$$\int_S \left[k_{\#}\left(\frac{x}{\varepsilon}\right) D^2\left(w^{\varepsilon}\right)\, D^2\tilde{w} - gv^{\varepsilon}\mathfrak{C}\left(\frac{x}{\varepsilon}\right) D^2\tilde{w} - b\tilde{w}\right] dx = 0, \tag{2.1}$$

which should hold for every admissible test function.

The previous statement may be made rigorous by the following definition:

DEFINITION 1. *A function $w^{\varepsilon} \in H_0^2(S)$ is a weak solution of the system (1.1), (1.3) and (1.2) if (2.1) holds for all $\tilde{w} \in H_0^2(S)$.*

2.2. A-priori estimates. The lemma below provides an important a-priori estimate on the solution which enables us to apply the fundamental results in [**Allaire (1992)**].

LEMMA 1. *For every ε there exists a unique weak solution w^{ε}. Furthermore, it is possible to find a constant C independent of ε such that:*

$$\left\|w^{\varepsilon}\right\|_{H^2(S)} < C. \tag{2.2}$$

PROOF. **Uniqueness:** the weak formulation in (2.1) may be written in the form

$$A\left(w^{\varepsilon}, \tilde{w}\right) = L\left(\tilde{w}\right), \quad w^{\varepsilon}, \tilde{w} \in H_0^2(S)$$

where

$$A\left(w^{\varepsilon}, \tilde{w}\right) = \int_S k_{\#}\left(\frac{x}{\varepsilon}\right) D^2\left(w^{\varepsilon}\right)\, D^2\tilde{w}\, dx, \quad L\left(\tilde{w}\right) = \int_S gv^{\varepsilon}\mathfrak{C}\left(\frac{x}{\varepsilon}\right) D^2\tilde{w} + b\tilde{w}\, dx.$$

It can be shown that A is bilinear, continuous and coercive in $H_0^2(S)$, and that L is a linear continuous functional on $H_0^2(S)$ (i.e. $L \in H^{-2}(S)$). Therefore, by the application of the well-known Lax-Milgram theorem (see e.g. [**Lebedev and Vorovich (2002)**] and [**Sanchez-Hubert and Sanchez-Palencia (1989)**]), we are guaranteed that there exists a unique solution of the considered problem and that

$$\left\|w^{\varepsilon}\right\|_{H^2(S)} \leq \frac{1}{\alpha}\left\|L\right\|_{H^{-2}(S)}, \tag{2.3}$$

where α is the coercivity constant. The bilinearity of A and the linearity of L are trivial. A is continuous since

$$\begin{aligned}\left|A\left(w^{\varepsilon}, \tilde{w}\right)\right| = \left|\int_S k_{\#}\left(\frac{x}{\varepsilon}\right) D^2\left(w^{\varepsilon}\right)\, D^2\tilde{w}\, dx\right| &\leq k_P\left\|D^2\left(w^{\varepsilon}\right)\right\|_{L^2(S)}\left\|D^2\tilde{w}\right\|_{L^2(S)} \\ &\leq k_P\left\|w^{\varepsilon}\right\|_{H^2(S)}\left\|\tilde{w}\right\|_{H^2(S)}.\end{aligned}$$

The first inequality stems from the stiffness definition and from the Cauchy-Schwartz inequality, and the second one from Sobolev spaces norm definition. A is coercive since

$$\left|A\left(w^{\varepsilon}, w^{\varepsilon}\right)\right| = \left|\int_S k_{\#}\left(\frac{x}{\varepsilon}\right)\left(D^2\left(w^{\varepsilon}\right)\right)^2\, dx\right| \geq k_B\left\|D^2\left(w^{\varepsilon}\right)\right\|_{L^2(S)}^2 \geq \alpha\left\|w^{\varepsilon}\right\|_{H^2(S)}.$$

The first inequality stems from the stiffness definition and the L^2 norm definition, and the second one from Poincaré-Friedrichs inequality. The linear functional L is continuous since it is bounded, indeed:

$$|L(\tilde{w})| = \left| \int_S g v^\varepsilon \mathfrak{C}\left(\frac{x}{\varepsilon}\right) D^2\tilde{w} + b\tilde{w}\, dx \right| \leq \left| \int_S g v^\varepsilon \mathfrak{C}\left(\frac{x}{\varepsilon}\right) D^2\tilde{w}\, dx \right| + \left| \int_S b\tilde{w}\, dx \right|$$
$$\leq |g| \left\|v^\varepsilon\right\|_{L^2(S)} \left\|D^2(\tilde{w})\right\|^2_{L^2(S)} + \|b\|_{L^2(S)} \|\tilde{w}\|_{L^2(S)} \leq \left(|g| \left\|v^\varepsilon\right\|_{L^2(S)} + \|b\|_{L^2(S)}\right) \|\tilde{w}\|_{H^2(S)}.$$

The first inequality is derived from the triangle inequality, the second one from the application of the Cauchy-Schwartz inequality and the last one from Sobolev spaces norm definition.

Inequality (2.2): The coercivity constant in (2.3) is clearly independent of ε. The norm of L is bounded by $\left(|g| \left\|v^\varepsilon\right\|_{L^2(S)} + \|b\|_{L^2(S)}\right)$, therefore we only need to prove that $\left\|v^\varepsilon\right\|_{L^2(S)}$ is independent of ε. To this aim

$$\left\|v^\varepsilon\right\|^2_{L^2(S)} = \int_{S/S_P} v^2 dx + \sum_{i=1}^{N_P} \left(\int_{S_{P_i}} v dx \right)^2 \leq \|v\|^2_{L^2(S/S_P)} + \sum_{i=1}^{N_P} \|v\|^2_{L^1\left(S_{P_i}\right)} \leq \|v\|^2_{L^2(S)}.$$

The applied inequalities follow directly from standard integration theory. □

REMARK 2. *Since $H^2_0(S)$ is a separable Hilbert Space, the boundedness of the sequence w^ε pointed out in the previous lemma, assures that the sequence w^ε contains a weak convergent subsequence in $H^2_0(S)$ (see e.g.* [**Lebedev and Vorovich (2002)**]*). Now we derive the equation that defines the limit function w (homogenized equation) and show that it admits a unique solution and that its coefficients are independent of the chosen subsequence.*

2.3. Two-scale homogenized system. Following the comments in the previous remark, we define two-scale convergence by (see [**Allaire (1992)**]):

DEFINITION 2. *Let $\zeta^\varepsilon \in L^2(S)$, $\zeta \in L^2(S \times Y)$. It is said that $\zeta^\varepsilon \overset{2-scale}{\rightarrow} \zeta$ if*

$$\lim_{\varepsilon \to 0} \int_S \zeta^\varepsilon(x)\, \psi\left(x, \frac{x}{\varepsilon}\right) dx = \int_S \int_Y \zeta(x,y)\, \psi(x,y)\, dy dx,$$

for every $\psi \in C^\infty_0\left(S; C^\infty_\#(Y)\right)$, $C^\infty_\#(Y)$ being the space of Y periodic functions of $C^\infty(-\infty,\infty)$, and $C^\infty_0(S)$ being the set of infinitely differentiable functions on S vanishing at 0 and l with all their derivatives.

The main result of the homogenization theory that we use (see [**Allaire (1992)**]) is based on the hypothesis that $\|w^\varepsilon\|_{H^2(S)} < C$ and yields the existence of ε_j, $w \in H^2_0(S)$ and $\bar{w} \in L^2\left(S; H^2_\#(Y)\right)$, $H^2_\#(Y)$ being the completion of $C^\infty_\#(Y)$ for the norm of $H^2(Y)$, such that

$$\begin{aligned} & w^{\varepsilon_j} \overset{weak}{\rightarrow} w, \quad \text{in } H^2_0(S); \\ & w^{\varepsilon_j} \overset{2-scale}{\rightarrow} w, \quad D\left(w^{\varepsilon_j}\right) \overset{2-scale}{\rightarrow} Dw, \quad D^2\left(w^{\varepsilon_j}\right) \overset{2-scale}{\rightarrow} D^2 w + D^2_y \bar{w}. \end{aligned} \tag{2.4}$$

In order to get the homogenized equations we set

$$\tilde{w}(x) = \eta(x) + \varepsilon^2 \xi\left(x, \frac{x}{\varepsilon}\right), \quad \eta \in C^\infty_0(S), \quad \xi \in C^\infty_0\left(S; C^\infty_\#(Y)\right)$$

in the weak formulation (2.1). We remark that, as suggested by [**Veiga (1995)**], only even powers in ε are sufficient for achieving at once the homogenized and the unit-cell

problem. Therefore, we get:

$$\int_S \left[k_\# \left(\frac{x}{\varepsilon}\right) D^2\left(w^\varepsilon\right) - g v^\varepsilon \mathfrak{C}\left(\frac{x}{\varepsilon}\right) - b\right] \left[D^2\eta\left(x\right) + D_y^2\xi\left(x, \frac{x}{\varepsilon}\right) + \varepsilon\, D_y D\xi\left(x, \frac{x}{\varepsilon}\right) + \varepsilon^2 D^2\xi\left(x, \frac{x}{\varepsilon}\right)\right] dx = 0. \tag{2.5}$$

By considering

$$\psi_1\left(x, \frac{x}{\varepsilon}\right) := k_\#\left(\frac{x}{\varepsilon}\right)\left[D^2\eta\left(x\right) + D_y^2\xi\left(x, \frac{x}{\varepsilon}\right) + \varepsilon\, D_y D\xi\left(x, \frac{x}{\varepsilon}\right) + \varepsilon^2 D^2\xi\left(x, \frac{x}{\varepsilon}\right)\right],$$

and

$$\psi_2\left(x, \frac{x}{\varepsilon}\right) := -g\mathfrak{C}\left(\frac{x}{\varepsilon}\right)\left[D^2\eta\left(x\right) + D_y^2\xi\left(x, \frac{x}{\varepsilon}\right) + \varepsilon\, D_y D\xi\left(x, \frac{x}{\varepsilon}\right) + \varepsilon^2 D^2\xi\left(x, \frac{x}{\varepsilon}\right)\right]$$

as test functions[1], we may pass (2.5) to the two-scale limit. We note that as ε goes to zero the terms multiplied by ε or ε^2 goes uniformly to zero, since for every $\xi \in C_0^\infty\left(S; C_\#^\infty\left(Y\right)\right)$ the following obvious bounds hold:

$$\min_{\substack{x\in S\\ y\in Y}} \xi\left(x, y\right) \leq \xi\left(x, y\right) \leq \max_{\substack{x\in S\\ y\in Y}} \xi\left(x, y\right).$$

Moreover we remind that v^ε converges to v in $L^2\left(S\right)$. Therefore, we obtain the following

$$\int_S \int_Y \left[k_\#\left(y\right)\left(D^2 w + D_y^2 \bar{w}\right)\right]\left[D^2\eta\left(x\right) + D_y^2\xi\left(x, y\right)\right] dydx = \int_S \int_Y g v \mathfrak{C}\left(y\right)\left[D^2\eta\left(x\right) + D_y^2\xi\left(x, y\right)\right] dydx + \int_S b\eta\left(x\right) dx, \tag{2.6}$$

which corresponds to two distinct equations:

$$\int_S \int_Y \left[k_\#\left(y\right)\left(D^2 w + D_y^2 \bar{w}\right) - g v \mathfrak{C}\left(y\right)\right] D^2\eta\left(x\right) dydx = \int_S b\eta\left(x\right) dx, \tag{2.7}$$

and

$$\int_S \int_Y \left[k_\#\left(y\right)\left(D^2 w + D_y^2 \bar{w}\right) - g v \mathfrak{C}\left(y\right)\right] D_y^2\xi\left(x, y\right) dydx = 0. \tag{2.8}$$

An easy integration by parts show that the above relation is a variational formulation associated to the following two-scale homogenized system:

$$\begin{cases} D_y^2\left(k_\#\left(y\right)\left(D^2 w + D_y^2 \bar{w}\right)\right) = D_y^2\left(g v \mathfrak{C}\left(y\right)\right), \quad \text{in } S \times Y \\ D^2\left(\int_Y \left(k_\#\left(y\right)\left(D^2 w + D_y^2 \bar{w}\right)\right) dy\right) = D^2\left(\int_Y g v \mathfrak{C}\left(y\right) dy\right) + b, \quad \text{in } S \\ w|_{x=0} = 0, \quad Dw|_{x=0} = 0, \quad w|_{x=l} = 0, \quad Dw|_{x=l} = 0, \\ y \to \bar{w}\left(x, y\right) \quad Y\text{-periodic.} \end{cases} \tag{2.9}$$

Endowing the Hilbert space $H_\#^2\left(S\right) \times L^2\left(S; H_\#^2\left(Y\right)\right)$ with the norm $\|D^2 w\|_{L^2(S)} + \left\|D_y^2 \bar{w}\right\|_{L^2(S\times Y)}$ we easily check the conditions of Lax-Milgram theorem on (2.6) and we therefore establish the uniqueness of the solution.

[1]The resulting test functions are not smooth, but we still can pass to the two-scale limit, since (see [**Allaire (1992)**]) they two-scale converge strongly to their limits.

2.4. Homogenized equation and cell problem. In order to give a better understanding of the limit problem, it is advisable to manipulate (2.9) in order to decouple the two equations into a homogenized equation on S and cell problem on Y. To this aim we express the auxiliary deflection field $\bar{w}$ as the linear combination

$$\bar{w}(x,y) = N_1(y) D^2 w(x) + N_2(y) g v(x) \tag{2.10}$$

of the voltage field and the curvature of the limit deflection. By substituting (2.10) into (2.8) and by taking test functions of the form $\xi = \xi_1(x)\xi_2(y)$ we obtain the following cell problems:

$$\begin{cases} \int_Y k_\#(y)\left(1 + D_y^2 N_1(y)\right) D_y^2 \xi_2(y)\, dy = 0 \\ \int_Y \left(k_\#(y) D_y^2 N_2(y) - \mathfrak{C}(y)\right) D_y^2 \xi_2(y)\, dy = 0 \end{cases}, \quad \xi_2 \in H^2_\#(Y). \tag{2.11}$$

By following [**Botkin (1999)**], it is possible to show that (2.11) is equivalent to

$$\begin{cases} k_\#(y)\left(1 + D_y^2 N_1(y)\right) = \left\langle \dfrac{1}{k_\#} \right\rangle_Y^{-1} \\ k_\#(y) D_y^2 N_2(y) - \mathfrak{C}(y) = -\left\langle \dfrac{1}{k_\#} \right\rangle_Y^{-1} \left\langle \dfrac{\mathfrak{C}}{k_\#} \right\rangle_Y \end{cases}, \quad \text{for a.e. } y \in Y. \tag{2.12}$$

The computation of the above mean values gives:

$$\left\langle \frac{1}{k_\#} \right\rangle_Y = \frac{1}{k_P}\left(c_f + \frac{k_P}{k_B}(1 - c_f)\right), \quad \left\langle \frac{\mathfrak{C}}{k_\#} \right\rangle_Y = \frac{1}{k_P} c_f \tag{2.13}$$

where the coverage factor $c_f = \dfrac{l_P}{\varepsilon}$ is introduced.

By substituting equations (2.12) into the second equation of (2.9) we obtain the homogenized equation:

$$\left\langle \frac{1}{k_\#} \right\rangle_Y^{-1} D^4 w = g \left\langle \frac{1}{k_\#} \right\rangle_Y^{-1} \left\langle \frac{\mathfrak{C}}{k_\#} \right\rangle_Y D^2 v + b,$$

or, by using the formulas in (2.13)

$$k_{\text{hom}} D^4 w = g_{\text{hom}} D^2 v + b, \tag{2.14}$$

where the homogenized bending stiffness k_{hom} and coupling coefficient g_{hom} are given by

$$k_{\text{hom}} = \frac{k_P}{c_f + \frac{k_P}{k_B}(1 - c_f)}, \quad g_{\text{hom}} = g\frac{c_f}{c_f + \frac{k_P}{k_B}(1 - c_f)}. \tag{2.15}$$

When the beam is fully covered by piezoelectric elements ($c_f = 1$), the homogenized constitutive coefficients become:

$$k_{\text{hom}} = k_P, \quad g_{\text{hom}} = g.$$

3. Numerical tests

When discarding the distributed load, the exact solution of the considered sample static problem in each beam segment is a third order polynomial. Therefore, by considering each segment to be an element of a FE mesh and using standard Hermitian basis functions as element trial function the exact solution is achieved. The global stiffness matrix is obtained by assembling alternating matrices of the type (3.5) of Chapter 3. The load

vector is obtained by assembling the element load vectors (assuming to excite the beam only with the piezoelectric elements):

$$\mathbf{F} = \left[\begin{array}{cccc} 0 & -g & 0 & g \end{array} \right]^{\mathrm{T}}$$

after multiplication with the element imposed voltage (V_i for piezocomposite segments and 0 for elastic ones).

We refer again to the aluminum beam and piezoceramic transducers described in Table 2 of Chapter 3. As an application sample, we consider a parabolic applied voltage in (2.14) of the following form:

$$v\left(x\right) = V_{\max} \frac{4x\left(l-x\right)}{l^2},$$

with $V_{\max} = 100\,\mathrm{V}$. The solution of the homogenized equation is

$$w\left(x\right) = V_{\max} \frac{g_{\mathrm{hom}} x^2 \left(l-x\right)^2}{3k_{\mathrm{hom}} l^2}.$$

On the other hand, in the refined model the applied voltages are given by (1.4), and the solution is derived by following the aforementioned finite-element type analysis. We consider two different distributions of piezoelectric transducers on the considered host beam; namely: we assume the covering factor to be 40% and we consider 5 and 15 transducers. In Figures 2 and 3 we report the deflection (in meters) of the homogenized model (solid line) and that of the refined model sampled at the boundary nodes of each beam segment (dots).

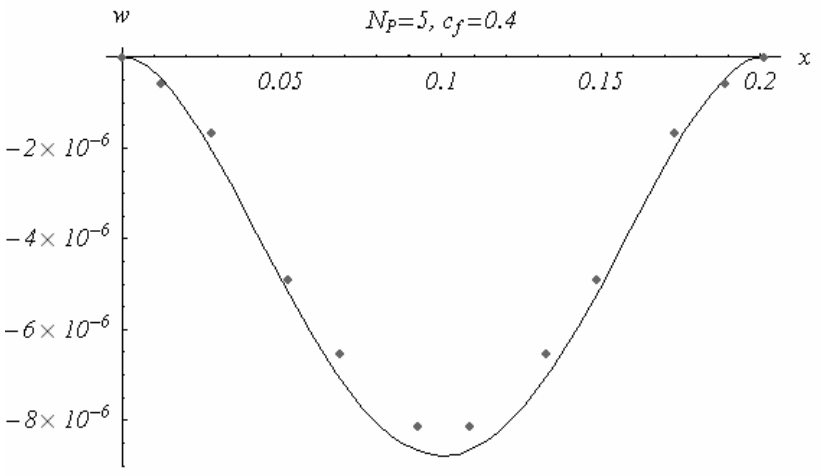

FIGURE 2. Comparison between the refined (dots) and homogenized predictions (solid lines) with 5 piezoelectric transducers (beam clamped at both ends).

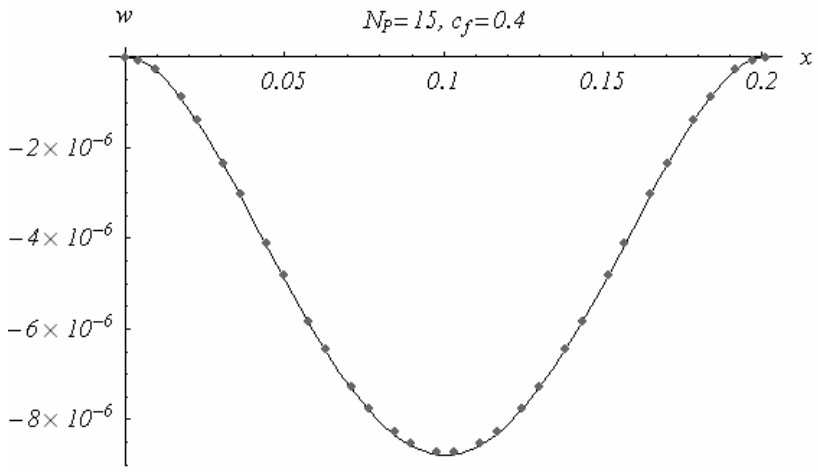

FIGURE 3. Comparison between the refined (dots) and homogenized predictions (solid lines) with 15 piezoelectric transducers (beam clamped at both ends).

Even if the proof has been presented for a beam clamped at both ends, the same results may be extended to other boundary conditions. For example, for a cantilever beam the governing equation (2.15) remains unchanged, but the function w is not in $H_0^2(S)$ and the proper boundary conditions are

$$w|_{x=0} = 0, \quad D(w)|_{x=0} = 0, \quad k_{\text{hom}} D^2(w) - g_{\text{hom}} v\big|_{x=l} = 0, \quad k_{\text{hom}} D^3(w) - g_{\text{hom}} D(v)\big|_{x=l} = 0.$$

As an application sample we consider a constant applied voltage

$$v(x) = V_{\max},$$

which yields the following homogenized solution:

$$w(x) = -V_{\max} \frac{g_{\text{hom}}}{2k_{\text{hom}}} x^2.$$

In Figures 4 and 5 we report the deflection of the homogenized model (solid line) and that of the refined model (dots) for the same cases analyzed above.

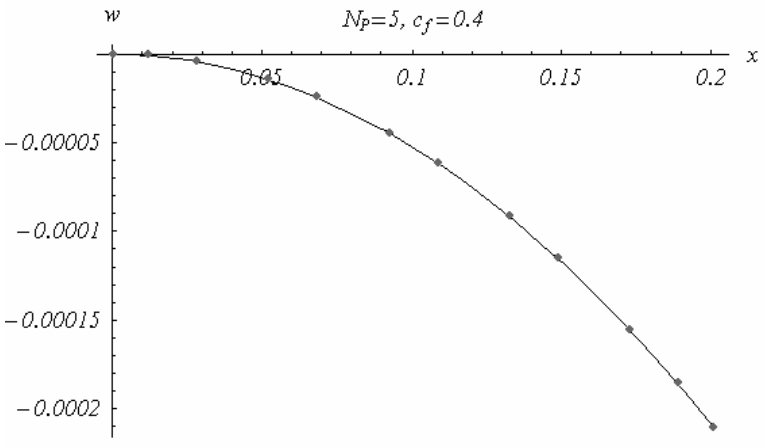

FIGURE 4. Comparison between the refined (dots) and homogenized predictions (solid lines) with 5 piezoelectric transducers (camtilever beam).

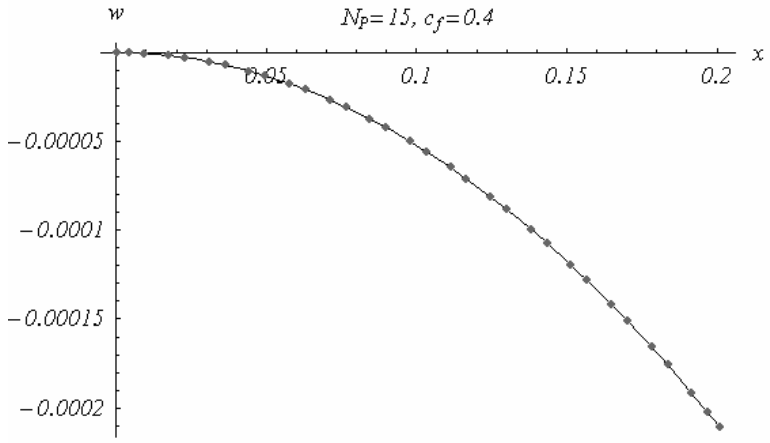

FIGURE 5. Comparison between the refined (dots) and homogenized predictions (solid lines) with 15 piezoelectric transducers (cantilever beam).

CHAPTER 5

Resonant piezoelectric shunting

The most popular passive single-mode damping technique consists in shunting a piezoelectric element with a resistor R and an inductor L as proposed firstly in [**Hagood and von Flotow (1991)**] (see Figure 1).

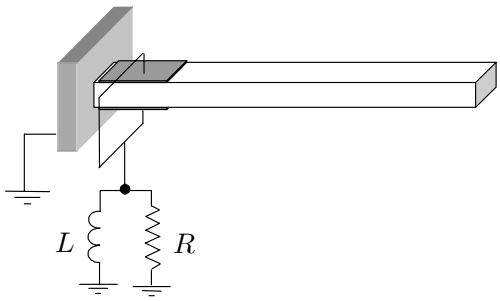

FIGURE 1. Sketch of a cantilever beam with a transducer shunted with a RL impedance.

As the structure vibrates, the mechanical energy is rapidly transformed into electric energy which is dissipated through the resistor. The damping efficiency of the used impedance is maximum when the resonance frequency of the shunt circuit is equal to the mechanical frequency of the structural eigenmode to be damped, i.e. the shunting network is tuned to the mechanical system. When this tuning condition is achieved the resistance R must be properly chosen so as to maximize the damping effectiveness.

In the present Chapter we present a suitable reduced-order model of the considered stepped piezoelectric beam (presented in Chapter 2) suitable for piezoelectric shunting. Next, we discuss the optimization of the circuit parameters by choosing the ∞-norm of the mobility function as the cost function ($\mathcal{H}_\infty$ control problem, see e.g. [**Zhou et al. (1996)**]). We treat the effects of large variations of the inductance, resistance and coupling coefficient and provide closed-form expressions for their small perturbations. The results of this sensitivity analysis are used to model the effects of uncertainties on the damping effectiveness. Finally we mention a possible application of piezoelectric shunting in identification processes and test the novel method on an experimental prototype.

1. Governing equations

We consider the same stepped beam as that presented in Chapter 2, where a given piezoelectric transducer (say the one occupying the s-th segment) is shunted with an RL impedance, a different one is used as an actuator driven by a voltage source (say the one occupying the a-th segment) and all the others are short-circuited to ground.

The mechanical governing equations are derived from (3.12) of Chapter 2

$$\sum_{h=1}^{N}\int_{S_h} k_h w''(x,t)\tilde{w}''(x)dx - g_s V_s(t)\left(\tilde{w}'(X_{s+1}) - \tilde{w}'(X_s)\right) - g_a V_a(t)\left(\tilde{w}'(X_{a+1}) - \tilde{w}'(X_a)\right) = -\sum_{h=1}^{N}\int_{S_h}\rho_h\ddot{w}(x,t)\tilde{w}(x)dx.$$

On the other hand the time evolution of the voltage $V_s(t)$ is (see equation (2.2b) of Chapter 2)

$$Q_s(t) = C_s V_s(t) + g_s\left(w'(X_{s+1},t) - w'(X_s,t)\right),$$

where C_s indicates the piezoelectric capacitance and Q_s the stored charge and the remaining summand represents the piezoelectric charge induced by the mechanical deformation. From the analysis of the circuit we easily see that Q_s is related to V_s by

$$\dot{Q}_s(t) - \dot{Q}_s(0) = -\frac{1}{L}\int_0^t V_s(\tau)\,d\tau - \frac{1}{R}V_s(t).$$

By considering vanishing initial conditions and introducing the flux linkages ψ_a and ψ_s, defined as the time integral of the corresponding voltages,we obtain the following two coupled electromechanical equations:

(1.1)
$$\sum_{h=1}^{N}\int_{S_h} k_h w''(x,t)\tilde{w}''(x)dx - g_s\dot{\psi}_s(t)\left(\tilde{w}'(X_{s+1}) - \tilde{w}'(X_s)\right) - g_a\dot{\psi}_a(t)\left(\tilde{w}'(X_{a+1}) - \tilde{w}'(X_a)\right) = -\sum_{h=1}^{N}\int_{S_h}\rho_h\ddot{w}(x,t)\tilde{w}(x)dx$$

(1.2)
$$\frac{1}{L}\psi_s(t) + \frac{1}{R}\dot{\psi}_s(t) + C_s\ddot{\psi}_s(t) + g_s\left(\dot{w}'(X_{s+1},t) - \dot{w}'(X_s,t)\right) = 0$$

In order to optimize the electric parameters (inductance and resistance) for a narrow band vibration damping in the neighborhood of the i-th structural frequency $\omega^{(i)}$, a design model is developed. In particular, the modal reduction of (1.1) and (1.2) onto the i-th mechanical mode shape $\mathsf{w}^{(i)}$ (derived by using one of methodologies indicated in Chapter 3) is developed. By assuming

$$w(x,t) = \mathsf{w}^{(i)}(x)\,W_i(t),$$

the following coupled evolution equations for the modal coefficient $W_i(t)$ and the flux-linkage $\psi_s(t)$ are obtained:

(1.3)
$$\begin{cases} m\ddot{W}_i(t) + m\omega_i^2 W_i(t) - G_{is}\dot{\psi}_s(t) = F_i(t) \\ \frac{1}{L}\psi_s(t) + \frac{1}{R}\dot{\psi}_s(t) + C_s\ddot{\psi}_s(t) + G_{is}\dot{W}_i(t) = 0 \end{cases},$$

where the modal parameters are defined by:

$$G_{is} := g_s\left(\left(\mathsf{w}^{(i)}\right)'(X_{s+1}) - \left(\mathsf{w}^{(i)}\right)'(X_s)\right),\ F_i(t) := g_a\left(\left(\mathsf{w}^{(i)}\right)'(X_{a+1}) - \left(\mathsf{w}^{(i)}\right)'(X_a)\right)\dot{\psi}_a(t).$$

We report the corresponding governing equations in the following non-dimensional form and, since it does not cause misunderstandings, the same symbols as for the dimensional

case are used:

$$\left\{ \begin{array}{l} \ddot{W}_i(t) + W_i(t) - \gamma\ddot{\psi}_s(t) = F_i(t) \\ \ddot{\psi}_s(t) + \delta\dot{\psi}_s(t) + \beta\psi_s(t) + \gamma\dot{W}_i(t) = 0 \end{array} \right. , \tag{1.4}$$

where the dimensionless parameters

$$\beta := \frac{1}{LC_s}\frac{1}{\left(\omega^{(i)}\right)^2}, \tag{1.5a}$$

$$\delta := \frac{1}{RC_s}\frac{1}{\omega^{(i)}}, \tag{1.5b}$$

$$\gamma := \frac{G_{is}}{\omega^{(i)}\sqrt{mC_s}} \tag{1.5c}$$

appear. Without loss of generality we assume that γ is positive. The time has been non-dimensionalized with respect of the inverse of the mechanical radian frequency $\omega^{(i)}$. The parameter β measures the tuning effectiveness of the electric network, since it is nothing than the square of the ratio of mechanical to electrical natural frequency, δ measures the electric damping and γ the electromechanical modal coupling.

The mechanical mobility function is defined by

$$H_p(\omega) := \frac{\mathcal{F}\left[\dot{W}_i\right](\omega)}{\mathcal{F}\left[F_i\right](\omega)} = -\frac{j\omega\left(-\omega^2 + \beta + j\omega\delta\right)}{-\omega^4 + \omega^3 j\delta + \omega^2\left(\beta + 1 + \gamma^2\right) - j\omega\delta - \beta},$$

where $\mathcal{F}$ indicates Fourier transform, ω the dimensionless radian frequency, and p the set of parameters $p = (\beta, \delta, \gamma)$.

2. Optimization

A widely adopted criterion for optimizing the considered shunting circuit consists in minimizing the ∞-norm of the mobility function, defined as the essential supremum of $|H_p|$ on the positive real axis:

$$\|H_p\|_\infty = \operatorname*{esssup}_{\omega \in \mathrm{R}^+} |H_p| .$$

In the literature, several criteria for optimizing passive controllers have been proposed, e.g. the pole placement ([**Hagood and von Flotow (1991)**], [**Porfiri et al. (accepted)**]) and the infinite horizon minimization ([**Juang (1984)**], [**Andreaus et al. (2004)**]). Our present choice is motivated by the simplicity of handling uncertainties within the $\mathcal{H}_\infty$ control theory.

In this case, by duplicating the argument of [**Den Hartog (1934)**], it is possible to derive an exact estimation of the optimal inductance and optimal resistance. Indeed, it is possible to show (by cumbersome and time consuming manipulations) that in the graph of $|H_p|$, there exists a pair of points, say $S = (\omega_S, |H_p(\omega_S)|)$ and $T = (\omega_T, |H_p(\omega_T)|)$ defined by:

$$\begin{array}{rcl} \forall\bar{\beta},\bar{\gamma} \in \mathrm{R}^+ & \quad \exists\omega_S,\omega_T : \forall\delta_1,\delta_2 \in \mathrm{R}^+ & \\ \left|H_{(\bar{\beta},\delta_1,\bar{\gamma})}(\omega_S)\right| = \left|H_{(\bar{\beta},\delta_2,\bar{\gamma})}(\omega_S)\right| & \quad \left|H_{(\bar{\beta},\delta_1,\bar{\gamma})}(\omega_T)\right| = \left|H_{(\bar{\beta},\delta_2,\bar{\gamma})}(\omega_T)\right| . & \end{array}$$

These two fixed points can be simply found by equating the square of transfer function absolute value evaluated in the limit of δ going to infinity to that evaluated when δ is zero

$$\left|H_{(\beta,0,\gamma)}(\omega)\right|^2 = \lim_{\delta\to+\infty}\left|H_{(\beta,\delta,\gamma)}(\omega)\right|^2 \Rightarrow \frac{\omega^2}{\left(1-\omega^2\right)^2} = \frac{\left(\omega^3 - \beta\omega\right)^2}{\left(\omega^4 - \omega^2\left(\beta + 1 + \gamma^2\right) + \beta\right)^2};$$

thus:

$$\omega_{T,S}(\beta,\gamma)=\frac{1}{2}\sqrt{2+2\beta+\gamma^2\pm\sqrt{-16\beta+(2+2\beta+\gamma^2)^2}}.$$

The ∞-norm of H_p is minimized by imposing that the values attained by $|H_p(\omega)|^2$ at these two points are the same, and by imposing that these values are its maxima, namely:

$$|H_p(\omega_S)|^2=|H_p(\omega_T)|^2\Rightarrow\beta_{opt}=1; \tag{2.1}$$

and subsequently

$$\frac{d}{d\omega}|H_p(\omega)|^2\bigg|_{\omega=\omega_S}=\frac{d}{d\omega}|H_p(\omega)|^2\bigg|_{\omega=\omega_T}=0\Rightarrow\delta_{opt}=\sqrt{\frac{3}{2}}\gamma; \tag{2.2}$$

yielding:

$$\min_{\beta\in\mathrm{R}^+,\,\delta\in\mathrm{R}^+}\left\|H_{(\beta,\delta,\gamma)}\right\|_\infty=\left\|H_{\left(\beta_{opt},\delta_{opt},\gamma\right)}\right\|_\infty=\frac{\sqrt{2}}{\gamma}. \tag{2.3}$$

Furthermore, when the tuning condition (2.1) is satisfied, the difference between the fixed point dimensionless radian frequencies is

$$\omega_T\left(\beta_{opt},\gamma\right)-\omega_S\left(\beta_{opt},\gamma\right)=\frac{\gamma}{\sqrt{2}}, \tag{2.4}$$

and their values are

$$\omega_{T,S}\left(\beta_{opt},\gamma\right)=\frac{1}{2}\sqrt{4+\gamma^2\pm\gamma\sqrt{4+\gamma^2}}. \tag{2.5}$$

Therefore from (1.5a) the optimal inductance is

$$L_{opt}=\frac{1}{\left(\omega^{(i)}\right)^2C_s}, \tag{2.6}$$

and from (1.5b) the optimal resistance is

$$R_{opt}=\sqrt{\frac{2}{3}}\frac{\sqrt{m}}{G_{is}\sqrt{C_s}}. \tag{2.7}$$

The electric damping ratio ζ defined by (see e.g. [**Meirovitch (2000)**])

$$\zeta=\frac{\delta}{2\sqrt{\beta}},$$

when conditions (2.1) and (2.2) are satisfied, becomes

$$\zeta_{opt}=\sqrt{\frac{3}{8}}\gamma.$$

REMARK 3. *An additional capacitance in parallel connection with the piezoelectric transducers decreases the needed optimal inductance according to (2.6), but at the same time reduces the damping effectiveness according to (2.3) together with (1.5c).*

REMARK 4. *The system performances may be strengthened by properly positioning the piezoelectric transducer on the host beam (see e.g.* [**Barboni et al. (2000)**]*). Indeed by maximizing the modal coupling γ, the system ∞-norm may be minimized.*

3. Effect of parameters variations

In this Section we analyze the effects of changes of the electric parameters on the system damping performances. We include in the analysis also variations of the coupling parameter γ, which may arise, for instance, after the partial debonding of the transducer on the beam and will be important for future discussions on distributed control. We split the analysis into two parts: we establish general numerical procedures to study the case of large variations of the system parameter and we provide simple closed-form formulas to tackle the effects of small variations (sensitivity analysis).

3.1. Effect of large variations. In order to compute the effects of large variations of the system parameters β, δ, γ on the system ∞-norm, we refer to [**Zhou et al. (1996)**], [**Chandrasekharan (1996)**] and [**Doyle et al. (1989)**]. To this aim, let us consider the state space realization of the system

$$\mathcal{R} = \left[\begin{array}{cc} A & B \\ C & 0 \end{array}\right],$$

with

$$A = \left[\begin{array}{cccc} 0 & 1 & 0 & 0 \\ -1 & 0 & 0 & \gamma \\ 0 & 0 & 0 & 1 \\ 0 & -\gamma & -\beta & -\delta \end{array}\right], \quad B = \left[\begin{array}{c} 0 \\ 1 \\ 0 \\ 0 \end{array}\right], \quad C = \left[\begin{array}{cccc} 0 & 1 & 0 & 0 \end{array}\right];$$

and define the Hamiltonian matrix

$$\mathrm{H} = \left[\begin{array}{cc} A & \eta^{-2} B B^{\mathrm{T}} \\ -C^{\mathrm{T}} C & -A^{\mathrm{T}} \end{array}\right], \quad \eta \in \mathrm{R}^{+}.$$

Since, A is stable the following lemma hold:

$$\|H_p\|_\infty < \eta \Leftrightarrow \mathrm{H} \text{ has no eigenvalues on the imaginary axis.}$$

Therefore, for arbitrary β, δ, γ the ∞-norm of H_p may be computed by applying the following bisection algorithm:

(1) choose two initial bounds for $\|H_p\|_\infty$, i.e. $\eta_l < \|H_p\|_\infty < \eta_u$[1];
(2) set $\eta = \dfrac{\eta_u + \eta_l}{2}$ and evaluate the eigenvalues of H at η;
(3) if there are any eigenvalues on the imaginary axis set $\eta_l = \eta$, otherwise $\eta_u = \eta$;
(4) compute the difference between η_l and η_u and if it is more than the desired precision go to the second step, otherwise $\|H_p\|_\infty \simeq \eta$.

3.2. Sensitivity analysis. When the considered variations, say $\Delta\beta$, $\Delta\delta$ and $\Delta\gamma$, are small, the first order approximation may be acceptable:

$$\begin{aligned} |H_p(\omega)|^2 = |H_p(\omega)|^2\big|_{p_{opt}} &+ \frac{\partial}{\partial\beta}|H_p(\omega)|^2\Big|_{p_{opt}} \Delta\beta + \frac{\partial}{\partial\delta}|H_p(\omega)|^2\Big|_{p_{opt}} \Delta\delta \\ &+ \frac{\partial}{\partial\gamma}|H_p(\omega)|^2\Big|_{p_{opt}} \Delta\gamma =: |H_p(\omega)|^2\big|_{p_{opt}} + \left[\begin{array}{ccc} \Delta\beta & \Delta\delta & \Delta\gamma \end{array}\right] S_{p_{opt}}(\omega) \end{aligned}$$

[1]Let us remark that, the Hamiltonian has eigenvalues with non zero real part when evaluated at η_u, on the contrary at η_l it has some eigenvalues on the imaginary axis.

where the subscript p_{opt} denotes the optimal configuration $\left(\beta_{opt}, \delta_{opt}, \gamma\right)$, and the sensitivity coefficients vector $S_{p_{opt}}$ has been introduced (see e.g. [**Lutes and, Sarkani (2004)**]). By working out the cumbersome algebra one gets:

$$\begin{aligned}
\frac{\partial}{\partial\beta}\left|H_p\left(\omega\right)\right|^2\Big|_{p_{opt}} &= \frac{4\gamma^2\omega^4\left(-1+\omega^2\right)\left(2-\left(4+5\gamma^2\right)\omega^2+2\omega^4\right)}{\left(-2+\left(8+\gamma^2\right)\omega^2-2\left(6+\gamma^2+\gamma^4\right)\omega^4+\left(8+\gamma^2\right)\omega^6-2\omega^8\right)^2};\\
\frac{\partial}{\partial\delta}\left|H_p\left(\omega\right)\right|^2\Big|_{p_{opt}} &= \frac{4\sqrt{6}\gamma^3\omega^6\left(-2+\left(4+\gamma^2\right)\omega^2-2\omega^4\right)}{\left(-2+\left(8+\gamma^2\right)\omega^2-2\left(6+\gamma^2+\gamma^4\right)\omega^4+\left(8+\gamma^2\right)\omega^6-2\omega^8\right)^2};\\
\frac{\partial}{\partial\gamma}\left|H_p\left(\omega\right)\right|^2\Big|_{p_{opt}} &= \frac{8\gamma_0\omega^4\left(1-\left(2+\gamma^2\right)\omega^2+\omega^4\right)\left(2+\left(-4+3\gamma^2\right)\omega^2+2\omega^4\right)}{\left(-2+\left(8+\gamma^2\right)\omega^2-2\left(6+\gamma^2+\gamma^4\right)\omega^4+\left(8+\gamma^2\right)\omega^6-2\omega^8\right)^2}.
\end{aligned}$$

Furthermore, one can show that the aforementioned functions are smooth functions in R^+.

For small variations $\Delta\beta$, $\Delta\delta$ and $\Delta\gamma$ the maxima of $\left|H_p\left(\omega\right)\right|^2$ are still attained at $\omega_{T,S}$. By substituting the expressions for $\omega_{S,T}$ in (2.5) into $S_{p_{opt}}\left(\omega\right)$ we get:

$$S_{p_{opt}}\left(\omega_{S,T}\right) = \begin{bmatrix} \dfrac{\gamma \pm \sqrt{8+\gamma^2}}{\gamma^3} \\ 0 \\ -\dfrac{4}{\gamma^3} \end{bmatrix},$$

where the minus (plus) sign in the first entry of $S_{p_{opt}}\left(\omega_{T,S}\right)$ corresponds to ω_T $\left(\omega_S\right)$. Therefore

$$\left\|\left|H_p\right|^2\right\|_\infty := \max_{\omega\in\mathrm{R}^+}\left|H_p\left(\omega\right)\right|^2 = \max_{\omega\in\mathrm{R}^+}\left|H_{p_{opt}}\left(\omega\right)\right|^2 + \frac{\sqrt{8+\gamma^2}}{\gamma^3}\left|\Delta\beta\right| + \frac{1}{\gamma^2}\Delta\beta - \frac{4}{\gamma^3}\Delta\gamma.$$

The above expression yields:

$$\left\|H_p\right\|_\infty = \left\|H_{p_{opt}}\right\|_\infty + \frac{\sqrt{8+\gamma^2}}{2\sqrt{2}\gamma^2}\left|\Delta\beta\right| + \frac{1}{2\sqrt{2}\gamma}\Delta\beta - \frac{\sqrt{2}}{\gamma^2}\Delta\gamma. \tag{3.1}$$

For small coupling equation (3.1) becomes:

$$\left\|H_p\right\|_\infty \simeq \left\|H_{p_{opt}}\right\|_\infty + \frac{1}{\gamma^2}\left|\Delta\beta\right| - \frac{\sqrt{2}}{\gamma^2}\Delta\gamma, \tag{3.2}$$

which provides the following representative relation between the perturbed and the optimal system ∞-norm:

$$\frac{\left\|H_p\right\|_\infty}{\left\|H_{p_{opt}}\right\|_\infty} \simeq 1 + \frac{1}{\gamma\sqrt{2}}\left|\Delta\beta\right| - \frac{1}{\gamma}\Delta\gamma.$$

REMARK 5. *The damping parameter δ is not influencing the damping performances of the shunting impedance as long as its variations stay small. On the other hand, the tuning parameter β strongly affects the system performances since its variations are amplified by a factor linear with γ^{-1} which is generally a large number.*

4. Effect of parameters uncertainties

Starting from equation (3.1), we study the effects of uncertainties on the system damping performance. We assume that the parameters $\Delta\beta$ and $\Delta\gamma$ are independent random

variables normally distributed with zero mean. The probability density functions are

$$f_{\Delta\beta}\left(\Delta\beta\right)=\frac{1}{\sqrt{2\pi}\sigma_{\Delta\beta}}\exp\left(-\frac{1}{2}\left(\frac{\Delta\beta}{\sigma_{\Delta\beta}}\right)^2\right),\quad f_{\Delta\gamma}\left(\Delta\gamma\right)=\frac{1}{\sqrt{2\pi}\sigma_{\Delta\gamma}}\exp\left(-\frac{1}{2}\left(\frac{\Delta\gamma}{\sigma_{\Delta\gamma}}\right)^2\right),$$

where $\sigma_{\Delta\beta}$ and $\sigma_{\Delta\gamma}$ denote the standard deviations of the considered random variables.

Even if the mean value of $\Delta\beta$ is zero the mean value of its absolute value is not zero:

$$E\left[\left|\Delta\beta\right|\right]=\int_{\mathrm{R}}\left|\Delta\beta\right|f_{\Delta\beta}\left(\Delta\beta\right)d\Delta\beta=\sqrt{\frac{2}{\pi}}\sigma_{\Delta\beta};$$

and its variance is

$$V\left[\left|\Delta\beta\right|\right]=\int_{\mathrm{R}}\left(\left|\Delta\beta\right|-E\left[\left|\Delta\beta\right|\right]\right)^2f_{\Delta\beta}\left(\Delta\beta\right)d\Delta\beta=\left(1-\frac{2}{\pi}\right)\left(\sigma_{\Delta\beta}\right)^2.$$

Obviously, the expected value of the product $\left|\Delta\beta\right|\Delta\beta$ is zero. Therefore, the mean value of the norm of H_p from (3.1) (see e.g. [**Breiman (1969)**]) is

$$E\left[\left\|H_p\right\|_\infty\right]=\left\|H_{p_{opt}}\right\|_\infty+\frac{\sqrt{8+\gamma^2}}{2\sqrt{2}\gamma^2}\sqrt{\frac{2}{\pi}}\sigma_{\Delta\beta},\tag{4.1}$$

that for small coupling becomes:

$$E\left[\left\|H_p\right\|_\infty\right]\simeq\left\|H_{p_{opt}}\right\|_\infty+\frac{1}{\gamma^2}\sqrt{\frac{2}{\pi}}\sigma_{\Delta\beta},\tag{4.2}$$

which shows that the standard deviation of the tuning parameter influences directly the expected value of the system norm, reducing the damping effectiveness. Similarly, the variance of the system ∞-norm is

$$V\left[\left\|H_p\right\|_\infty\right]=\left(\left(1-\frac{2}{\pi}\right)\frac{1}{\gamma^4}+\left(1-\frac{1}{\pi}\right)\frac{1}{4\gamma^2}\right)\left(\sigma_{\Delta\beta}\right)^2+\left(\frac{\sqrt{2}}{\gamma^2}\right)^2\left(\sigma_{\Delta\gamma}\right)^2,\tag{4.3}$$

which for small coupling becomes:

$$V\left[\left\|H_p\right\|_\infty\right]\simeq\left(1-\frac{2}{\pi}\right)\frac{1}{\gamma^4}\left(\sigma_{\Delta\beta}\right)^2+\frac{2}{\gamma^4}\left(\sigma_{\Delta\gamma}\right)^2.\tag{4.4}$$

From equations (4.1) and (4.3) we notice that the electric damping δ is not influencing the system damping performance. Therefore, the uncertainties on the resistance are not important in a first order approximation theory and only the uncertainties of the inductance are significant.

The uncertainties on the dimensionless parameters can be immediately related to the uncertainties on the inductance. Indeed, we assume that the inductance is given as the sum of the optimal value L_{opt} and a random variable ΔL, normally distributed with zero mean and standard deviation $\sigma_{\Delta L}$, i.e.:

$$L=L_{opt}+\Delta L.$$

Thus, for small deviations of the inductance with respect of its optimal value, the random variable $\Delta\beta$ can be related to ΔL by (see (1.5a))

$$\Delta\beta=-\frac{\Delta L}{L_{opt}}.$$

Therefore, for small coupling γ, the system norm moments are expressed by the following relations:

$$\frac{E\left[\|H_p\|_\infty\right] - \left\|H_{p_{opt}}\right\|_\infty}{\left\|H_{p_{opt}}\right\|_\infty} = \frac{1}{\gamma\sqrt{\pi}}\frac{\sigma_{\Delta L}}{L_{opt}}, \quad \frac{\sqrt{V\left[\|H_p\|_\infty\right]}}{\left\|H_{p_{opt}}\right\|_\infty} = \frac{1}{\gamma}\sqrt{\frac{1}{2}\left(1-\frac{2}{\pi}\right)}\frac{\sigma_{\Delta L}}{L_{opt}}. \tag{4.5}$$

From the above relations we can give an estimate of the tolerance needed in realizing the shunting impedance for achieving a certain vibration damping within a prescribed accuracy.

5. Experimental and numerical results

We refer to the experimental setup described in Section 4 of Chapter 3. We use the first piezoelectric transducer for damping the first structural mode, and the second transducer for exciting the beam. The capacitances of the used transducer can be computed from (2.3) in Chapter 2:

$$C_2 = C_4 = 0.1326\ \mu\text{F},$$

while the piezoelectric coupling are given by equation (5.1b) in Chapter 3. The first circular resonance frequency from Table 3 in Chapter 3 is

$$\omega^{(1)} = 2\pi \times 65.3662\ \text{Hz},$$

while the average modal curvatures at the transducers' locations are computed from the exact (LEN) modal shapes:

$$\left(\left(\mathsf{w}^{(1)}\right)'(X_3) - \left(\mathsf{w}^{(1)}\right)'(X_2)\right) = 5.185\,\text{m}^{-1}, \qquad \left(\left(\mathsf{w}^{(1)}\right)'(X_5) - \left(\mathsf{w}^{(1)}\right)'(X_4)\right) = 3.397\,\text{m}^{-1}.$$

The dimensionless modal coupling parameter γ is from (1.5c)

$$\gamma = 0.183,$$

since the system mass is

$$m = 36.35\,\text{g}.$$

The predicted values of the optimal inductance and resistance are computed by the use of (2.6) and (2.7):

$$L_{opt} = 44.7\ \text{H}, \qquad R_{opt} = 81.9\ \text{k}\Omega.$$

5.1. Numerical results. We start our discussion by considering the effects of the variations of the dimensionless parameters β, δ and γ with respect of the optimal configuration p_{opt}, described by formulas (2.1) and (2.2). We compare the numerical results achieved by using the procedure described in Section 3.1 with those implied by equation (3.1) in Figures 2, 3 and 4.

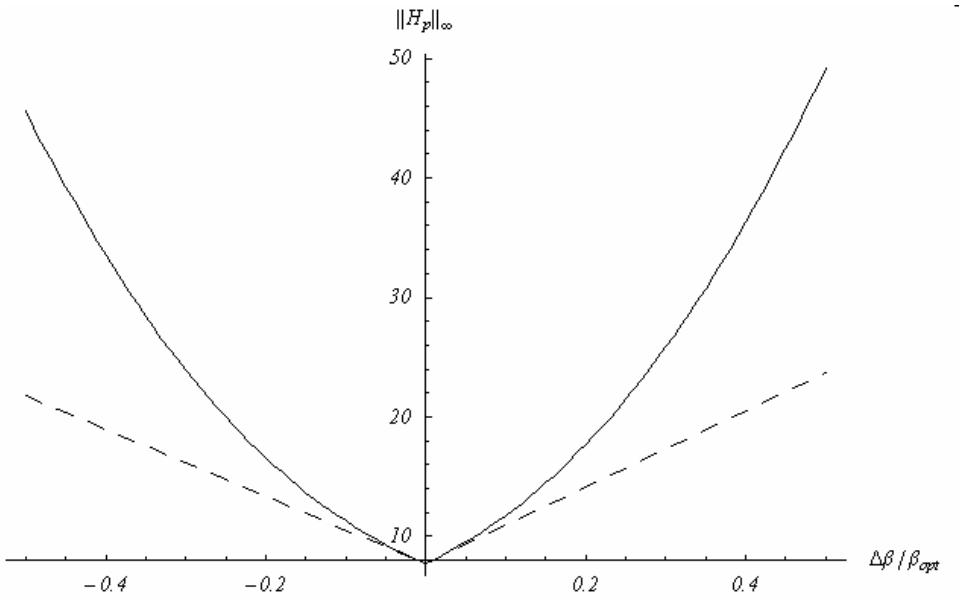

FIGURE 2. Variations of the system infinity norm with respect to the tuning parameter β (solid line: exact behavior, dashed line: results from linearization).

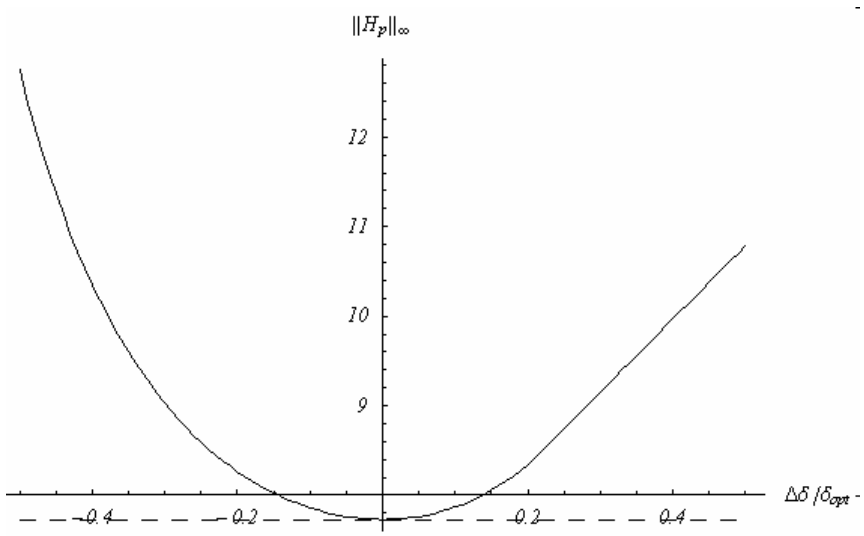

FIGURE 3. Variations of the system infinity norm with respect to the damping parameter δ (solid line: exact behavior, dashed line: results from linearization).

From Figure 2 we can see that the tuning parameter strongly affects the system performances and that even small changes in the electric resonance may lead to dramatic losses in the damping efficiency. On the other hand, the electric damping coefficient does

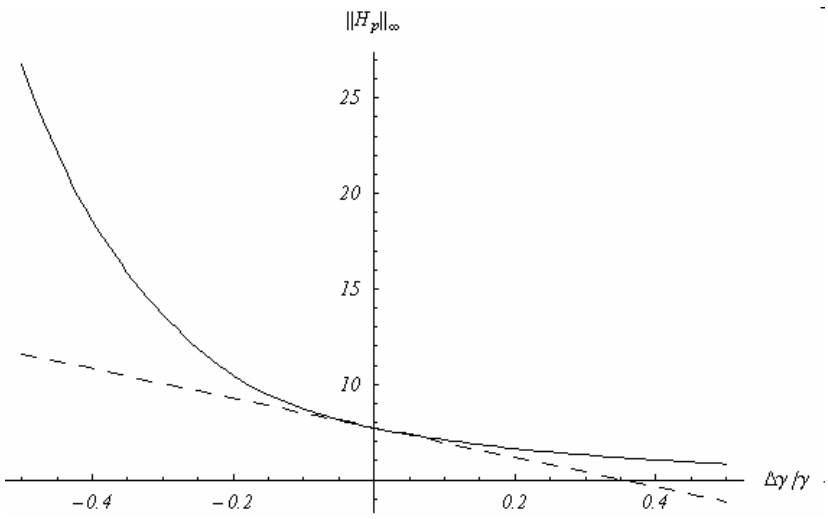

FIGURE 4. Variations of the system infinity norm with respect to the coupling coefficient γ (solid line: exact behavior, dashed line: results from linearization).

not represent a critical parameter and it does only marginally determine the control effectiveness. As a general comment, we remark that the approximate formulas (3.1) represent a valuable tool for easily establishing the effects of parameters variation on the system performances.

In order to validate the results in Section 4 (i.e. equations (4.1) and (4.3)), we have applied the Monte Carlo method (see e.g. [**Buslenko et al. (1966)**]) to the considered system by choosing a population of 10000 samples for each numerical test. Several tests have been performed, by choosing with different values of the parameters standard deviations, ranging from 0 to one tenth of the nominal value. The results are reported in Figure 5, where it is easily understood that for small deviations the approximate formulas derived in (4.1) and (4.3) give satisfactory results.

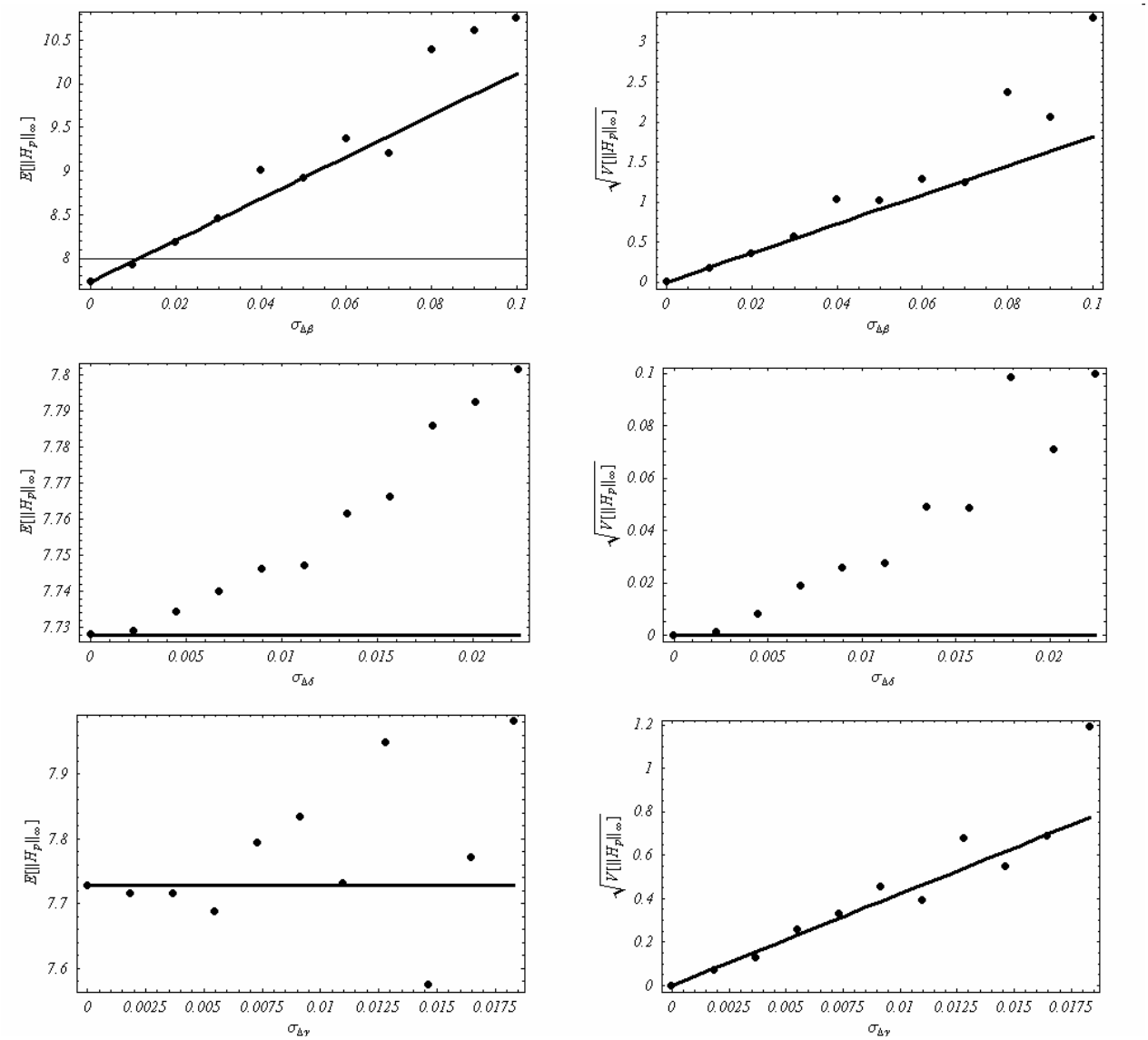

FIGURE 5. Results of MonteCarlo simulations by using normal random variables with zero mean and computing exact system infinity norms (dots: MonteCarlo results, solid line: approximate estimations)

5.2. Experimental evidence. The piezoelectric shunting requires an adjustable inductor, whose inductance is very high. An inductor with these characteristics has been simulated by exploiting the two operational amplifiers RC-circuit depicted in Figure 6 and pictured in Figure 7 (modified Antoniou circuit [**Senani (1996)**] and [**Bruton (1980)**]).

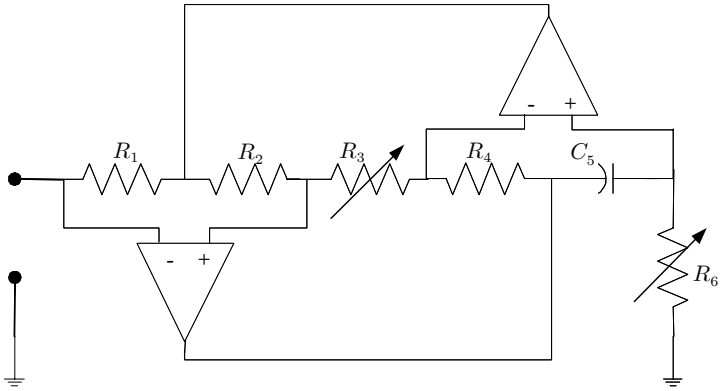

FIGURE 6. Adjustable inductor.

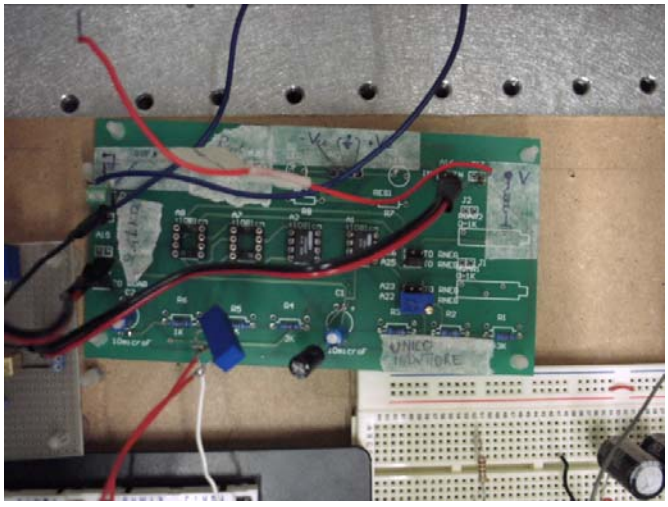

FIGURE 7. Picture of the realized inductor.

The corresponding equivalent inductance is given as a function of its components as follows:

$$L = \frac{R_1 R_4 R_6}{R_2} C_5.$$

Moreover, high quality factors can be achieved by varying the resistance R_3. It adds to the equivalent impedance a series negative resistance which can be exploited to cancel out parasitic losses, see [**Senani (1996)**]. High-voltages FET-input operational amplifiers Burr-Brown OPA445AP driven by a dual outputs power supply TTi EX752M at ± 30 V and high-precision resistors ($\pm 1\%$) have been used.

In Figure 8, we report the mobility functions obtained by exciting the structure at transducer 4 and either shunting transducer 2 with the adjustable inductor tuned so to have the S and T points at the same height, or leaving it open-circuited.

TABLE 1. Experimental ecidence versus theoretical predictions of the reduced order model.

	f_S	f_T	L_{opt}	R_{opt}	f_{short}	f_{open}
Experiments	61.95 Hz	70.70 Hz	58.1 H	119 kΩ	66.25 Hz	67.40 Hz
Theory	61.27 Hz	69.73 Hz	44.1 H	81.9 kΩ	65.37 Hz	67.63 Hz
Percentage Errors	1.10%	1.37%	24.1%	31.2%	1.33%	−0.341%

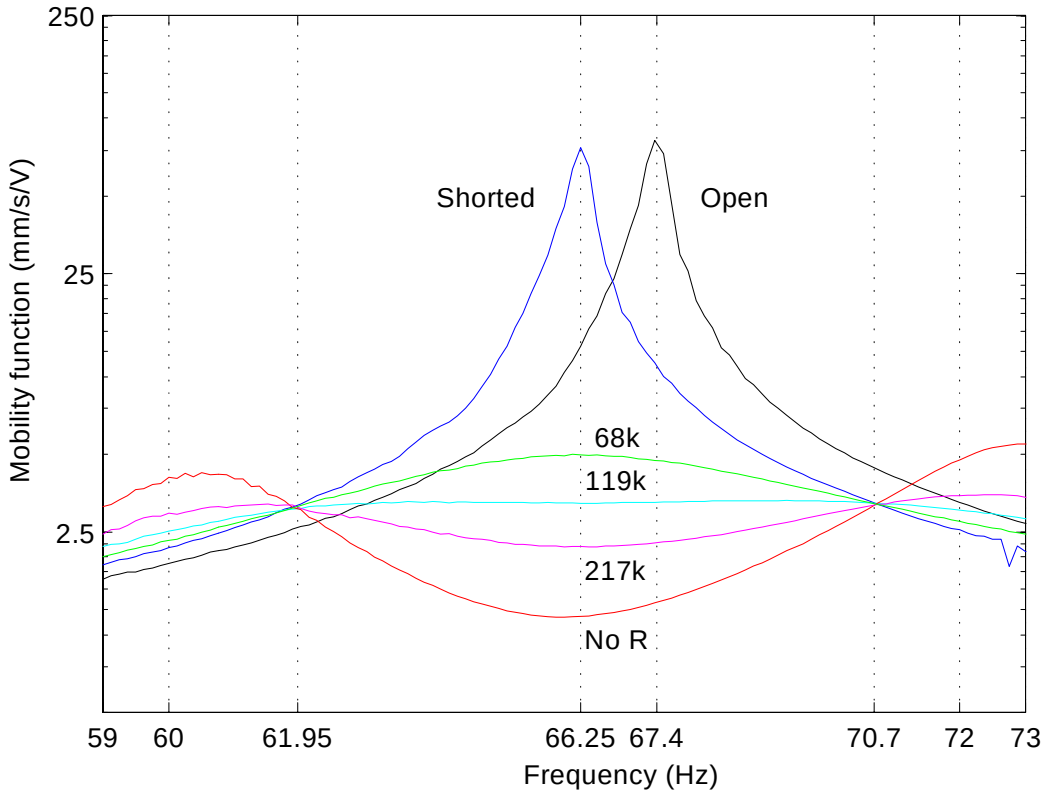

FIGURE 8. Experimental mobility function with optimized inductance and different resistances.

In Table 1, we report the experimental observations compared with the theoretical predictions. The subscripts *short* and *open* indicate measurements performed by leaving the transducer 2 short or open-circuited. From the analysis of Table 1 the following comments may be drawn:

- The presented model provides a satisfactory estimation of the system frequencies when the transducer is open or short-circuited;
- The fixed point frequencies are accurately estimated, enabling a prediction of the piezoelectric shunting damping effectiveness;
- The experimental optimal inductance is much different than the predicted one. This occurrence is imputed to a coarse estimation of the piezoelectric capacitance which determine the predicted inductance according to (2.6). More accurate estimation of the piezoelectric capacitance may be derived by applying the results in [**Maurini et al. (2004, 2)**];

- The experimental optimal resistance is much different than the predicted one. This circumstance may be attributed to parasitic effects in the synthetic inductance, to the mechanical modal damping which has been completely discarded and to the improper capacitance estimate.

5.3. Discussions. The piezoelectric shunting technique so far presented, may be used also for identification purposes. From the knowledge of the stepped beam behavior under different shunting conditions, it is possible to measure indirectly the values of the needed coupling coefficients and capacitances. In the following, we propose two different methods for their identification and underline their advantages and disadvantages.

5.3.1. *Open-circuit vs short-circuit (OvS).* The piezoelectric coupling coefficient γ, accounting for the modal coupling of the s-th segment to the i-th mode, is usually found with the identification method followed in [**Hagood and von Flotow (1991)**], where a piezoelectric beam hosting a single transducer is studied. It is determined by the following measurements:

- resonance frequency $\omega^{(i)}$ of the beam with every element short-circuited (sometimes we write ω_{short}),
- resonance frequency, say ω_{open}, of the beam with every element short-circuited except of the s-th segment left open-circuited.

From equations (1.4) the open-circuit frequency ω_{open} can be readily calculated to be

$$\omega_{open} = \omega_{short}\sqrt{1+\gamma^2}$$

upon substituting δ and γ with zeros, corresponding to the open circuit condition. Hence, the coupling coefficient is estimated by

$$\gamma = \sqrt{-1+\left(\frac{\omega_{open}}{\omega_{short}}\right)^2}. \tag{5.1}$$

With this method, assuming that the frequencies are measured with an uncertainty σ_ω, the uncertainty of the coupling estimate is

$$\frac{\sigma_\gamma}{\gamma} = \frac{1}{\gamma}\sqrt{\left(\frac{d\gamma}{d\omega_{open}}\right)^2+\left(\frac{d\gamma}{d\omega_{short}}\right)^2}\sigma_\omega = \frac{\omega_i}{\gamma\left(\omega_{open}\right)^2}\sqrt{\frac{\left(\omega_{open}\right)^2+\left(\omega_{short}\right)^2}{\left(\omega_{open}\right)^2-\left(\omega_{short}\right)^2}}\sigma_\omega \simeq \frac{1}{\gamma^2}\frac{\sigma_\omega}{\omega_{short}}. \tag{5.2}$$

The last approximation holds for small differences between the two frequencies, i.e. for small coupling. Thus, for small couplings, the amplification factor of the uncertainty is very large.

5.3.2. *Resonant shunt vs short-circuit (RvS).* An alternative identification method stems directly from the piezoelectric shunting technique presented above. Indeed by adjusting the synthetic inductance for having the S and T points at the same height we obtain from (2.6):

$$C_s = \frac{1}{\left(\omega_{short}\right)^2 L_{opt}}.$$

Next, by measuring the difference of the frequencies of the S and T points, we obtain from (2.4)

$$\gamma = \sqrt{2}\frac{(\omega_T-\omega_S)}{\omega_{short}}, \tag{5.3}$$

TABLE 2. Comparison between the two identification methods.

	OvS	RvS
Measured quantities	Natural frequencies: ω_{open} and ω_{short}	Frequency responses: H Inductance: L
Identifiable variables	Coupling coefficient γ	Coupling coefficient: γ Capacitance
Accuracy	Poor	Good
Difficulty	Little	Considerable

TABLE 3. Experimentally identified coupling parameters and capacitance.

	γ	C_2
OvS	0.184	-
RvS	0.187	99.3 nF
Theory	0.183	132.6 nF

where ω_T and ω_S are the dimensional frequencies.

For this method when the frequencies are measured with an uncertainty σ_ω, the uncertainty of the estimated coupling is

$$\frac{\sigma_\gamma}{\gamma} = \left(\sqrt{\frac{4}{\gamma^2}+1}\right)\frac{\sigma_\omega}{\omega_{short}} \simeq \frac{2}{\gamma}\frac{\sigma_\omega}{\omega_{short}}; \tag{5.4}$$

the last approximation being acceptable only for small coupling. By comparing the estimation results in (5.4) and (5.2) the second method is shown to be more accurate. Furthermore, the second approach enables to estimate also the piezoelectric capacitance. At the same time, it relies on a more complicated experimental setup (a simulated inductor is required) and more experimental data (the whole frequency response around the natural frequency is required).

In Table 2 these comments are summarized and the required measures together with the identifiable variables are listed. In Table 3 the results of the two identification methods applied to the considered sample are reported.

CHAPTER 6

Second order transmission line

In this Chapter we consider the performances of a second order transmission line interconnecting the electric terminals of an array of piezoelectric transducers positioned on a host beam. Each piezoelectric element is connected to the adjacent one via a floating RL impedance, i.e. a resistor in parallel connection with an inductor.

We initially model the PEM structure as a continuum by exploiting the results of the two-scale homogenization in Chapter 4. Arbitrary boundary conditions are considered for the electric circuit. By considering a reduced modal model of the PEM structure in the neighborhood of a structural frequency the line inductance and resistance are optimized and a criterion for determining the optimal electric boundary conditions is proposed. As an application sample, we study a cantilever beam and optimize the electric network for achieving the maximum damping effectiveness in the neighborhood of the lowest structural mode.

Next, we consider a more refined model of the PEM structure, where the discrete nature of the electric circuit is accounted for. Optimal values of the line inductance and line resistance are found and compared to the prediction of the homogenized model. Closed form solutions of the eigenproperties of the electric network are provided, based on an auxiliary boundary value difference problem (see e.g. [**Samarskii and Nikolaev (1989)**]).

The effects of uncertainties on the line-inductances are studied. The sensitivity of the electrical eigenproperties with respect to the variations of any inductance is examined. Next, the inductances are treated as independent random variables and a simple formula for evaluating the consequent loss of damping performance is worked out.

Finally an experimental setup is described, and the modeling results are validated. The PEM beam prototype consists of a cantilever beam with 5 piezoelectric ceramics used for control purposes and 1 additional transducer used for exciting the beam in the neighborhood of its lowest structural frequency. The floating inductances are realized by the use of RC-circuits and the internal resonance in between the electrical and the mechanical system is achieved by the use of a variable grounded inductor located at the beam free end.

1. Homogenized model

1.1. Governing equations. The homogenized governing equations of a PEM beam exploiting a second-order RL transmission line may derived by the use of a procedure similar to the one presented for the simple static case in Chapter 4. We refrain from tackling the involved mathematical issues related to the time dependence and to the presence of the discrete electric network. We refer to [**Canon and Lenczner (1999)**], [**Hoffman and Botkin (2000)**] and [**Lenczner and Mercier (2004)**] for a complete and rigorous treatment. As a rule of thumb, we may claim that the forecasts of the homogenized model are acceptable for mechanical wave lengths larger than the structure period ε. Indeed, high frequency oscillations are not captured by the effective models, which, basically, averages the key descriptors on any periodic cell.

In particular it may be shown that the governing equation for the mechanical deflection field w is:

$$\rho_{\text{hom}}\ddot{w} + k_{\text{hom}} w^{IV} - g_{\text{hom}}\dot{\psi}'' = b, \tag{1.1}$$

where ψ is the electric flux-linkage field and the homogenized bending stiffness k_{hom} and coupling coefficient g_{hom} are given in equation (2.15) of Chapter 4, while the homogenized linear mass density ρ_{hom} is

$$\rho_{\text{hom}} = \rho_P c_f + \rho_B \left(1 - c_f\right). \tag{1.2a}$$

On the other hand, the governing equation for the electric flux-linkage is

$$c_{\text{hom}}\ddot{\psi} - \frac{1}{l_{\text{hom}}}\psi'' - \frac{1}{r_{\text{hom}}}\dot{\psi}'' + g_{\text{hom}}\dot{w}'' = 0, \tag{1.3}$$

where the homogenized capacitance per unit length c_{hom}, inductance per unit length l_{hom} and resistance per unit length r_{hom} have been introduced

$$c_{\text{hom}} = \frac{C}{\varepsilon}, \quad l_{\text{hom}} = \frac{L}{\varepsilon}, \quad r_{\text{hom}} = \frac{R}{\varepsilon},$$

C being the piezoelectric capacitance, L the line inductance and R the line resistance.

In what follows, we consider a cantilever beam. The boundary conditions at the clamped left end are

$$w\left(0,t\right) = 0, \quad w'\left(0,t\right) = 0, \quad \left(\psi'\left(0,t\right) + \frac{l_{\text{hom}}}{r_{\text{hom}}}\dot{\psi}'\left(0,t\right)\right) - \alpha_0\left(\psi\left(0,t\right) + \frac{l_{\text{hom}}}{r_{\text{hom}}}\dot{\psi}\left(0,t\right)\right) = 0, \tag{1.4}$$

where the positive constant α_0 has been introduced to account for a generic RL boundary impedance. At the free end we have

$$\begin{gathered}\left(k_{\text{hom}} w''\left(l,t\right) - g_{\text{hom}}\dot{\psi}\left(l,t\right)\right) = 0, \quad \left(k_{\text{hom}} w'''\left(l,t\right) - g_{\text{hom}}\dot{\psi}'\left(l,t\right)\right) = 0, \\ \left(\psi'\left(l,t\right) + \frac{l_{\text{hom}}}{r_{\text{hom}}}\dot{\psi}'\left(l,t\right)\right) + \alpha_l\left(\psi\left(l,t\right) + \frac{l_{\text{hom}}}{r_{\text{hom}}}\dot{\psi}\left(l,t\right)\right) = 0,\end{gathered} \tag{1.5}$$

where another positive constant α_l has been introduced. We assume that the constants α_0 and α_l belong to $\bar{\mathrm{R}}^+ = \mathrm{R}^+ \cup \{+\infty\}$, where $+\infty$ corresponds to short-circuit the electric end to ground. We remark that the chosen boundary conditions provide a proportional damping in the electric circuit, without altering its modal characteristics.

1.2. Reduced model. We consider structural vibrations in the neighborhood of the i-th mechanical frequency $\omega^{(i)}$, and we assume that in that frequency band the electric circuit is resonating at its j-th mode. In order to optimize the electric parameters, inductances and resistances for this narrow band vibration damping, a reduced order design model is developed. The modal reduction of (1.1) and (1.3) onto the i-th mechanical mode shape $\mathsf{w}^{(i)}$ and j-th electrical mode shape $\psi^{(j)}$ is developed. Each of the considered mode shape is found by discarding the piezoelectric coupling, i.e. they represent the mode shapes of the two uncoupled systems. In particular,

$$\left(\psi^{(j)}\right)'' = -\lambda_{\text{hom}}^{(j)}\psi^{(j)}, \qquad \left(\psi^{(j)}\right)'\left(0\right) - \alpha_0\psi^{(j)}\left(0\right) = 0, \quad \left(\psi^{(j)}\right)'\left(l\right) + \alpha_l\psi^{(j)}\left(l\right) = 0,$$

and

$$\begin{gathered}k_{\text{hom}}\left(\mathsf{w}^{(i)}\right)^{IV} = \left(\omega^{(i)}\right)^2 \rho_{\text{hom}}\mathsf{w}^{(i)}, \\ \mathsf{w}^{(i)}\left(0\right) = 0, \quad \left(\mathsf{w}^{(i)}\right)'\left(0\right) = 0, \quad \left(\mathsf{w}^{(i)}\right)''\left(l\right) = 0, \quad \left(\mathsf{w}^{(i)}\right)'''\left(l\right) = 0.\end{gathered}$$

As usual, the mechanical mode shape is normalized in order to have

$$\int_0^l \rho_{\text{hom}} \left(\mathsf{w}^{(i)}\right)^2 dx = m \Rightarrow \int_0^l \left(\mathsf{w}^{(i)}\right)^2 dx = l,$$

and similarly the electric one

$$\int_0^l \left(\psi^{(j)}\right)^2 dx = l.$$

By assuming

$$w(x,t) = \mathsf{w}^{(i)}(x) W_i(t), \quad \psi(x,t) = \psi^{(j)}(x) \Psi_j(t),$$

the following coupled evolution equations for the modal coefficients $W_i(t)$ and $\Psi_j(t)$ are obtained:

$$\begin{cases} m\ddot{W}_i(t) + m\omega_i^2 W_i(t) - G_{\text{hom } ij}\, \dot{\Psi}_j(t) = F_i(t) \\ l c_{\text{hom}} \ddot{\Psi}_j(t) + \dfrac{l}{l_{\text{hom}}} \lambda_{\text{hom}}^{(j)} \Psi_j(t) + \dfrac{l}{r_{\text{hom}}} \lambda_{\text{hom}}^{(j)} \dot{\Psi}_j(t) + G_{\text{hom } ij}\, \dot{W}_i(t) = 0 \end{cases}, \tag{1.6}$$

where the modal parameters are defined by:

$$G_{\text{hom } ij} := g_{\text{hom}} \int_0^l \left(\mathsf{w}^{(i)}\right)''(x) \psi^{(j)}(x)\, dx, \tag{1.7a}$$

$$F_i(t) := \int_0^l b(x,t)\, \mathsf{w}^{(i)}(x)\, dx. \tag{1.7b}$$

Without loss of generality, we assume that $G_{\text{hom } ij}$ is positive.

1.3. Optimization. The system (1.6) shares the same structure of that in (1.3) of Chapter 5 for the resonant piezoelectric shunting. Therefore, it may be cast into the dimensionless form (1.4) of Chapter 5 by properly defining the key dimensionless parameters β, δ and γ as follows:

$$\beta := \frac{\lambda_{\text{hom}}^{(j)}}{l_{\text{hom}} c_{\text{hom}}} \frac{1}{\left(\omega^{(i)}\right)^2}, \tag{1.8a}$$

$$\delta := \frac{\lambda_{\text{hom}}^{(j)}}{r_{\text{hom}} c_{\text{hom}}} \frac{1}{\omega^{(i)}}, \tag{1.8b}$$

$$\gamma := \frac{G_{\text{hom } ij}}{\omega^{(i)} \sqrt{m c_{\text{hom}} l}}. \tag{1.8c}$$

Next we optimize the system infinity norm, by exploiting the results in Section 2 of Chapter 5. The optimality condition (2.1) of Chapter 5 together with (1.8a) yield:

$$\beta = 1 \Rightarrow \frac{\lambda_{\text{hom}}^{(j)}}{l_{\text{hom}}} = c_{\text{hom}} \left(\omega^{(i)}\right)^2, \tag{1.9}$$

while the optimality condition (2.2) of Chapter 5 together with (1.8b) give:

$$\delta = \sqrt{\frac{3}{2}}\gamma \Rightarrow \frac{\lambda_{\text{hom}}^{(j)}}{r_{\text{hom}}} = \frac{G_{\text{hom } ij}}{l} \sqrt{\frac{3}{2}} \sqrt{\frac{c_{\text{hom}}}{\rho_{\text{hom}}}}. \tag{1.10}$$

On the other hand, from (2.3) of Chapter 5 we have that the system norm is minimized when the modal coupling is maximized. Therefore, we choose the boundary conditions

α_0 and α_l in order to maximize the coupling coefficient $G_{\text{hom } ij}$ between the two chosen electrical and mechanical modes. The following optimization problem arises:

$$\text{find } (\alpha_0, \alpha_l) \in \bar{\mathrm{R}}^+ \times \bar{\mathrm{R}}^+ : \int_0^l \left(\mathsf{w}^{(i)}\right)'' (x)\, \psi^{(j)}(x)\, dx \text{ is maximized,}$$

where we notice that $\psi^{(j)}(x)$ is dependent on the two design parameters.

It is evident that the integral defining $G_{\text{hom } ij}$ is maximized whenever ψ_j is equal to the normalized i-th modal curvature, i.e.

$$\psi_j(x) = \frac{\left(\mathsf{w}^{(i)}\right)'' (x)}{\sqrt{\frac{1}{l}\int_0^l \left(\left(\mathsf{w}^{(i)}\right)'' (x)\right)^2 dx}} = \frac{\left(\mathsf{w}^{(i)}\right)'' (x)}{\omega^{(i)}} \sqrt{\frac{k_{\text{hom}}}{\rho_{\text{hom}}}}.$$

In this instance its value is

$$\max G_{\text{hom } ij} = g_{\text{hom}} \omega^{(i)} \sqrt{\frac{\rho_{\text{hom}}}{k_{\text{hom}}}} l, \tag{1.11}$$

and consequently the modal coupling is

$$\max \gamma = \frac{g_{\text{hom}}}{\sqrt{k_{\text{hom}} c_{\text{hom}}}}. \tag{1.12}$$

REMARK 6. *For a second order line, this condition cannot be satisfied, in general, by a proper choice of the constants α_0, α_l since the modal beam curvature involves hyperbolic functions which cannot represent the electric mode shape. This problem will be solved in Chapter 7 when dealing with the fourth order transmission line.*

1.4. Application sample. As an application sample we focus on the vibration suppression of the lowest mechanical mode shape ($i = 1$) by its coupling with the lowest ($j = 1$) electric mode shape. Thus,

$$\mathsf{w}^{(1)}(x) = A_1 \cos\left(\eta^{(1)} \frac{x}{l}\right) + A_2 \cosh\left(\eta^{(1)} \frac{x}{l}\right) + A_3 \sin\left(\eta^{(1)} \frac{x}{l}\right) + A_4 \sinh\left(\eta^{(1)} \frac{x}{l}\right), \tag{1.13}$$

$$\left(\omega^{(1)}\right)^2 = \left(\frac{\eta^{(1)}}{l}\right)^4 \frac{k_{\text{hom}}}{\rho_{\text{hom}}}, \tag{1.14}$$

with

$$\begin{cases} A_1 = -A_2 = -1 \\ A_3 = -A_4 = 0.734095 \\ \eta^{(1)} = 1.875104 \end{cases}.$$

On the other hand the electric mode shape is

$$\psi^{(1)}(x) = C_1 \cos\left(\zeta^{(1)} \frac{x}{l}\right) + C_2 \sin\left(\zeta^{(1)} \frac{x}{l}\right), \quad \zeta^{(1)} = l\sqrt{\lambda^{(1)}_{\text{hom}}}, \tag{1.15}$$

where the eigenvalue $\zeta^{(1)}$ is the lowest root of

$$\tan\left(\zeta^{(1)}\right) = \frac{\left(\bar{\alpha}_0 + \bar{\alpha}_l\right)\zeta^{(1)}}{\zeta^{(1)} - \bar{\alpha}_0 \bar{\alpha}_l}, \quad \bar{\alpha}_0 = \alpha_0 l, \quad \bar{\alpha}_l = \alpha_l l. \tag{1.16}$$

The constants C_1 and C_2 are given in terms of the constant $\bar{\alpha}_0$ and the eigenvalue $\zeta^{(1)}$ by the following:

(1.17a)

$$(C_1)^2 = \frac{4\left(\zeta^{(1)}\right)^3}{\left(\frac{1}{2}\left(\left(\zeta^{(1)}\right)^2 - (\bar{\alpha}_0)^2\right)\sin\left(2\bar{\eta}^{(1)}\right) + 2\bar{\lambda}_1\left(\left(\zeta^{(1)}\right)^2 + (\bar{\alpha}_0)^2 + 2\bar{\alpha}_0\sin^2\left(\zeta^{(1)}\right)\right)\right)},$$

(1.17b)

$$C_2 = \frac{C_1\bar{\alpha}_0}{\zeta^{(1)}}.$$

By substituting (1.13) and (1.15) into (1.7a), the modal coupling becomes

(1.18)

$$G_{\text{hom }11}(\bar{\alpha}_0, \bar{\alpha}_l) = \left(\eta^{(1)}\right)^2 \frac{g_{\text{hom}}}{l}\int_0^1 \left[-A_1\cos\left(\eta^{(1)}\xi\right) + A_2\cosh\left(\eta^{(1)}\xi\right) - A_3\sin\left(\eta^{(1)}\xi\right) + A_4\sinh\left(\eta^{(1)}\xi\right)\right] \left[C_1\cos\left(\zeta^{(1)}\xi\right) + C_2\sin\left(\zeta^{(1)}\xi\right)\right] d\xi,$$

where, after cumbersome manipulations, each integral can be expressed as the product of two trigonometric functions evaluated at $\eta^{(1)}$ or $\zeta^{(1)}$. The optimization problem can be numerically solved as any standard two dimensional minimization problem in terms of the unknown positive variables $\bar{\alpha}_0$, $\bar{\alpha}_l$. Indeed for any pair $(\bar{\alpha}_0, \bar{\alpha}_l)$ we can find the corresponding lowest electric eigenvalue $\zeta^{(1)}$ by solving the trascendental equation (1.16); from the eigenvalue $\zeta^{(1)}$ and the parameter $\bar{\alpha}_0$, the constants C_1 and C_2 can be found by evaluating formulas (1.17). Thus for each pair $(\bar{\alpha}_0, \bar{\alpha}_l)$ the modal coupling $G_{\text{hom }11}$ is computed by the use of (1.18) and its absolute value is maximized.

We remark that the same approach may be applied to any mechanical boundary condition, and to any choice of the mechanical and electric mode to be resonantly coupled.

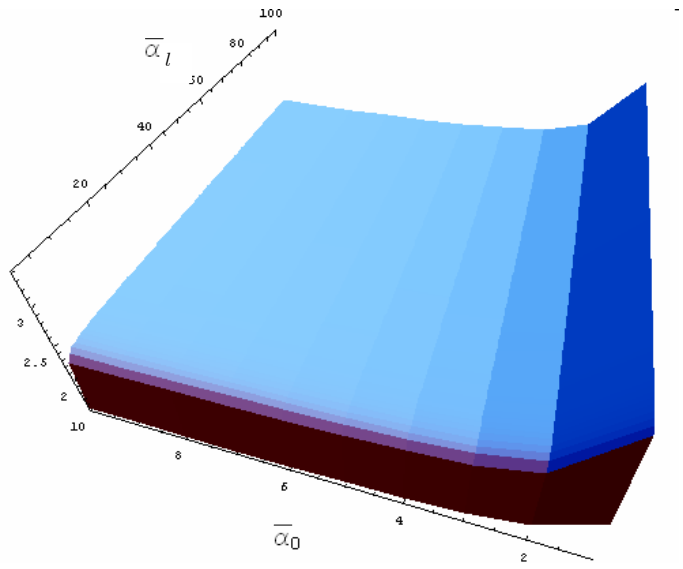

FIGURE 1. Plot of $lG_{\text{hom }11}/g_{\text{hom}}$ for $\bar{\alpha}_0 \in [0, 10]$ and $\bar{\alpha}_l \in [0, 100]$.

In this instance, as shown in Figure 1, the numerical maximization yields

$$\bar{\alpha}_0 = 0, \quad \bar{\alpha}_l = +\infty.$$

Thus, the electric circuit should be open circuited at the left hand and short circuited to ground at the right end. The trascendental equation (1.16) gives

$$\cos\left(\zeta^{(1)}\right) = 0 \Rightarrow \zeta^{(1)} = \frac{\pi}{2}. \tag{1.19}$$

and the generic circuit eigenvalue is:

$$\zeta^{(j)} = \frac{\pi}{2}(2j-1) \Rightarrow \lambda^{(j)}_{\text{hom}} = \frac{1}{l^2}\left(\frac{\pi}{2}(2j-1)\right)^2.$$

The constants C_1 and C_2 are found from (1.17):

$$C_1 = \sqrt{2}, \quad C_2 = 0, \tag{1.20}$$

and the generic circuit mode shapes is

$$\psi^{(j)}(x) = \frac{\sqrt{2}}{l}\cos\left(\frac{\pi}{2}(2j-1)\frac{x}{l}\right).$$

By substituting (1.19) and (1.20) into (1.18) and the coupling becomes:

$$G_{\text{hom }11}(\bar{\alpha}_0, \bar{\alpha}_l) = \frac{g_{\text{hom}}}{l}\varrho, \qquad \varrho = 3.3706.$$

When it is compared to the maximum achievable coupling in (1.11) we have

$$\frac{G_{\text{hom }11}(\bar{\alpha}_0, \bar{\alpha}_l)}{\max G_{\text{hom }11}} = \frac{\varrho}{\left(\eta^{(1)}\right)^2} = 89.9\%,$$

and similarly, from (1.12), the modal coupling is

$$\frac{\gamma}{\max \gamma} = \frac{\varrho}{\left(\eta^{(1)}\right)^2}.$$

From (1.9), the value of the optimal inductance is

$$l_{\text{hom}} = \frac{\pi^2}{4l^2 c_{\text{hom}}\left(\omega^{(1)}\right)^2} \Rightarrow L = \varepsilon\frac{\pi^2}{4c_{\text{hom}}\left(\omega^{(1)}\right)^2 l^2}, \tag{1.21}$$

and from (1.10), the value of the optimal resistance is

$$r_{\text{hom}} = \frac{1}{g_{\text{hom}}}\frac{\pi^2}{4\varrho}\sqrt{\frac{2}{3}}\sqrt{\frac{\rho_{\text{hom}}}{c_{\text{hom}}}} \Rightarrow R = \varepsilon\frac{1}{g_{\text{hom}}}\frac{\pi^2}{4\varrho}\sqrt{\frac{2}{3}}\sqrt{\frac{\rho_{\text{hom}}}{c_{\text{hom}}}}. \tag{1.22}$$

The optimal inductances and resistances are decreasing linearly with the cell size ε, for prescribed capacitance per unit length. The quality factor of the floating impedance

$$Q_{RL} := \frac{R}{\omega^{(i)}L} = \frac{1}{\gamma}\sqrt{\frac{2}{3}}$$

is constant with the cell size ε.

REMARK 7. *By looking at Figure 1, we notice that the dimensionless coupling parameter γ is almost insensitive to variations of the right boundary impedance. This may be used to design adaptive networks, where all of the floating inductors are fixed and only the right boundary impedance is slightly adjusted for fine tuning.*

2. Refined model

2.1. Governing equations. For ordinary engineering applications the number of available transducers is limited and the exact periodicity of the system is not guaranteed. Therefore, the forecasts of the homogenized model may not be sufficiently reliable when dimensioning PEM beams. In this Section we start from the design rules stemming from the homogenized model and account for the discrete nature of the electric circuit, together with the material discontinuities of the stepped beam.

The optimization of the homogenized PEM beam suggests to short-circuit the last piezoelectric element to ground and leave the first one open circuited (see equations (1.4) and (1.5)).

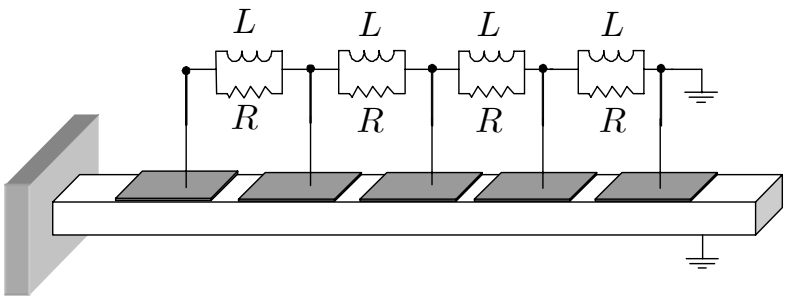

FIGURE 2. Sketch of the cantilever PEM beam equipped with the optimized second order transmission line.

We consider N_P piezoelectric elements as transducers for the vibration control system, while one additional element labeled with a as an actuator (in this case, we have N_P+1 transducers and N segments). In this case, it is convenient to number the piezoelectric elements used for control purposes from 0 to N_P-1, as we move from the free end to the clamped end as shown in Figure 3. This renumbering rule[1] will be named $\mathfrak{r}$,

$$\mathfrak{r} : \{0, ..., N_P - 1\} \to \{1, ..., N + 1\}.$$

The mechanical governing equations are derived from (3.12) of Chapter 2:

$$\sum_{h=1}^{N} \int_{S_h} k_h w''(x,t)\tilde{w}''(x)dx - g \sum_{h=1}^{N_P-1} \dot{\psi}_h(t) \left(\tilde{w}'(X_{\mathfrak{r}(h)+1}) - \tilde{w}'(X_{\mathfrak{r}(h)})\right) - g\dot{\psi}_a(t) \left(\tilde{w}'(X_{a+1}) - \tilde{w}'(X_a)\right) = -\sum_{h=1}^{N} \int_{S_h} \rho_h \ddot{w}(x,t)\tilde{w}(x)dx,$$

where the contribution of the piezoelectric actuator has been isolated and equal transducers are employed (all the g's and C's are equal). Since it does not cause misunderstandings, we use the same letter for either the flux-linkages with the two different numbering.

On the other hand, by considering vanishing initial conditions, the time evolution of the flux linkages are

$$C\,\ddot{\boldsymbol{\psi}} + \frac{1}{L}\mathring{\mathcal{N}}\boldsymbol{\psi} + \frac{1}{R}\mathring{\mathcal{N}}\dot{\boldsymbol{\psi}} + \mathbf{i} = 0, \tag{2.1}$$

[1]The map $\mathfrak{r}$ associates to each transducer the location of its left node on the stepped beam.

where the dimensionless $(N_P-1)\times(N_P-1)$ matrix

$$\mathring{\mathcal{N}}=\begin{bmatrix} 2 & -1 & 0 & ... & 0 \\ -1 & 2 & -1 & ... & ... \\ 0 & -1 & ... & ... & 0 \\ ... & ... & ... & 2 & -1 \\ 0 & ... & 0 & -1 & 1 \end{bmatrix},$$

the (N_P-1)-vectors $\boldsymbol{\psi}$ and $\mathbf{i}$ collecting the non-vanishing transducers flux-linkages and the corresponding piezoelectric currents induced by the mechanical vibrations have been introduced. In particular, the h-th entry of the piezoelectric currents vector is

$$i_h = g\left(\dot{w}'(X_{\mathfrak{r}(h)+1},t)-\dot{w}'(X_{\mathfrak{r}(h)},t)\right).$$

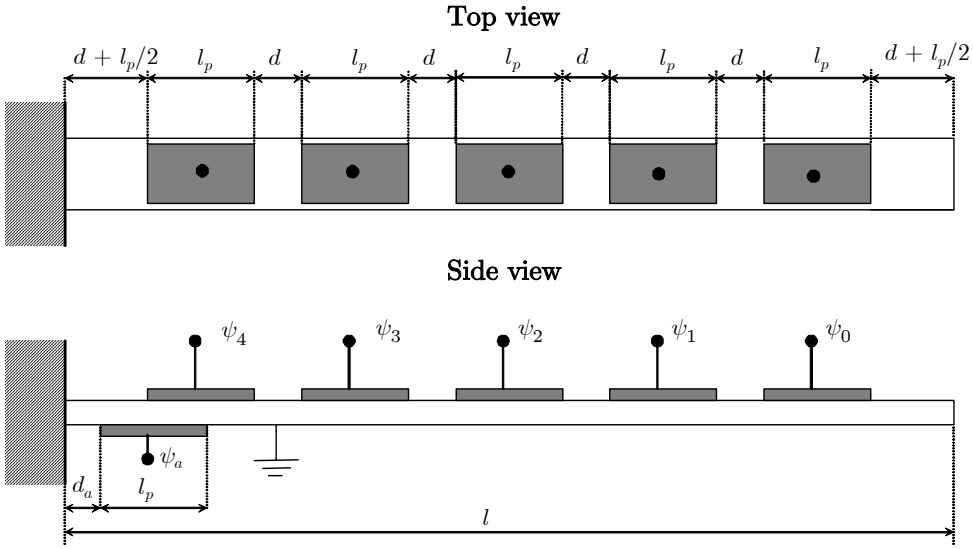

FIGURE 3. Sketch of the stepped beam used for testing the transmission line.

2.2. Reduced model and optimization. We consider the same problem treated within the homogenized model. We follow the same procedure for deriving a two degrees of freedom model of the PEM beam, but, instead of using the homogenized modal properties, we exploit the modal characteristics of the stepped beam and of the lumped circuit. The modal reduction onto the i-th mechanical mode shape $\mathsf{w}^{(i)}$ and j-th electrical mode shape $\mathring{\mathbf{v}}^{(j)}$ is developed. The mechanical mode shape is determined by the use of the LEN method, or any other approximate method, as explained in Chapter 3, while the electric mode shape is the j-th eigenvector of the matrix $\mathring{\mathcal{N}}$, i.e.:

$$\mathring{\mathcal{N}}\mathring{\mathbf{v}}^{(j)}=\mathring{\lambda}^{(j)}\mathring{\mathbf{v}}^{(j)}. \tag{2.2}$$

where we normalize $\mathring{\mathbf{v}}^{(j)}$ to one. By assuming

$$w(x,t)=\mathsf{w}^{(i)}(x)\,W_i(t), \quad \boldsymbol{\psi}(t)=\mathring{\mathbf{v}}^{(j)}\Psi_j(t),$$

the following coupled evolution equations for the modal coefficients $W_i(t)$ and $\Psi_j(t)$ are obtained:

$$\begin{cases} m\ddot{W}_i(t)+m\omega_i^2 W_i(t)-G_{ij}\,\dot{\Psi}_j(t)=F_i(t), \\ C\ddot{\Psi}_j(t)+\dfrac{1}{L}\mathring{\lambda}^{(j)}\Psi_j(t)+\dfrac{1}{R}\mathring{\lambda}^{(j)}\dot{\Psi}_j(t)+G_{ij}\,\dot{W}_i(t)=0 \end{cases}, \tag{2.3}$$

where the modal parameters are defined by:

$$G_{ij} := \mathbf{d}^{\mathrm{T}}\mathring{\mathbf{v}}^{(j)}, \qquad F_i(t) := g\left(\mathsf{w}_i'(X_{a+1}) - \mathsf{w}_i'(X_a)\right)\dot{\Psi}_a(t),$$

with

$$\mathbf{d} = g\left[\begin{array}{cccc} \mathsf{w}_i'(X_{\mathfrak{r}(0)+1}) - \mathsf{w}_i'(X_{\mathfrak{r}(0)}) & \cdots & \mathsf{w}_i'(X_{\mathfrak{r}(N_P-1)+1}) - \mathsf{w}_i'(X_{\mathfrak{r}(N_P-1)}) \end{array}\right]^{\mathrm{T}},$$

estimating the average beam curvatures at the piezoelectric transducers. The non-dimensio-

-nalization of (2.3) into the form (1.4) of Chapter 5, yields:

$$\beta = \frac{\mathring{\lambda}^{(j)}}{LC}\frac{1}{\left(\omega^{(i)}\right)^2}, \quad \delta = \frac{\mathring{\lambda}^{(j)}}{RC}\frac{1}{\omega^{(i)}}, \quad \gamma = \frac{G_{ij}}{\omega^{(i)}\sqrt{mC}}. \tag{2.4}$$

The optimal inductance and resistance are found by the use of (2.1) and (2.2) in Chapter 5:

$$L = \frac{\mathring{\lambda}^{(j)}}{C}\frac{1}{\left(\omega^{(i)}\right)^2}, \quad R = \sqrt{\frac{2}{3}}\frac{\mathring{\lambda}^{(j)}}{\gamma\omega^{(i)}C}. \tag{2.5}$$

We remark that the radian frequency appearing in (2.5) accounts for the material discontinuities of the segmented beam, while that used in (1.21) and (1.22) is based on the homogenized model. In the following Section we derive closed-form formulas for evaluating the eigenproperties of the matrix $\mathring{\mathcal{N}}$.

2.3. Eigenproperties of $\mathring{\mathcal{N}}$. We consider the eigenvalue problem (2.2). We write the tridiagonal system in the form of three-point boundary value difference problem:

$$\left\{\begin{array}{l} -\mathring{v}_{i-1} + \left(2 - \mathring{\lambda}\right)\mathring{v}_i - \mathring{v}_{i+1} = 0, \quad 1 \le i \le N_P - 2, \\ \mathring{v}_0 = 0, \quad -\mathring{v}_{N_P-2} + \left(1 - \mathring{\lambda}\right)\mathring{v}_{N_P-1} = 0. \end{array}\right. . \tag{2.6}$$

By following [**Samarskii and Nikolaev (1989)**], the general solution to the given constant coefficients second order difference equation is

$$\mathring{v}_i = c_1 T_i(z) + c_2 U_{i-1}(z), \quad z = 1 - \frac{\mathring{\lambda}}{2}, \tag{2.7}$$

where c_1 and c_2 are arbitrary constants, and the Chebysev polynomials of the first (T) and second (U) type have been introduced:

$$T_i(x) = \left\{\begin{array}{ll} \cos\left[i\arccos\left[x\right]\right], & |x| \le 1 \\ \frac{1}{2}\left[\left(x + \sqrt{x^2-1}\right)^i + \left(x + \sqrt{x^2-1}\right)^{-i}\right], & |x| \ge 1 \end{array}\right. , \tag{2.8a}$$

$$U_i(x) = \left\{\begin{array}{ll} \dfrac{\sin\left[(i+1)\arccos\left[x\right]\right]}{\sin\left[\arccos\left[x\right]\right]}, & |x| \le 1 \\ \dfrac{1}{2\sqrt{x^2-1}}\left[\left(x + \sqrt{x^2-1}\right)^{i+1} - \left(x + \sqrt{x^2-1}\right)^{-(i+1)}\right], & |x| \ge 1 \end{array}\right. . \tag{2.8b}$$

We remark that these polynomials frequently arise in mathematical physics and that they may also be obtained by the following recursive relations:

$$\begin{cases} T_{i+2}(x) = 2xT_{i+1}(x) - T_i(x), & i \geq 0 \\ T_0(x) = 1, \qquad T_1(x) = x \\ T_{-i}(x) = T_i(x) \end{cases}, \tag{2.9a}$$

$$\begin{cases} U_{i+2}(x) = 2xU_{i+1}(x) - U_i(x), & i \geq 0 \\ U_0(x) = 1, \qquad U_1(x) = 2x \\ U_{-i}(x) = -U_{i-2}(x) \end{cases}. \tag{2.9b}$$

The constants c_1 and c_2 are found by imposing the boundary conditions

$$\mathring{v}_0 = c_1 = 0, \quad -\mathring{v}_{N_P-2} + \left(1 - \mathring{\lambda}\right)\mathring{v}_{N_P-1} = c_2\left(-U_{N_P-3}(z) + 2zU_{N_P-2}(z)\right) = 0,$$

where the above definitions of the Chebysev polynomials have been accounted for. Since we are seeking a non-trivial solution to (2.6), $c_2 \neq 0$, we have the condition

$$\left(-U_{N_P-3}(z) + 2zU_{N_P-2}(z)\right) = 0, \tag{2.10}$$

which determines the solution in the form

$$v_i = c_2 U_{i-1}(z). \tag{2.11}$$

The roots of the polynomial equation (2.10) are found by the use of (2.9b)

$$\left(-U_{N_P-3}(z) + (2z-1)U_{N_P-2}(z)\right) = U_{N_P-1}(z) - U_{N_P-2}(z) = 0.$$

Therefore, from (2.8b) we get

$$\frac{\sin\left[N_P \arccos[z]\right]}{\sin\left[\arccos[z]\right]} = \frac{\sin\left[(N_P-1)\arccos[z]\right]}{\sin\left[\arccos[z]\right]} \Rightarrow z = \cos\frac{(2k-1)}{(2N_P-1)}\pi, \quad k = 1, ..., N_P - 1,$$

and from the definition of z, the eigenvalues become

$$\mathring{\lambda}^{(j)} = 2\left(1 - \cos\frac{(2j-1)}{(2N_P-1)}\pi\right) = 4\sin^2\frac{(2j-1)}{2(2N_P-1)}\pi, \quad j = 1, ..., N_P - 1. \tag{2.12}$$

Similarly from (2.11), the eigenvectors are

$$\mathring{v}_i^{(j)} = \frac{2}{\sqrt{2N_P-1}}\sin\left[i\frac{(2j-1)\pi}{(2N_P-1)}\right], \quad i, j = 1, ..., N_P - 1. \tag{2.13}$$

where the constant c_2 has been chosen in order to have an orthonormal set.

Therefore, the optimal values of the inductance and resistance can be computed by substituting (2.12) and (2.13) into (2.5).

It is worthwhile to notice that the eigenvalues $\lambda_{\text{hom}}^{(j)}$ represent an approximation of the eigenvalues $\mathring{\lambda}^{(j)}$ divided by the squared step size ε^2:

$$\frac{\left(\mathring{\lambda}^{(j)}/\varepsilon^2\right)}{\mathring{\lambda}_{\text{hom}}^{(j)}} = (N_P)^2\frac{4\sin^2\dfrac{\pi(2j-1)}{2(2N_P-1)}}{\left(\dfrac{\pi}{2}(2j-1)\right)^2} = 1 + \frac{1}{N_P} + o\left(\frac{1}{N_P}\right),$$

where we used $N_P = l/\varepsilon$. Similar considerations may be drawn for the eigenvectors.

3. Sensitivity analysis

In this Section we consider the effects of variations of the inductances, with respect to their optimal common value, on the system damping performances. The different inductances are counted from the free end as shown in Figure 4.

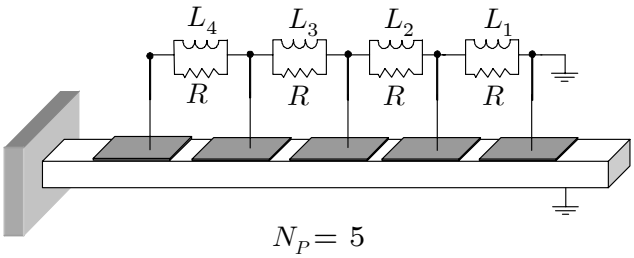

FIGURE 4. Numbering of the unequal inductors in the second order transmission line.

The electric governing equation (2.1) becomes

$$C\,\ddot{\boldsymbol{\psi}} + \mathcal{L}\boldsymbol{\psi} + \frac{1}{R}\mathring{\mathcal{N}}\dot{\boldsymbol{\psi}} + \mathbf{i} = 0,$$

with

$$\mathcal{L} = \begin{bmatrix} \frac{1}{L_1}+\frac{1}{L_2} & -\frac{1}{L_2} & 0 & ... & 0 \\ -\frac{1}{L_2} & \frac{1}{L_2}+\frac{1}{L_3} & -\frac{1}{L_3} & ... & ... \\ 0 & -\frac{1}{L_3} & ... & ... & 0 \\ ... & ... & ... & \frac{1}{L_{N_P-2}}+\frac{1}{L_{N_P-1}} & -\frac{1}{L_{N_P-1}} \\ 0 & ... & 0 & -\frac{1}{L_{N_P-1}} & \frac{1}{L_{N_P-1}} \end{bmatrix}.$$

Each inductance L_i is deviating with respect to the optimal value in (2.5) of a quantity ΔL_i. For small variations, the matrix $\mathcal{L}$ may be written as

$$\mathcal{L} \simeq \frac{1}{L}\mathcal{N},$$

where the dimensionless matrices

$$\mathcal{N} = \mathring{\mathcal{N}} + \Delta\mathcal{N}, \qquad \Delta\mathcal{N} = \begin{bmatrix} X_1+X_2 & -X_2 & 0 & ... & 0 \\ -X_2 & X_2+X_3 & -X_3 & ... & ... \\ 0 & -X_3 & ... & ... & 0 \\ ... & ... & ... & X_{N_P-2}+X_{N_P-1} & -X_{N_P-1} \\ 0 & ... & 0 & -X_{N_P-1} & X_{N_P-1} \end{bmatrix},$$

and the dimensionless variations

$$X_k = -\frac{\Delta L_k}{L},$$

have been introduced.

The presence of these deviations induces changes in the modal parameters β and γ, which affect the system effectiveness according to the sensitivity formula for the small coupling case (3.2) of Chapter 5, which is here recalled:

$$\|H_p\|_\infty = \left\|H_{p_{opt}}\right\|_\infty + \frac{1}{\gamma^2}\,|\Delta\beta| - \frac{\sqrt{2}}{\gamma^2}\Delta\gamma. \tag{3.1}$$

The parameters β depends linearly on the j-th eigenvalue of the matrix $\mathcal{N}$, while γ depends linearly on the j-th eigenvector (see equation (2.4)). Therefore, it is crucial to

determine the eigenproperties sensitivity of $\mathcal{N}$ with respect to the X_j. In particular the variations of β and γ are related to the deviations X_k and can be expressed by:

$$\Delta\beta = \frac{1}{\mathring{\lambda}^{(j)}} \sum_{k=1}^{N_P-1} \mathring{\partial}_{,k} \left[\lambda^{(j)}\right] X_k, \qquad \Delta\gamma = \frac{\gamma}{\mathbf{d}^{\mathrm{T}}\mathring{\mathbf{v}}^{(j)}} \mathbf{d}^{\mathrm{T}} \sum_{k=1}^{N_P-1} \mathring{\partial}_{,k} \left[\mathbf{v}^{(j)}\right] X_k, \tag{3.2}$$

where $\mathring{\partial}_{,k}$ denotes partial differentiation with respect to X_k and consequent evaluation at the unperturbed state.

3.1. Problem statement. The eigenvalue problem is written as

$$\mathcal{N}\mathbf{v}^{(j)} = \lambda^{(j)}\mathbf{v}^{(j)}, \tag{3.3a}$$

$$\left(\mathbf{v}^{(j)}\right)^{\mathrm{T}} \mathbf{v}^{(j)} = 1, \tag{3.3b}$$

where also the normalization condition has been accounted for.

To obtain the derivatives of the eigenpair $\left(\lambda^{(j)}, \mathbf{v}^{(j)}\right)$ with respect to the perturbation X_k, we differentiate equation (3.3) with respect to X_k and evaluate it at the unperturbed state (see e.g. [**El-Kady and Al-Ohaly (1997)**]):

$$\left(\mathring{\mathcal{N}} - \mathring{\lambda}^{(j)}\mathbf{1}\right)\left(\mathring{\partial}_{,k}\left[\mathbf{v}^{(j)}\right]\right) - \mathring{\mathbf{v}}^{(j)}\left(\mathring{\partial}_{,k}\left[\lambda^{(j)}\right]\right) = -\left(\mathring{\partial}_{,k}\left[\Delta\mathcal{N}\right]\right)\mathring{\mathbf{v}}^{(j)}, \tag{3.4a}$$

$$\left(\mathring{\mathbf{v}}^{(j)}\right)^{\mathrm{T}}\left(\mathring{\partial}_{,k}\left[\mathbf{v}^{(j)}\right]\right) = 0, \tag{3.4b}$$

where $\mathbf{1}$ denotes the $(N_P-1)\times(N_P-1)$ identity matrix.

The matrix $\left(\mathring{\partial}_{,k}\left[\Delta\mathcal{N}\right]\right)$ has the very simple form:

$$\left(\mathring{\partial}_{,k}\left[\Delta\mathcal{N}\right]\right) = \mathbf{e}_k\mathbf{e}_k^{\mathrm{T}}, \tag{3.5}$$

where

$$\mathbf{e}_k^{\mathrm{T}} = \left[\begin{array}{ccccccc} 0 & \cdots & -1 & 1 & 0 & \cdots & 0 \end{array}\right],$$

and the -1 is at the$(k-1)$-th entry, and for k equal to 1 only the first element of $\mathbf{e}_k^{\mathrm{T}}$ is not vanishing and equal to 1.

3.2. Eigenvalues sensitivity. In order to find the eigenvalues sensitivity, we simply multiply equation (3.4a) by $\left(\mathring{\mathbf{v}}^{(j)}\right)^{\mathrm{T}}$ and obtain

$$\mathring{\partial}_{,k}\left[\lambda^{(j)}\right] = \left(\mathring{\mathbf{v}}^{(j)}\right)^{\mathrm{T}}\left(\mathring{\partial}_{,k}\left[\Delta\mathcal{N}\right]\right)\mathring{\mathbf{v}}^{(j)}, \tag{3.6}$$

where the unperturbed eigenvalue problem (2.2), with orthonormal eigenvectors, has been employed.

By using equation (3.5) the sensitivity in (3.6) can be written as

$$\mathring{\partial}_{,k}\left[\lambda^{(j)}\right] = \left(\left(\mathring{\mathbf{v}}^{(j)}\right)^{\mathrm{T}}\mathbf{e}_k\right)^2 = \left(\frac{1}{2N_P-1}\sin\left[j\frac{(2j-1)\,\pi}{(2N_P-1)}\right] - \frac{1}{2N_P-1}\sin\left[(j-1)\frac{(2j-1)\,\pi}{(2N_P-1)}\right]\right)^2,$$

which, after some algebraic manipulations becomes:

$$\mathring{\partial}_{,k}\left[\lambda^{(j)}\right] = \frac{4}{2N_P-1}\mathring{\lambda}^{(j)}\cos^2\left[\frac{(2j-1)\,(2k-1)\,\pi}{2\,(2N_P-1)}\right]. \tag{3.7}$$

The sensitivity of the eigenvalues of the considered system may be found also following the procedure developed by [**Soong and Bogdanoff (1963)**], dealing with transmission

matrices in disordered chains. We remark that the sensitivity (3.7) is positive; therefore, small deviations X_k always increase the eigenvalues.

By substituting (3.7) into (3.2) we obtain

$$\Delta\beta = \frac{4}{2N_P - 1} \sum_{k=1}^{N_P-1} \cos^2 \left[\frac{(2j-1)(2k-1)\pi}{2(2N_P-1)} \right] X_k,$$

which provides the global tuning-loss induced by the deviations of the inductances.

3.3. Eigenvectors sensitivity. We multiply equation (3.4a) by $\left(\mathring{\mathbf{v}}^{(n)}\right)^{\mathrm{T}}$ with $n \neq j$ and obtain

$$\left(\mathring{\lambda}^{(n)} - \mathring{\lambda}^{(j)}\right) \left(\mathring{\mathbf{v}}^{(n)}\right)^{\mathrm{T}} \left(\mathring{\partial}_{,k} \left[\mathbf{v}^{(j)}\right]\right) = - \left(\mathring{\mathbf{v}}^{(n)}\right)^{\mathrm{T}} \left(\mathring{\partial}_{,k} \left[\Delta\mathcal{N}\right]\right) \mathring{\mathbf{v}}^{(j)}.$$

Hence by accounting also for equation (3.4b) we obtain the following modal expansion for the eigenvector sensitivity:

$$\mathring{\partial}_{,k} \left[\mathbf{v}^{(j)}\right] = - \sum_{\substack{n=1 \\ n\neq j}}^{N_P-1} \frac{\left(\mathring{\mathbf{v}}^{(n)}\right)^{\mathrm{T}} \left(\mathring{\partial}_{,k} \left[\Delta\mathcal{N}\right]\right) \mathring{\mathbf{v}}^{(j)}}{\left(\mathring{\lambda}^{(n)} - \mathring{\lambda}^{(j)}\right)} \mathring{\mathbf{v}}^{(n)}. \tag{3.8}$$

By using equation (3.5) the sensitivity (3.8) becomes:

$$\mathring{\partial}_{,k} \left[\mathbf{v}^{(j)}\right] = - \sum_{\substack{n=1 \\ n\neq j}}^{N_P-1} \frac{\left(\mathbf{e}_k^{\mathrm{T}} \mathring{\mathbf{v}}^{(j)}\right) \left(\mathbf{e}_k^{\mathrm{T}} \mathring{\mathbf{v}}^{(n)}\right)}{\left(\mathring{\lambda}^{(n)} - \mathring{\lambda}^{(j)}\right)} \mathring{\mathbf{v}}^{(n)} =$$

$$\frac{4}{2N_P - 1} \sum_{\substack{n=1 \\ n\neq j}}^{N_P-1} \frac{\sqrt{\mathring{\lambda}^{(n)} \mathring{\lambda}^{(j)}}}{\left(-\mathring{\lambda}^{(n)} + \mathring{\lambda}^{(j)}\right)} \cos \left[\frac{(2k-1)(2n-1)\pi}{2(2N_P-1)} \right] \cos \left[\frac{(2k-1)(2j-1)\pi}{2(2N_P-1)} \right] \mathring{\mathbf{v}}^{(n)}.$$

By substituting the above expression into (3.2) we obtain the variation of the modal coupling $\Delta\gamma$ induced by the inductances deviations.

4. Effect of parameters uncertainties

Starting from the sensitivities of the system eigenpairs with respect to the perturbations X_k, we study the effects of uncertainties. We assume that the parameters X_k are equally distributed independent random variables normally distributed with zero mean. The probability density functions are

$$f_X(x) = \frac{1}{\sqrt{2\pi}\sigma_X} \exp\left(-\frac{1}{2} \left(\frac{x}{\sigma_X} \right)^2 \right),$$

where σ_X denotes the common standard deviation.

It is well known (see [**Breiman (1969)**]) that if the random variables are independent

$$\forall c_1, c_2, ..., c_N \qquad E\left[\sum_{j=1}^{N} c_j X_j \right] = \sum_{j=1}^{N} c_i E\left[X_j\right],$$

and

$$\forall c_1, c_2, ..., c_N \qquad V\left[\sum_{j=1}^{N} c_j X_j \right] = \sum_{j=1}^{N} c_j^2 V\left[X_j\right].$$

Furthermore, the linear combination of independent normal variables is still normal.

4.1. Moments of $\Delta\beta$. Therefore from (3.2) we know hat $\Delta\beta$ is a normal variables whose mean value and variance are

$$E\left[\Delta\beta\right]=0, \qquad V\left[\Delta\beta\right]=\left(\frac{1}{\mathring{\lambda}^{(j)}}\right)^2\left[\sum_{k=1}^{N_P-1}\left(\mathring{\partial}_{,k}\left[\lambda^{(j)}\right]\right)^2\right](\sigma_X)^2.$$

The factor in square brackets may be evaluated from (3.7):

$$\sum_{k=1}^{N_P-1}\left(\mathring{\partial}_{,k}\left[\lambda^{(j)}\right]\right)^2=4^2\left(\frac{4}{2N+1}\right)^2\sin^4\left(\frac{(2j-1)}{2\,(2N+1)}\pi\right)$$
$$\sum_{k=1}^{N_P-1}\left(\cos^4\left[\frac{(2j-1)\,(2k-1)\,\pi}{2\,(2N+1)}\right]\right)=\frac{3}{2N_P-1}\left(\mathring{\lambda}^{(j)}\right)^2.$$

Hence, the variance of $\Delta\beta$ is

$$V\left[\Delta\beta\right]=\frac{3}{2N_P-1}\left(\sigma_X\right)^2.$$

Its standard deviation $\sigma_{\Delta\beta}$ decreases to zero with the square root of the matrix dimension, i.e.:

$$\sigma_{\Delta\beta}=\sqrt{\frac{3}{2N_P-1}}\sigma_X.$$

4.2. Moments of $\Delta\gamma$. From (3.2), also the random variable $\Delta\gamma$ is Gaussian and its mean value and variance are

$$E\left[\Delta\gamma\right]=0, \qquad V\left[\Delta\gamma\right]=\left(\frac{\gamma}{\mathbf{d}^{\mathrm{T}}\mathring{\mathbf{v}}^{(j)}}\right)^2\left[\sum_{k=1}^{N_P-1}\left(\mathbf{d}^{\mathrm{T}}\left(\mathring{\partial}_{,k}\left[\mathbf{v}^{(j)}\right]\right)\right)^2\right](\sigma_X)^2.$$

In this case it is not possible to derive a simple closed-form formula as that presented for the variance of $\Delta\beta$. Nevertheless, the variance can be easily computed in terms of the vector $\mathbf{d}$ and the number of transducers N_P:

$$V\left[\Delta\gamma\right]=\gamma^2 f_1^{(j)}\left(\mathbf{d},N_P\right)\left(\sigma_X\right)^2,$$

where

$$f_1^{(j)}\left(\mathbf{d},N_P\right)=\left(\frac{1}{\mathbf{d}^{\mathrm{T}}\mathring{\mathbf{v}}^{(j)}}\right)^2\left(\frac{4}{2N_P-1}\right)^2$$
$$\sum_{k=1}^{N_P-1}\left(\sum_{\substack{n=1\\n\neq j}}^{N_P-1}\frac{\sqrt{\mathring{\lambda}^{(n)}\mathring{\lambda}^{(j)}}}{\left(-\mathring{\lambda}^{(n)}+\mathring{\lambda}^{(j)}\right)}\cos\left[\frac{(2k-1)\,(2n-1)\,\pi}{2\,(2N_P-1)}\right]\cos\left[\frac{(2k-1)\,(2j-1)\,\pi}{2\,(2N_P-1)}\right]\mathbf{d}^{\mathrm{T}}\mathring{\mathbf{v}}^{(n)}\right)^2,$$

is a function which depends only on the number of piezoelectric elements N_P and on the modal curvature $\mathbf{d}$. We explicitly remark that if the modal curvature is parallel to the j-th unperturbed eigenvector $\mathring{\mathbf{v}}^{(j)}$, the function $f_1^{(j)}$ vanishes for every N_P.

For example, when the modal curvature is not parallel to the j-th unperturbed eigenvector $\mathring{\mathbf{v}}^{(j)}$, but can be expressed as $\mathring{\mathbf{v}}^{(j)}+\varepsilon\mathring{\mathbf{v}}^{(h)}$, the function $f_1^{(j)}$ gives the following simple result:

$$f_1^{(j)}\left(\mathring{\mathbf{v}}^{(j)}+\varepsilon\mathring{\mathbf{v}}^{(h)},N_P\right)=\varepsilon^2\frac{\mathring{\lambda}^{(h)}\mathring{\lambda}^{(j)}}{\left(-\mathring{\lambda}^{(h)}+\mathring{\lambda}^{(j)}\right)^2}\left(\frac{2}{2N_P-1}\right).$$

As another example, if the modal curvature is instead expressed as $\mathring{\mathbf{v}}^{(j)}+\varepsilon_1\mathring{\mathbf{v}}^{(h_1)}+\varepsilon_2\mathring{\mathbf{v}}^{(h_2)}$, with $h_1\neq h_2$, then the function $f_1^{(j)}$ gives:

$$f_1^{(j)}\left(\mathring{\mathbf{v}}^{(j)}+\varepsilon_1\mathring{\mathbf{v}}^{(h_1)}+\varepsilon_2\mathring{\mathbf{v}}^{(h_2)},N_P\right)=(\varepsilon_1)^2\frac{\mathring{\lambda}^{(h_1)}\mathring{\lambda}^{(j)}}{\left(-\mathring{\lambda}^{(h_1)}+\mathring{\lambda}^{(j)}\right)^2}\left(\frac{2}{2N_P-1}\right)+$$
$$+(\varepsilon_2)^2\frac{\mathring{\lambda}^{(h_2)}\mathring{\lambda}^{(j)}}{\left(-\mathring{\lambda}^{(h_2)}+\mathring{\lambda}^{(j)}\right)^2}\left(\frac{2}{2N_P-1}\right)+$$
$$\frac{\mathring{\lambda}^{(j)}\sqrt{\mathring{\lambda}^{(h_1)}\mathring{\lambda}^{(h_2)}}}{\left(-\mathring{\lambda}^{(h_1)}+\mathring{\lambda}^{(j)}\right)\left(-\mathring{\lambda}^{(h_2)}+\mathring{\lambda}^{(j)}\right)}\varepsilon_1\varepsilon_2\left(\frac{2}{2N_P-1}\right)\delta_{|h_1-h_2|1},$$

where δ_{ij} is the Kronecker delta, being 1 if i is equal to j and 0 otherwise. In the general case for an arbitrary modal curvature

$$\mathbf{d}=\sum_{h=1}^{N_P-1}\varepsilon_h\mathring{\mathbf{v}}^{(j)},$$

we obtain

$$f_1^{(j)}(\mathbf{d},N_P)=\frac{1}{(\varepsilon_j)^2}\left(\frac{2}{2N_P-1}\right)\left[\sum_{\substack{k=1\\k\neq j}}^{N_P-1}(\varepsilon_k)^2\frac{\mathring{\lambda}^{(k)}\mathring{\lambda}^{(j)}}{\left(-\mathring{\lambda}^{(k)}+\mathring{\lambda}^{(j)}\right)^2}+\sum_{\substack{k=1\\k\neq j,j-1}}^{N_P-2}\frac{\mathring{\lambda}^{(j)}\sqrt{\mathring{\lambda}^{(k)}\mathring{\lambda}^{(k+1)}}}{\left(-\mathring{\lambda}^{(k)}+\mathring{\lambda}^{(j)}\right)\left(-\mathring{\lambda}^{(k+1)}+\mathring{\lambda}^{(j)}\right)}\varepsilon_k\varepsilon_{k+1}\right]. \tag{4.1}$$

We explicitly remark that $f_1^{(j)}(\mathbf{d},N_P)$ does not depend on the absolute value of $\mathbf{d}$ and that depends only on its direction. The standard deviation is

$$\sigma_{\Delta\gamma}=\gamma\sigma_X\sqrt{f_1^{(j)}(\mathbf{d},N_P)}.$$

4.3. Mixed moments. In this case the random variables $\Delta\gamma$ and $\Delta\beta$ are not independent, since they both depend on the same deviations X_k. Their correlation is

$$\Gamma[\Delta\gamma,\Delta\beta]=E[(\Delta\gamma-E[\Delta\gamma])(\Delta\beta-E[\Delta\beta])]=$$
$$\frac{\gamma}{\mathbf{d}^{\mathrm{T}}\mathring{\mathbf{v}}^{(j)}}\frac{1}{\mathring{\lambda}^{(j)}}\left(\sum_{k=1}^{N_P-1}\mathbf{d}^{\mathrm{T}}\left(\mathring{\partial}_{,k}\left[\mathbf{v}^{(j)}\right]\right)\mathring{\partial}_{,k}\left[\lambda^{(j)}\right]\right)(\sigma_X)^2.$$

Also in this case no closed-form expressions are available, and the following computer oriented formula may be worthwhile:

$$\Gamma[\Delta\gamma,\Delta\beta]=\gamma f_2^{(j)}(\mathbf{d},N_P)(\sigma_X)^2,$$

with

$$f_2^{(j)}(\mathbf{d}, N_P) = \frac{1}{\mathbf{d}^{\mathrm{T}}\mathring{\mathbf{v}}^{(j)}}\left(\frac{4}{2N_P-1}\right)^2$$
$$\sum_{k=1}^{N_P-1}\cos^3\left[\frac{(2k-1)(2j-1)\pi}{2(2N+1)}\right]\sum_{\substack{n=1\\n\neq j}}^{N_P-1}\frac{\sqrt{\mathring{\lambda}^{(n)}\mathring{\lambda}^{(j)}}}{\left(-\mathring{\lambda}^{(n)}+\mathring{\lambda}^{(j)}\right)}\cos\left[\frac{(2k-1)(2n-1)\pi}{2(2N_P-1)}\right]\mathbf{d}^{\mathrm{T}}\mathring{\mathbf{v}}^{(n)}.$$

4.4. Moments of the system norm. From the knowledge of the statistics of $\Delta\beta$ and $\Delta\gamma$ we can compute the expected value of the system infinity norm in (3.1) as we have done in (4.2) of Chapter 5:

$$E\left[\|H_p\|_\infty\right] = \left\|H_{p_{opt}}\right\|_\infty + \sqrt{\frac{2}{\pi}}\frac{1}{\gamma^2}\sqrt{\frac{3}{2N_P-1}}\sigma_X. \tag{4.2}$$

The computation of the variance of $\|H_p\|_\infty$, for small coupling, yields the same result of (4.3) of Chapter 5, even if $\Delta\beta$ and $\Delta\gamma$ are correlated (when the coupling cannot be considered small the results should be modified by accounting for the correlation between $\Delta\beta$ and $\Delta\gamma$, and using the above expression for $f_2^{(j)}(\mathbf{d}, N_P)$).

Indeed, the expected value of the product between $|\Delta\beta|$ and $\Delta\gamma$ is:

$$E\left[(|\Delta\beta|)(\Delta\gamma)\right] = \frac{1}{\mathring{\lambda}^{(j)}}\frac{\gamma}{\mathbf{d}^{\mathrm{T}}\mathring{\mathbf{v}}^{(j)}}\mathbf{d}^{\mathrm{T}}E\left[\left(\left|\sum_{k=1}^{N_P-1}\mathring{\partial}_{,k}\left[\lambda^{(j)}\right]X_k\right|\right)\left(\sum_{k=1}^{N_P-1}\mathring{\partial}_{,k}\left[\mathbf{v}^{(j)}\right]X_k\right)\right],$$

which is equal to

$$\frac{1}{\mathring{\lambda}^{(j)}}\frac{\gamma}{\mathbf{d}^{\mathrm{T}}\mathring{\mathbf{v}}^{(j)}}\mathbf{d}^{\mathrm{T}}\int_{\mathrm{R}^{N_P-1}}\mathrm{E}\left(x_1,..x_{N_P-1}\right)\mathrm{O}\left(x_1,..,x_{N_P-1}\right)dx_1...dx_{N_P-1},$$

where we defined:

$$\left|\sum_{k=1}^{N_P-1}\mathring{\partial}_{,k}\left[\lambda^{(j)}\right]x_k\right|\prod_{k=1}^{N_P-1}f_X(x_k) =: \mathrm{E}\left(x_1,..,x_{N_P-1}\right)$$

and

$$\sum_{k=1}^{N_P-1}\mathring{\partial}_{,k}\left[\mathbf{v}^{(j)}\right]x_k =: \mathrm{O}\left(x_1,..,x_{N_P-1}\right).$$

By noticing that

$$\mathrm{O}\left(x_1,..x_{N_P-1}\right) = -\mathrm{O}\left(-x_1,..,-x_{N_P-1}\right),$$

and

$$\mathrm{E}\left(x_1,..x_{N_P-1}\right) = \mathrm{E}\left(-x_1,..,-x_{N_P-1}\right),$$

it is easy to recognize that

$$E\left[(|\Delta\beta|)(\Delta\gamma)\right] = 0.$$

Thus, from (4.4) we obtain

$$V\left[\|H_p\|_\infty\right] = \left[\left(1-\frac{2}{\pi}\right)\frac{1}{\gamma^4}\left(\frac{3}{2N_P-1}\right)+\frac{2}{\gamma^2}f_1^{(j)}(\mathbf{d}, N_P)\right]\sigma_X^2. \tag{4.3}$$

As the number of transducers increases the effect of the uncertainties X_j on the expected value of the system norm becomes smaller and smaller (see (4.2)). Similarly, from (4.1) and (4.3) we can also see that as the number of transducers is increasing the variance of the system norm is decreasing. Hence, by comparing the achieved results, with

TABLE 1. Beam and PZT transducers geometrical properties

l	a_B	h	l_p	a_P	δ	d	d_a
273.6 mm	19.5 mm	1.90 mm	35.6 mm	17.8 mm	0.27 mm	10.0 mm	5.0 mm

those in equation (4.5) of Chapter 5 we may state that the use of several piezoelectric elements in a transmission line network allows for the mitigation of the effects of statistical uncertainties on the system performances.

5. Experimental Setup

Experiments were conducted to validate the theoretical models presented above[2].

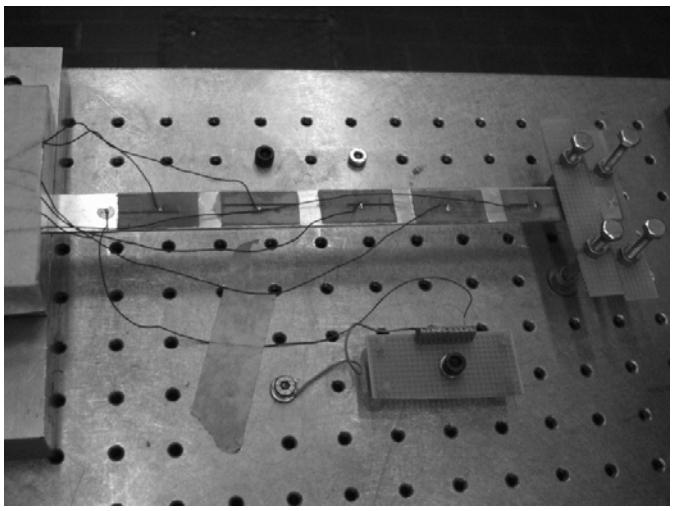

FIGURE 5. Picture of the PEM beam

Frequency response tests were performed on a cantilever aluminum (Al6061-T6) beam with five surface-bonded piezoelectric transducers made of PZT-5H piezoelectric ceramics (Piezo-System T110-H4E-602), sketched in Figure 5 (the corresponding geometrical properties are reported in Table 1, while the constitutive ones are found in Table 2 of Chapter 3).

The same experimental setup, as in Section 4 of Chapter 3 has been used to conduct the tests. The first resonance frequency of the beam when all the piezoelectric elements are short-circuited is

$$\omega^{(1)} = 2\pi \times 20.44\,\text{Hz}.$$

The piezoelectric capacitances have been measured by using the technique described in Section 5.3 and their average value is $C = 52.846$ nF. They differ from the average within 3% (see e.g. [**dell'Isola et al. (2004)**]).

The optimal line inductance can be computed by the use of (2.5), (2.12), the measured resonance frequency $\omega^{(1)}$ and the average capacitance C:

$$L = 138.38 \text{ H}.$$

[2]All the experimental tests have been performed in the Laboratory of "Meccanica delle Vibrazioni" of the University of Rome "La Sapienza" directed by Prof. Sestieri.

TABLE 2. Measured non-dimensional coupling parameters. .

γ_4	γ_3	γ_2	γ_1	γ_0
12.2×10^{-2}	9.54×10^{-2}	5.77×10^{-2}	2.98×10^{-2}	0.083×10^{-2}

In order to compute the optimal resistance in (2.5) we should know the coupling coefficient γ and the capacitance C. The coupling coefficient γ can be expressed as

$$\gamma = \sum_{h=0}^{N_P-1} \mathring{v}_h^{(1)} \gamma_h,$$

where the modal coupling of the separate transducers have been introduced

$$\gamma_j = g \frac{\left(\mathsf{w}^{(1)}\right)'\left(X_{\mathfrak{r}(j)+1}\right) - \left(\mathsf{w}^{(1)}\right)'\left(X_{\mathfrak{r}(j)}\right)}{\omega^{(1)}\sqrt{mC}} = \frac{d_j}{\omega^{(1)}\sqrt{mC}}.$$

These parameters may be measured by the technique presented in Section 5.3 of Chapter 5, and their values are listed in Table 2. They convey all the necessary information about the beam modal curvature and will be used in what follows to study the statistical properties of the control system. Therefore the value of the modal coupling coefficient is

$$\gamma = 0.16670,$$

and the optimal resistance is

$$R = 87.046 \text{ k}\Omega.$$

The floating inductor can be simulated, according to [**Deboo (1967)**], by exploiting the three operational amplifiers RC-circuit depicted in Figure 6.

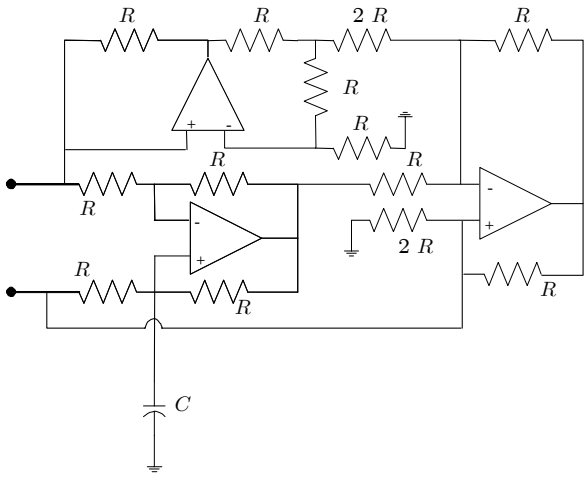

FIGURE 6. Schematics of floating inductors.

High-precision resistors must be used in order to reduce circuit losses, and guarantee a two-terminals behavior of the simulated inductor. A careful dimensioning of the circuit components may yield very high quality factors, without affecting the maximum allowed voltage. Meanwhile, attention must be paid towards undesired instability phenomena, which may eventually be compensated by introducing additional resistors connecting the circuit terminals to ground. From the analysis of the introduced RC-circuit, it is possible

TABLE 3. Nominal values of the electric components used to implement the floating and grounded inductors

Deboo ($L = 130.5$ H)	$R = 2.7$ kΩ
	$C = 17.9$ μF (polyester)
Antoniou ($L = 19.01$ H)	$R_1 = 3$ kΩ
	$R_2 = 1$ kΩ
	$R_3 = 0$ kΩ
	$R_4 = 1$ kΩ
	$R_6 = 198$ Ω
	$C_5 = 32$ μF (polyester)

to show that the circuit is equivalent to a sole floating inductor, the inductance of which is:

$$L = R^2 C.$$

From a practical point of view, inductance can be varied only by tuning the loading capacitance C, since otherwise the simultaneous change of all the resistances is required. The breadboard implementation of the floating inductor is shown in Figure 7.

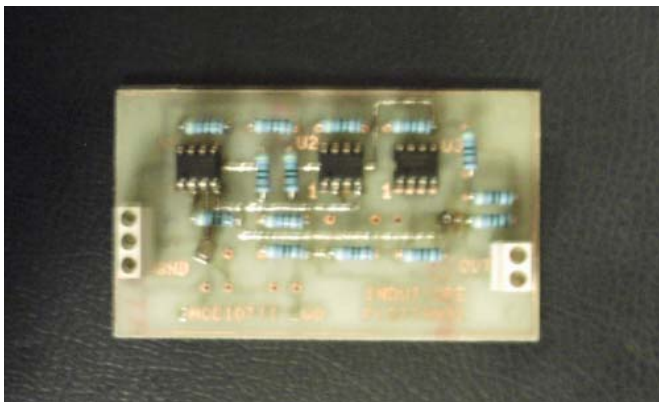

FIGURE 7. Picture of the realized inductor.

In order to avoid the simultaneous tuning of all the used inductors, the internal resonance condition (2.1) is achieved by following a simpler approach. Indeed, by looking at the plot in Figure 1, it is clear that variations of the boundary impedance at the transducer located at the free end in the range $[0, L]$ do not sensibly affect the electromechanical modal coupling γ, but, on the other hand, influence the electric resonance frequency. Therefore, the electric network can be tuned to the structural modal frequency by changing only that boundary inductance.

The modified Antoniou's circuit in Figure 6 of Chapter 5 was used to simulate the tuning grounded inductor.

The values of the components employed for the realization of the five floating inductors and the grounded one are reported in Table 3. High-voltages FET-input operational amplifiers Burr-Brown OPA445AP driven by a dual outputs power supply TTi EX752M at ±30 V and high-precision resistors (±1%) have been used.

In Figure 8, we report corresponding mobility function for different values of the line resistances R (a boundary resistance in parallel connection with the tuning grounded

Antoniou inductor was chosen to achieve a proportional damping). From equation (2.4) of Chapter 5, the difference between the frequencies of the fixed points S and T, can be evaluated to be 2.41 Hz. These theoretical predictions, based on the previous modeling on the experimental identification technique in Section 5.3 of Chapter 5, are in very close agreement with the experimental results implied by Figure 8 where it can be shown that a reduction of the mechanical mobility maximum value of 95.8% occurs around the first mode. The discrepancy between the theoretically predicted and experimentally measured optimal line resistance may be attributed to the parasitic resistances of the simulated inductors and to the neglect of the structural damping.

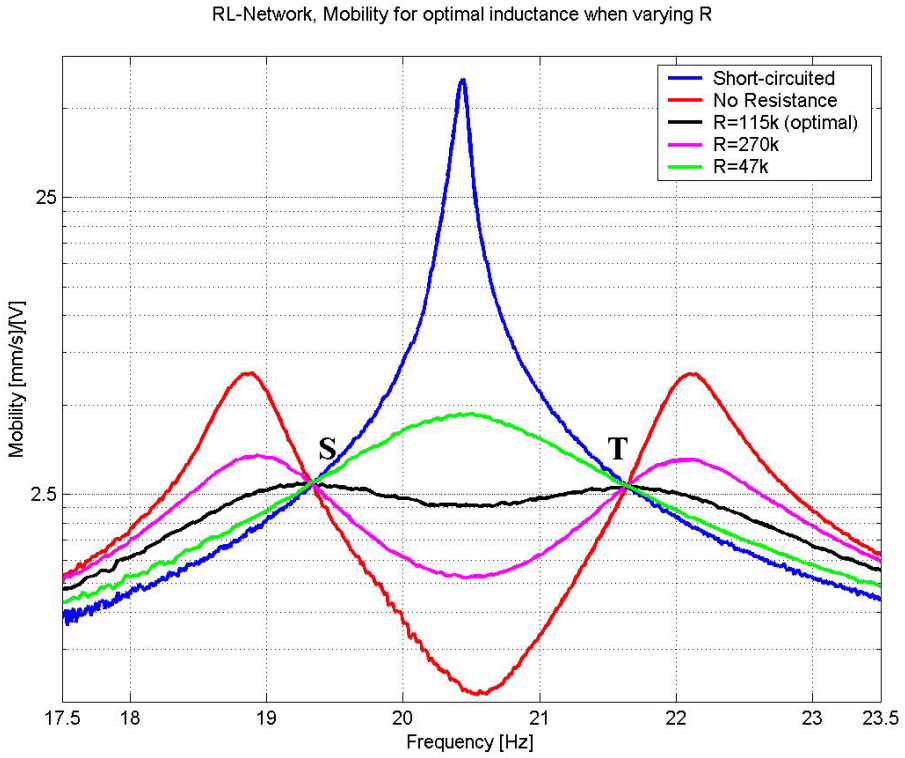

FIGURE 8. First mode mechanical mobility with different the line resistances.

From equation (4.2) and the experimental value of the coupling γ, the difference between the expected value of the system norm and the optimal one is:

$$\frac{E\left[\|H_p\|_\infty\right] - \left\|H_{p_{opt}}\right\|_\infty}{\left\|H_{p_{opt}}\right\|_\infty} = \sqrt{\frac{1}{\pi}}\frac{1}{\gamma}\sqrt{\frac{3}{2N_P - 1}}\sigma_X = 1.954\,\sigma_X,$$

where we used

$$\left\|H_{p_{opt}}\right\|_\infty = \frac{\sqrt{2}}{\gamma} = 8.484$$

The computation of the variance of the system infinity norm requires the knowledge of the beam modal curvature, which is conveyed by the parameters in Table 2, since, as we already pointed out dealing with equation (4.1), the function $f_1^{(j)}$ depends only on the direction of $\mathbf{d}$. Therefore we can evaluate $f_1^{(j)}$ from the couplings in Table 2:

$$f_1^{(j)}\left(\left[\begin{array}{cccc}\gamma_1 & \gamma_2 & \gamma_3 & \gamma_4\end{array}\right]^{\mathrm{T}}, 5\right) = 0.451 \times 10^{-3}.$$

which is an extremely small number, since $\mathbf{d}$ is almost parallel to the first eigenvector of the unperturbed circuit. Therefore, from (4.4) we obtain

$$\sqrt{V\left[\|H_p\|_\infty\right]} = 12.53\,\sigma_X,$$

and

$$\frac{\sqrt{V\left[\|H_p\|_\infty\right]}}{\left\|H_{p_{opt}}\right\|_\infty} = 1.477\,\sigma_X.$$

CHAPTER 7

Fourth order transmission line

In this Chapter, we consider the performances of an electric circuit analog[1] to an Euler-Bernoulli beam with structural damping[2], interconnecting the electrical terminals of the array of piezoelectric transducers positioned on the host beam. The used circuit is named fourth order transmission line in order to emphasize the presence of the fourth derivative in the electric evolution equation and to preserve the same terminology of Chapter 6.

We initially analyze the resulting PEM structure as a continuum, by making use of the results in Chapter 4. The eigenvalue problem for the fourth derivative operator with natural (in the sense of [**Russell (1988)**]) boundary conditions is reviewed. The concept of dual boundary conditions is presented and the relations between the spectral properties of the original and the dual problem are explained. The dual boundary conditions are used to define the domain of the electric fourth derivative operator. The electric damping is modeled by the square root of the fourth derivative. It is shown that the distributed circuit governed by the fourth derivative with dual boundary conditions and inherent square root damping allows for the simultaneous damping of every structural mode and that the damping performances are mode independent.

Next, we tackle the problem of synthesizing a lumped electric circuit approximating the beam circuit analog, i.e. governed by a discrete version of the beam equation. This problem has been analyzed in [**dell'Isola and Vidoli (1998, 2)**], [**Alessandroni et al. (2002)**] and [**dell'Isola et al. (2001)**], but the proposed circuits have stern practical inconveniences, either due to active transconductances, or negative inductors, or multiport transformers. In the present work two distinct synthesis techniques are exploited to achieve the same electric analog, being constituted only by inductors, capacitors and two-port transformers. Both the approaches involves a Timoshenko beam model and derive the Euler-Bernoulli beam analog circuit as a limit case. In the first approach, (see [**Porfiri et al. (2004)**] for details) the equilibrium and constitutive equations of a Timoshenko beam element are finite-difference approximated and a four port circuit analog to the beam element is conceived. In the second approach, (see [**Andreaus et al. (2004)**] for details) a Lagrangian based approach is used: the Lagrangian of a Timoshenko beam is discretized and by establishing an electromechanical analogy between the flux-linkages and the displacements a discrete circuit governed by the discretized beam Lagrangian is assembled. The first method is more intricate and difficult but gives necessary and sufficient conditions for the transformerless synthesis of analog circuits. On the other hand, the second method can be easily applied to more complicated problems (see e.g. [**Alessandroni et al. (2004)**] and [**Alessandroni et al. (2005)**]).

[1] In order to be more rigorous we should say that the circuit is the analog of a massless Euler-Bernoulli beam with structural damping and equipped with dual boundary conditions with respect to those prescribed on the stepped piezoelectric beam. Indeed, the inertia term in the electric evolution equation is provided by the piezoelectric elements, rather than the interconnecting network, and only dual boundary conditions assure the maximum modal coupling.

[2] The structural damping of the host beam is still neglected, only the electric circuit is dissipative.

Once a satisfactory beam circuit analog is available the problem of suitably inserting resistors for achieving the multimodal damping is tackled. A PEM beam prototype is designed and the broadband damping effectiveness of the proposed device is assessed. Finally the circuit analog is analyzed as a lumped system.

1. Problem formulation

When studying the second order transmission line (Chapter 6) we have applied the results found in Chapter 5 to a reduced order model based on the projection of the electromechanical solution on two modes of the uncoupled systems. We have seen that by the use of that distributed network it is impossible to simultaneously damp different structural modes. Indeed, the inductance per unit length is determined for achieving the internal resonance between two particular electrical and mechanical modes. Also, the boundary conditions are chosen once for all according to the chosen modes, in order to maximize the inner product between the beam modal curvature and the electric mode shape, which is maximum when the electric mode shapes are equal to the mechanical modal curvatures. Similarly, the resistance per unit length is determined by requiring that the electric modal damping is proportional to the modal coupling by the factor $\sqrt{3/2}$.

All the shortcomings of the second order transmission line may be overcame by the use of an electric circuit characterized by the following three properties:

(1) it is resonating at all the structural modes,
(2) its mode shapes are the beam modal curvatures,
(3) it is endowed with an inherent modal damping proportional with the modal coupling.

In the present Section we present the governing equations of the optimal circuit fulfilling all the above specifications. We start by analyzing the modal properties of the fourth derivative operator and its square root. Following [**Russell (1988)**] we introduce the concept of dual boundary conditions. We exploit this knowledge to derive the modal properties of the optimal distributed network.

1.1. Eigenvalue problem.

1.1.1. *Properties of the fourth derivative operator.* We denote by $\mathfrak{K}$ the fourth derivative operator in $L^2(0,1)$:

$$(\mathfrak{K}w)(x) = w^{IV}(x), \qquad x \in (0,1),$$

with $\mathcal{D}(\mathfrak{K})$, the domain of $\mathfrak{K}$, a subspace of $H^4(0,1)$ dense in $L^2(0,1)$, characterized by boundary conditions for which the operator is self-adjoint (in $L^2(0,1)$) and nonnegative definite.

It is possible to show that $\mathfrak{K}$ is self-adjoint and nonnegative definite for every choice of natural[3] boundary conditions (in the sense of [**Russell (1988)**]). In order to define natural boundary conditions we need to define the preliminary concept of symmetric boundary conditions. To this aim we take two functions w and v in $\mathcal{D}(\mathfrak{K})$ and by integration by parts we get

$$\int_0^1 (\mathfrak{K}w)\, v dx = \int_0^1 w'' v'' dx + (w''' v - w'' v')\big|_0^1,$$

[3]The natural boundary conditions in the classical literature on variational boundary value problems is completely unrelated to what we are studying now.

and

$$\int_0^1 (\mathfrak{K}v)\, w dx = \int_0^1 w''v'' dx + \left(v'''w - v''w'\right)\Big|_0^1 .$$

The boundary conditions that ensure the symmetry of $\mathfrak{K}$, i.e.:

$$\int_0^1 (\mathfrak{K}w)\, v dx = \int_0^1 (\mathfrak{K}v)\, w dx, \qquad \forall w, v \in \mathcal{D}(\mathfrak{K}),$$

are called symmetric. The symmetry of the fourth-derivative operator does not imply its self-adjointness[4]. We call natural boundary conditions the symmetric boundary conditions that:

- assure that $\mathfrak{K}$ is self-adjoint, i.e. that

$$\mathfrak{K}^* = \mathfrak{K}, \text{ with} \qquad \mathcal{D}(\mathfrak{K}) = \mathcal{D}(\mathfrak{K}^*),$$

  $\mathfrak{K}^*$ being the adjoint of $\mathfrak{K}$;
- render the quantity

$$w'w'' - ww''' \tag{1.1}$$

  nonpositive at 1 and nonnegative at 0.

Under natural boundary conditions the spectrum of $\mathfrak{K}$ consists of eigenvalues

$$0 \leq \left(\eta^{(1)}\right)^4 < \left(\eta^{(2)}\right)^4 < \cdots < \left(\eta^{(k)}\right)^4 < \left(\eta^{(k+1)}\right)^4 < \cdots$$

of single multiplicity when $\eta^{(k)}$ is different from zero. Moreover, they have the following form (see e.g. [**Russell (1988)**])

$$\eta^{(k)} = k + \nu + \varepsilon_k,$$

where ε_k is a sequence in l^2 and ν is a constant. The corresponding orthonormal eigenfunctions $\mathsf{w}^{(k)}$ form an orthonormal basis for $L^2(0,1)$ themselves or may be modified (in the case $\eta^{(1)} = 0$) to include a pair of orthonormalized eigenfunctions corresponding to the zero eigenvalue.

For any positive eigenvalue $\left(\eta^{(k)}\right)^4$ the corresponding eigenfunction is

$$\mathsf{w}^{(k)} = A_1 \cos\left(\eta^{(k)}x\right) + A_2 \cosh\left(\eta^{(k)}x\right) + A_3 \sin\left(\eta^{(k)}x\right) + A_4 \sinh\left(\eta^{(k)}x\right). \tag{1.2}$$

The modal curvatures are simply

$$\left(\mathsf{w}^{(k)}\right)'' = C_1 \cos\left(\eta^{(k)}x\right) + C_2 \cosh\left(\eta^{(k)}x\right) + C_3 \sin\left(\eta^{(k)}x\right) + C_4 \sinh\left(\eta^{(k)}x\right),$$

where

$$C_1 = -A_1\left(\eta^{(k)}\right)^2, \quad C_2 = A_2\left(\eta^{(k)}\right)^2, \quad C_3 = -A_3\left(\eta^{(k)}\right)^2, \quad C_4 = A_4\left(\eta^{(k)}\right)^2.$$

Alternatively the coefficients of the mode shape A_i and modal curvature C_i may be related by the following matrix relation:

$$\mathbf{C} = \left(\eta^{(k)}\right)^2 \mathbf{TA},$$

with

$$\mathbf{C} = \begin{bmatrix} C_1 \\ C_2 \\ C_3 \\ C_4 \end{bmatrix}, \quad \mathbf{A} = \begin{bmatrix} A_1 \\ A_2 \\ A_3 \\ A_4 \end{bmatrix}, \quad \mathbf{T} = \begin{bmatrix} -1 & 0 & 0 & 0 \\ 0 & 1 & 0 & 0 \\ 0 & 0 & -1 & 0 \\ 0 & 0 & 0 & 1 \end{bmatrix}.$$

[4]For instance in $\mathcal{D}(\mathfrak{K}) = H_0^4(S)$ the operator $\mathfrak{K}$ is symmetric. Its adjoint $\mathfrak{K}^*$ is the fourth-derivative defined on the domain $\mathcal{D}(\mathfrak{K}^*) = H^4(S)$, being strictly larger than $\mathcal{D}(\mathfrak{K})$.

The effect of the unitary transformation matrix $\mathbf{T}$ on a given vector consists of the multiplication by a constant and the change in the sign of the first and third component.

1.1.2. *Dual boundary conditions.* Natural boundary conditions account for lumped elastic elements at the beam ends (either rotational or extensional springs), therefore the resulting strain energy is not strictly distributed in general and boundary terms may appear. In the present work, we refrain from considering lumped elastic elements by accounting for the sole boundary conditions constituted by clamped, free, hinged, and guided boundary conditions. Thus, the expression in (1.1) is simultaneously vanishing at both the beam ends[5] and the strain energy takes the strictly distributed form:

$$\frac{1}{2}\int_0^1 (w'')^2\, dx.$$

Following [**Russell (1988)**], the boundary conditions may be written in the form

$$\mathbf{w}_0 = \mathbf{E}\mathbf{z}, \qquad \mathbf{w}_1 = \boldsymbol{\varepsilon}\boldsymbol{\zeta},$$

with

$$\mathbf{w}_0 = \begin{bmatrix} w(0) \\ w'(0) \\ w''(0) \\ w'''(0) \end{bmatrix}, \quad \mathbf{w}_1 = \begin{bmatrix} w(1) \\ w'(1) \\ w''(1) \\ w'''(1) \end{bmatrix}, \quad \mathbf{E} = \begin{bmatrix} \mathbf{E}_1 & \mathbf{E}_2 \end{bmatrix}, \quad \boldsymbol{\varepsilon} = \begin{bmatrix} \boldsymbol{\varepsilon}_1 & \boldsymbol{\varepsilon}_2 \end{bmatrix}, \tag{1.3}$$

and where $\mathbf{E}_1$ and $\mathbf{E}_2$ ($\boldsymbol{\varepsilon}_1$ and $\boldsymbol{\varepsilon}_2$) are independent four vectors whose entries are all zeros but one which is equal to a constant, $\mathbf{z}$ ($\boldsymbol{\zeta}$) is an arbitrary two vector.[6] In this way we select which are the components of the vectors $\mathbf{w}_0$ and $\mathbf{w}_1$ that may attain values different from zero.

The boundary conditions in terms of the coefficient vector $\mathbf{A}$ are

$$\mathbf{B}\mathbf{A} = \mathbf{E}\mathbf{z}, \quad \boldsymbol{\beta}\mathbf{A} = \boldsymbol{\varepsilon}\boldsymbol{\zeta},$$

where the following matrices have been introduced:

$$\mathbf{B} := \begin{bmatrix} 1 & 1 & 0 & 0 \\ 0 & 0 & 1 & 1 \\ -1 & 1 & 0 & 0 \\ 0 & 0 & -1 & 1 \end{bmatrix}, \quad \boldsymbol{\beta} := \begin{bmatrix} \cos\left(\eta^{(k)}\right) & \cosh\left(\eta^{(k)}\right) & \sin\left(\eta^{(k)}\right) & \sinh\left(\eta^{(k)}\right) \\ -\sin\left(\eta^{(k)}\right) & \sinh\left(\eta^{(k)}\right) & \cos\left(\eta^{(k)}\right) & \cosh\left(\eta^{(k)}\right) \\ -\cos\left(\eta^{(k)}\right) & \cosh\left(\eta^{(k)}\right) & -\sin\left(\eta^{(k)}\right) & \sinh\left(\eta^{(k)}\right) \\ \sin\left(\eta^{(k)}\right) & \sinh\left(\eta^{(k)}\right) & -\cos\left(\eta^{(k)}\right) & \cosh\left(\eta^{(k)}\right) \end{bmatrix}.$$

The corresponding boundary conditions that are satisfied by the modal curvature coefficient vector at the beam ends, called dual boundary conditions, are

$$\mathbf{B}\mathbf{T}^{-1}\mathbf{C} = \mathbf{E}\mathbf{z}, \quad \boldsymbol{\beta}\mathbf{T}^{-1}\mathbf{C} = \boldsymbol{\varepsilon}\boldsymbol{\zeta},$$

which, by recalling that $\mathbf{T}$ is unitary, become:

$$\mathbf{B}\mathbf{T}\mathbf{C} = \mathbf{E}\mathbf{z}, \quad \boldsymbol{\beta}\mathbf{T}\mathbf{C} = \boldsymbol{\varepsilon}\boldsymbol{\zeta}.$$

The product $\mathbf{B}\mathbf{T}$ ($\boldsymbol{\beta}\mathbf{T}$) is simply the matrix $\mathbf{B}$ ($\boldsymbol{\beta}$) after changing the sign of the first and third column, therefore it is equal to the matrix $\mathbf{B}$ ($\boldsymbol{\beta}$) after inverting the first with the third row and the second with the fourth. Hence, the dual boundary conditions are simply obtained from the matrices $\mathbf{E}$ and $\boldsymbol{\varepsilon}$ by changing the first row with the third one, and the second row with the fourth one. The corresponding matrices are indicated by $\mathbf{E}^{\#}$ and $\boldsymbol{\varepsilon}^{\#}$. We explicitly point out that the dual constraint of the clamped is the free end,

[5] In mechanics these constraints are sometimes referred to as perfect.

[6] The discussion may be extended to any natural boundary condition, if the vectors $\mathbf{E}_1$ and $\mathbf{E}_2$ ($\boldsymbol{\varepsilon}_1$ and $\boldsymbol{\varepsilon}_2$) are treated as generic independent vectors varying with $\eta^{(k)}$ and the boundary matrices $\mathbf{B}$ and $\boldsymbol{\beta}$ are treated as functions of $\eta^{(k)}$, as well.

of the hinged the hinged itself, of the free end is the clamped, of the guided is the guided end itself (see Figure 1)

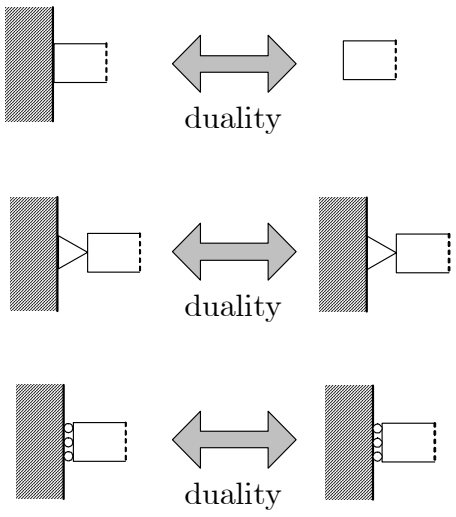

FIGURE 1. Sketch of duality relations between mechanical constraints.

Therefore, given the fourth derivative operator $\mathfrak{K}$ with domain $\mathcal{D}(\mathfrak{K})$ characterized by the matrices $\mathbf{E}$ and $\boldsymbol{\varepsilon}$ we can define the dual operator $\mathfrak{K}^{\#}$ with domain $\mathcal{D}\left(\mathfrak{K}^{\#}\right)$, by requiring that $\mathfrak{K}^{\#}$ is still the fourth derivative and its domain $\mathcal{D}\left(\mathfrak{K}^{\#}\right)$ is individuated by the matrices $\mathbf{E}^{\#}$ and $\boldsymbol{\varepsilon}^{\#}$ constructed as explained above. Obviously, $\mathfrak{K}^{\#}$ is self-adjoint and nonnegative definite too, its eigenfunctions may form an orthonormal basis in $L^2(0,1)$, and the dual of the dual problem is the original problem. The eigenvalues of the dual problem are the same of those of the original problem, while the eigenfunctions, say $\mathsf{w}^{\#(k)}$, are computed from those of the original ones, $\mathsf{w}^{(k)}$, after double differentiation[7] and normalization.

The inner product of $\mathsf{w}^{\#(j)}$ and $\left(\mathsf{w}^{(i)}\right)''$

- vanishes if $\eta^{(i)}$ is zero (since $\left(\mathsf{w}^{(i)}\right)''$ is zero consequently),
- vanishes if $\mathsf{w}^{\#(j)}$ is not corresponding to a 0 eigenvalue and i is different from j,
- is equal to $\left(\eta^{(k)}\right)^2$ if i is equal to j and none of the eigenfunctions correspond to a zero eigenvalue.

We remark that a distributed electric circuit governed by the dual operator, with its own boundary conditions, may resonate at all the mechanical mode frequencies and provide, meanwhile, electric mode shapes parallel to the beam modal curvatures.

1.1.3. *Square root of the fourth derivative.* In [**Chen and Russell (1982)**], in order to account for observed relationships between modal damping and modal frequencies in structural systems, the square root damping model is introduced. Indeed, this model leads to mode independent modal damping.

[7]The zero eigenvalues of the original problem are not inherited by the dual problem. In the dual problem, zero eigenvalues may arise and the corresponding eigenfunctions are not the second derivative of any eigenfunction of the original problem.

The fourth derivative $\mathfrak{K}$, with natural boundary conditions, admits a unique nonnegative self-adjoint square root $\mathfrak{K}^{1/2}$ whose domain $\mathcal{D}\left(\mathfrak{K}^{1/2}\right)$ is a subset of $\mathcal{D}\left(\mathfrak{K}\right)$ (see e.g. [**Kato (1966)**]). The eigenfunctions of $\mathfrak{K}^{1/2}$ are the same of those of $\mathfrak{K}$, and the eigenvalues are simply the square root of those of $\mathfrak{K}$.

In [**Russell (1988)**], its mathematical properties are deeply analyzed, and it is shown that it coincides with the negative second order derivative operator when special natural boundary conditions (called trigonometric) are prescribed. Those boundary conditions ensure purely trigonometric eigenfunctions for the fourth derivative operator, i.e. vanishing A_2 and A_4 in (1.2). When such boundary conditions are imposed the dissipative operator is actually a differential operator and by exploiting finite difference approximations it is possible to synthesize a lumped approximating network. Otherwise, it "is not a differential operator and its interpretation is rather obscure", [**Russell (1988)**].

As mentioned before, in the present work we are interested only in a particular class of natural boundary conditions constituted only by clamped, free, hinged and guided boundary. Within this small admissible set of constraints the only trigonometric boundary conditions are the hinges at both ends. Indeed for a simply supported beam the only non zero term in (1.2) is A_3.

1.2. Vibrations of a PEM beam endowed with the optimal circuit. The governing equation for the mechanical deflection field w is (see equation (1.1) in Chapter 6):

$$\rho_{\hom}\ddot{w} + k_{\hom}w^{IV} - g_{\hom}\dot{\psi}'' = b,$$

where the same notation as in Chapter 6 is used; in particular the constitutive parameters are defined in (2.15) of Chapter 4 and (1.2a) of Chapter 6.

The governing equation for the electric flux-linkage is

$$c_{\hom}\ddot{\psi} + a_{\hom}\psi^{IV} + b_{\hom}\left(\dot{\psi}^{IV}\right)^{1/2} + g_{\hom}\dot{w}'' = 0, \tag{1.4}$$

where the homogenized capacitance per unit length $c_{\hom}$ is given in (1.4) of Chapter 4, and the positive parameters $a_{\hom}$ and $b_{\hom}$ are design parameters. These two parameters represent the main properties of the distributed electric circuit and are related to the circuit topology and the electric components' values. They are treated as unknowns and their optimal values are the result of the infinity norm minimization problem for the i-th electromechanical mode.

Once the mechanical boundary conditions are prescribed, the electric ones are chosen to be their dual in the sense above specified. Hence, by adapting the notation of equations (1.3) to the present electromechanical problem, the boundary conditions become:

$$\mathbf{w}_0 - \frac{g_{\hom}}{k_{\hom}}\mathbf{Q}\,\dot{\boldsymbol{\psi}}_0 = \mathbf{E}\mathbf{z}, \qquad \boldsymbol{\psi}_0 = \mathbf{E}^{\#}\mathbf{x}, \tag{1.5a}$$

$$\mathbf{w}_l - \frac{g_{\hom}}{k_{\hom}}\mathbf{Q}\,\dot{\boldsymbol{\psi}}_l = \boldsymbol{\varepsilon}\boldsymbol{\zeta}, \qquad \boldsymbol{\psi}_l = \boldsymbol{\varepsilon}^{\#}\boldsymbol{\xi}, \tag{1.5b}$$

with

$$\mathbf{w}_0 = \begin{bmatrix} w(0,t) \\ w'(0,t) \\ w''(0,t) \\ w'''(0,t) \end{bmatrix}, \quad \boldsymbol{\psi}_0 = \begin{bmatrix} \psi(0,t) \\ \psi'(0,t) \\ \psi''(0,t) \\ \psi'''(0,t) \end{bmatrix},$$
$$\mathbf{w}_l = \begin{bmatrix} w(l,t) \\ w'(l,t) \\ w''(l,t) \\ w'''(l,t) \end{bmatrix}, \quad \boldsymbol{\psi}_l = \begin{bmatrix} \psi(l,t) \\ \psi'(l,t) \\ \psi''(l,t) \\ \psi'''(l,t) \end{bmatrix},$$

and

$$\mathbf{Q} = \begin{bmatrix} 0 & 0 & 0 & 0 \\ 0 & 0 & 0 & 0 \\ 1 & 0 & 0 & 0 \\ 0 & 1 & 0 & 0 \end{bmatrix},$$

$\mathbf{z}$, $\boldsymbol{\zeta}$, $\mathbf{x}$ and $\boldsymbol{\xi}$ being arbitrary two vectors. We remark that the effect of the matrix $\mathbf{Q}$ on a generic vector is to invert the first component with the third one, the second with the fourth and then set to zero the first two. Therefore $\mathbf{QE}^{\#}$ is the matrix $\mathbf{E}$ with the first two rows set to zero and $\mathbf{QE}^{\#}\mathbf{x}$ can always be written as $\mathbf{Ez}$. Similar arguments hold for the right boundary. With this choice of electrical boundary conditions the mechanical field may be expressed in terms of the eigenfunctions of the fourth derivative with boundary conditions prescribed by $\mathbf{E}$ and $\boldsymbol{\varepsilon}$ and the flux-linkage in terms of the eigenfunctions of the dual problem.

We assume that the system is initially at rest, that there are no zero eigenvalues in both the problems and we write the solution in terms of the two orthonormal bases constituted by the normalized[8] eigenfunctions $\mathsf{w}^{(i)}$ and $\mathsf{w}^{(j)\#}$ (see e.g. [**Sanchez-Hubert and Sanchez-Palencia (1989)**] and [**Curtain and Zwart (1995)**]):

$$w(x,t) = \sum_{i=1}^{\infty} W_i(t)\,\mathsf{w}^{(i)}(x), \qquad \psi(x,t) = \sum_{j=1}^{\infty} \Psi_j(t)\,\mathsf{w}^{(j)\#}(x).$$

Therefore, the following problem arises

$$\begin{cases} m\ddot{W}_i(t) + m\left(\omega^{(i)}\right)^2 W_i(t) - g_{\text{hom}}\dfrac{\left(\eta^{(i)}\right)^2}{l}\dot{\Psi}_i(t) = F_i(t) \\ l\,c_{\text{hom}}\ddot{\Psi}_i(t) + a_{\text{hom}}\dfrac{(\lambda_i)^4}{l^3}\Psi_i(t) + b_{\text{hom}}\dfrac{\left(\eta^{(i)}\right)^2}{l}\dot{\Psi}_i(t) + g_{\text{hom}}\dfrac{\left(\eta^{(i)}\right)^2}{l}\dot{W}_i(t) = 0 \end{cases},$$

where the i-th modal force and radian frequency are:

$$F_i(t) := \int_0^l b(x,t)\,\mathsf{w}^{(i)}dx, \qquad \left(\omega^{(i)}\right)^2 = \frac{k_{\text{hom}}\left(\eta^{(i)}\right)^4}{\rho_{\text{hom}}l^4}.$$

[8]As usual we normalize the eigenfunctions for having

$$\int_0^l \left(\mathsf{w}^{(k)}\right)^2 dx = l, \qquad \int_0^l \left(\mathsf{w}^{(k)\#}\right)^2 dx = l,$$

and we still denote with λ_i the eigenvalues of the fourth derivative with the given natural boundary conditions in the domain $(0,1)$.

The resulting coupled ordinary differential equations may be cast in the widely discussed dimensionless form (1.4):

$$\begin{cases} \ddot{W}_i(t) + W_i(t) - \gamma\dot{\Psi}_i(t) = F_i(t) \\ \ddot{\Psi}_i(t) + \delta\dot{\Psi}_i(t) + \beta\Psi_i(t) + \gamma\dot{W}_i(t) = 0 \end{cases},$$

where each set of modal equations has been non-dimensionalized with respect of a different time scale and the key modal parameters are:

$$\beta := \frac{a_{\text{hom}}}{c_{\text{hom}}}\frac{\rho_{\text{hom}}}{k_{\text{hom}}}, \quad \delta := \frac{b_{\text{hom}}}{c_{\text{hom}}}\sqrt{\frac{\rho_{\text{hom}}}{k_{\text{hom}}}}, \quad \gamma := \frac{g_{\text{hom}}}{\omega_i\sqrt{mc_{\text{hom}}l}}\frac{\left(\eta^{(i)}\right)^2}{l} = \max\gamma. \tag{1.6}$$

REMARK 8. *Let us remark that the above calculated modal parameters are frequency independent and that the modal coupling attains its maximum defined in equation (1.12) of Chapter 6. Thus the tuning and damping parameters can be chosen once for all in order to optimize the damping of every structural mode.*

In particular, by the application of the internal resonance condition in (2.1) of Chapter 5 we obtain:

$$\frac{a_{\text{hom}}}{c_{\text{hom}}}\frac{\rho_{\text{hom}}}{k_{\text{hom}}} = 1 \Rightarrow \frac{c_{\text{hom}}}{a_{\text{hom}}} = \frac{\rho_{\text{hom}}}{k_{\text{hom}}}. \tag{1.7}$$

Similarly, the optimal choice of the damping parameters in (2.2) of Chapter 5 yields:

$$\frac{b_{\text{hom}}}{c_{\text{hom}}}\sqrt{\frac{\rho_{\text{hom}}}{k_{\text{hom}}}} = \sqrt{\frac{3}{2}}\frac{g_{\text{hom}}}{\sqrt{k_{\text{hom}}c_{\text{hom}}}} \Rightarrow b_{\text{hom}} = \sqrt{\frac{3}{2}}\sqrt{\frac{c_{\text{hom}}}{\rho_{\text{hom}}}}g_{\text{hom}}. \tag{1.8}$$

Therefore, the ∞-norm of the i-th mobility function is (2.3) of Chapter 5:

$$\left\|H_{(\beta_{opt},\delta_{opt},\gamma)}\right\|_\infty = \frac{\sqrt{2}}{\gamma} = \frac{\sqrt{2}}{g_{\text{hom}}}\sqrt{k_{\text{hom}}c_{\text{hom}}}.$$

1.2.1. *Electromechanical modal analysis.* Here we study the modal properties of the gyroscopically coupled partial differential equations governing the vibrations of the beam and the optimized fourth order line. Thus, when the electric dissipation and the external load are discarded, and the internal resonance condition in (1.7) is satisfied the governing equations are:

$$\begin{cases} \ddot{w} + \mathfrak{a}^4 w^{IV} - \mathfrak{b}^2\dot{\psi}'' = 0 \\ \ddot{\psi} + \mathfrak{a}^4\psi^{IV} + \mathfrak{b}^2\dot{w}'' = 0 \end{cases}, \tag{1.9}$$

where non-dimensionalized variables have been used and the following non-dimensional constants appear:

$$\mathfrak{a}^4 = \frac{1}{l^4\left(\omega^*\right)^2}\frac{k_{\text{hom}}}{\rho_{\text{hom}}}, \qquad \mathfrak{b}^2 = \frac{1}{l^2\omega^*}\frac{g_{\text{hom}}}{\sqrt{c_{\text{hom}}\rho_{\text{hom}}}}.$$

The parameter ω^* represents a characteristic radian frequency, the abscissa has been scaled with the beam length and the characteristic flux-linkage and deflection have been introduced:

$$\sqrt{\frac{c_{\text{hom}}}{\rho_{\text{hom}}}} = \frac{w^*}{\psi^*}.$$

The boundary conditions for the electromechanical coupled equations are the non-dimensio-

-nalized version of (1.5):

$$\mathbf{w}_0 - \frac{\mathfrak{b}^2}{\mathfrak{a}^4}\mathbf{Q}\,\dot{\boldsymbol{\psi}}_0 = \mathbf{E}\mathbf{z}, \qquad \boldsymbol{\psi}_0 = \mathbf{E}^{\#}\mathbf{x}, \tag{1.10a}$$

$$\mathbf{w}_1 - \frac{\mathfrak{b}^2}{\mathfrak{a}^4}\mathbf{Q}\,\dot{\boldsymbol{\psi}}_1 = \boldsymbol{\varepsilon}\boldsymbol{\zeta}, \qquad \boldsymbol{\psi}_1 = \boldsymbol{\varepsilon}^{\#}\boldsymbol{\xi}. \tag{1.10b}$$

The electromechanical modal properties are obtained by looking for a solution of (1.9) together with the boundary conditions (1.10) in the form

$$\begin{bmatrix} w(x,t) \\ \psi(x,t) \end{bmatrix} = \begin{bmatrix} \mathsf{m}(x) \\ \mathsf{e}(x) \end{bmatrix} \exp(\varpi t), \qquad \varpi \in \mathrm{C}.$$

Therefore, the following eigenvalue problem is obtained

$$\begin{cases} \varpi^2\mathsf{m} + \mathfrak{a}^4\mathsf{m}^{IV} - \mathfrak{b}^2\varpi\mathsf{e}'' = 0 \\ \varpi^2\mathsf{e} + \mathfrak{a}^4\mathsf{e}^{IV} + \mathfrak{b}^2\varpi\mathsf{m}'' = 0 \end{cases},$$

with boundary conditions directly obtained from (1.10).

By adapting the results obtained in [**Yang (1991)**] to the considered (generalized Sturm-Liouville) eigenvalue problem we obtain:

$$\varpi^{(\pm k)} = \pm i\omega^{(k)}, \qquad \begin{bmatrix} \mathsf{m}^{(\pm k)} \\ \mathsf{e}^{(\pm k)} \end{bmatrix} = \begin{bmatrix} \mathsf{m}_{\mathrm{R}}^{(k)} \\ \mathsf{e}_{\mathrm{R}}^{(k)} \end{bmatrix} \pm i \begin{bmatrix} \mathsf{m}_{\mathrm{I}}^{(k)} \\ \mathsf{e}_{\mathrm{I}}^{(k)} \end{bmatrix}, \qquad k = 1, 2, ...;$$

$$\omega^{(k)} \in \mathrm{R}^+, \qquad \begin{bmatrix} \mathsf{m}_{\mathrm{R}}^{(k)} \\ \mathsf{e}_{\mathrm{R}}^{(k)} \end{bmatrix}, \begin{bmatrix} \mathsf{m}_{\mathrm{I}}^{(k)} \\ \mathsf{e}_{\mathrm{I}}^{(k)} \end{bmatrix} \in \mathrm{R}^2;$$

where $\omega^{(k)}$ and $\begin{bmatrix} \mathsf{m}^{(\pm k)} & \mathsf{e}^{(\pm k)} \end{bmatrix}^{\mathrm{T}}$ are the dimensionless modal angular frequency and eigenvector of the k-th electromechanical mode of vibration of the distributed gyroscopic system and are given by:

$$\omega^{(k)} = \frac{1}{2}\left(\eta^{(k)}\right)^2 \mathfrak{b}^2 \left(1 \pm \sqrt{1 + \left(\frac{2\alpha^2}{\beta^2}\right)^2}\right), \qquad k = 1, 2, ...,$$

$$\begin{bmatrix} \mathsf{m}_{\mathrm{R}}^{(k)} \\ \mathsf{e}_{\mathrm{R}}^{(k)} \end{bmatrix} = \begin{bmatrix} 1 \\ 0 \end{bmatrix} \mathsf{w}^{(k)}, \qquad \begin{bmatrix} \mathsf{m}_{\mathrm{I}}^{(k)} \\ \mathsf{e}_{\mathrm{I}}^{(k)} \end{bmatrix} = \begin{bmatrix} 0 \\ (-1)^k \end{bmatrix} \mathsf{w}^{\#(k)}, \qquad k = 1, 2, ... \tag{1.11}$$

Hence, the pair of eigenvectors $\begin{bmatrix} \mathsf{m}^{(\pm k)} & \mathsf{e}^{(\pm k)} \end{bmatrix}^{\mathrm{T}}$ is associated simultaneously to both the $\omega^{(k)}$'s above introduced.

2. Multiport synthesis of the analog circuit

In this Section we find a completely passive lumped electric circuit analog to a vibrating beam, that consists only of inductors, capacitors and elementary two-port transformers. The proposed electric circuit will be synthesized following the subsequent design steps:

(1) finite difference discretization of the constitutive and balance equations for a vibrating Timoshenko beam,
(2) mobility representation of a beam element,

(3) synthesis of a four-port grounded circuit[9] (i.e., a four-port network containing only five terminals, one of which is a common ground terminal for all the ports), the admittance matrix of which parallels the beam element mobility matrix,
(4) cascade connection of the so-found networks to simulate the whole beam,
(5) neglect of beam shear deformability and rotatory inertia terms in the electric analog to achieve the Euler-Bernoulli beam electric analog.

2.1. Finite difference approximation of the mobility matrix. Every material particle of the considered Timoshenko beam is labelled by an abscissa x and its state is characterized by the transverse displacement w and the rotation of the beam cross-section ϑ.

The governing equations for the vibrations of a Timoshenko beam are, (see for instance [**Soedel (1993)**] and [**Meirovitch (2000)**]):

$$M' + T = \mathfrak{I}\,\dot{\Omega}, \tag{2.1a}$$

$$T' = \rho\,\dot{v}, \tag{2.1b}$$

$$\dot{M} = k\,\Omega', \tag{2.1c}$$

$$T = \mathfrak{k}\,(v' - \Omega), \tag{2.1d}$$

where M indicates the bending moment, T the shear contact action, $\mathfrak{I}$ the rotatory inertia, $v = \dot{w}$ the deflection velocity, $\Omega = \dot{\vartheta}$ the angular velocity of the cross sections, ρ the mass per unit length, $\mathfrak{k}$ the shear stiffness, and k the bending stiffness.

The partial differential equations (2.1a) and (2.1b) indicate balance equations of the couple and shear contact actions, respectively, while (2.1c) and (2.1d) the assumed linear constitutive behavior.

Let us subdivide the interval from 0 to l on the x axis putting equally spaced points $\varepsilon = l/N$ units apart, where N is the number of intervals (see Figure 2), and label

$$x_i = i\varepsilon,$$

for $i = 0, ..., N$, so $x_0 = 0$ and $x_N = l$. When using the circuit analog for control purposes the grid size ε coincides with the period of the PEM structure, see Chapter 4, and the number of intervals N with the number of piezoelectric elements N_P.

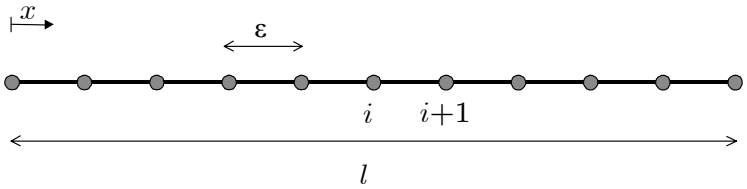

FIGURE 2. Discretization grid on the beam.

By introducing a suitable finite differences approximation for the previous set of equations with respect to the space variable, it is straightforward to achieve the following set

[9]The reason why we are not interested in multiport ungrounded networks lies in the impossibility of guaranteeing that a certain pair of terminals behaves as a port when interconnected with another pair of terminals.

of first order ordinary differential equations:

$$\frac{1}{\varepsilon}\left(M_{i+1}-M_i\right)+T_{i+1}=\mathfrak{I}\,\dot{\Omega}_{i+1}, \tag{2.2a}$$

$$\frac{1}{\varepsilon}\left(T_{i+1}-T_i\right)=\rho\,\dot{v}_i, \tag{2.2b}$$

$$\dot{M}_i=\frac{1}{\varepsilon}k\,\left(\Omega_{i+1}-\Omega_i\right), \tag{2.2c}$$

$$T_{i+1}=\mathfrak{k}\,(\frac{1}{\varepsilon}\left(v_{i+1}-v_i\right)-\Omega_{i+1}), \tag{2.2d}$$

where we use the subscript i to indicate the sampled value at the i-th node. Let us explicitly remark that the adopted finite differences schemes alternate between the forward and the backward rule; this mixed approach will permit us to obtain symmetric higher order schemes when dealing with higher order governing equations expressed in terms of the kinematical descriptors, e.g. when determining the finite difference scheme for the beam equations. Once a finite differences approximation for the mechanical impedance matrix of a beam element has been found, one well-established synthesis technique (see e.g. [**Alessandroni et al. (2002)**]) requires paralleling the velocity with the voltage, and the contact actions with the currents. The velocities at the beam element ends are regarded as across variables and the contact actions as through variables.

The correspondence between the mechanical variables in (2.2) and the electrical variables describing the analog network is:

$$\left(V_1,I_1\right)=\left(\frac{V^*}{\Omega^*}\Omega_i,-\frac{I^*}{M^*}M_i\right), \tag{2.3a}$$

$$\left(V_2,I_2\right)=\left(\frac{V^*}{v^*}v_i,-\frac{I^*}{T^*}T_i\right), \tag{2.3b}$$

$$\left(V_3,I_3\right)=\left(\frac{V^*}{\Omega^*}\Omega_{i+1},\frac{I^*}{M^*}M_{i+1}\right), \tag{2.3c}$$

$$\left(V_4,I_4\right)=\left(\frac{V^*}{v^*}V_{i+1},\frac{I^*}{T^*}T_{i+1}\right), \tag{2.3d}$$

where V^* and I^* denote, respectively, the characteristic voltage and current and M^*, T^*, v^* and Ω^* denote, respectively, the characteristic bending moment, shear force, velocity and angular velocity.

By means of this analogy, the impedance matrix representation for the beam element parallels the admittance matrix representation for the analog four-port grounded network. The mechanical impedance matrix of a beam element (see e.g. [**Molloy (1958)**]) is defined by:

$$\begin{bmatrix} -\widetilde{M}_i \\ -\widetilde{T}_i \\ \widetilde{M}_{i+1} \\ \widetilde{T}_{i+1} \end{bmatrix} = \mathbf{Z}^m\left(s\right) \begin{bmatrix} \widetilde{\Omega}_i \\ \widetilde{v}_i \\ \widetilde{\Omega}_{i+1} \\ \widetilde{v}_{i+1} \end{bmatrix},$$

where superimposed tilde denotes the one-sided Laplace transform[10], and s denotes the Laplace variable.

[10]Unless explicitly assumed, we set the initial conditions to zero.

From equations (2.2), one can immediately obtain:

$$\mathbf{Z}^m(s) = \begin{bmatrix} \frac{1}{s}\frac{k}{\varepsilon} & 0 & -\frac{1}{s}\frac{k}{\varepsilon} & 0 \\ 0 & \frac{1}{s}\frac{1}{\varepsilon} + s\rho\varepsilon & \frac{1}{s}\mathfrak{k} & -\frac{1}{s}\frac{\mathfrak{k}}{\varepsilon} \\ -\frac{1}{s}\frac{k}{\varepsilon} & \frac{1}{s}\mathfrak{k} & \frac{1}{s}\left(\frac{k}{\varepsilon} + \mathfrak{k}\varepsilon\right) + s\mathfrak{I}\,\varepsilon & -\frac{1}{s}\mathfrak{k} \\ 0 & -\frac{1}{s}\frac{\mathfrak{k}}{\varepsilon} & -\frac{1}{s}\mathfrak{k} & \frac{1}{s}\frac{1}{\varepsilon} \end{bmatrix}. \tag{2.4}$$

The mechanical impedance matrix $\mathbf{Z}^m(s)$ in (2.4) can be decomposed in the Foster canonical form as follows, see [**Newcomb (1966)**]:

$$\mathbf{Z}^m(s) = \frac{1}{s}\mathbf{Z}_0^m + s\mathbf{Z}_\infty^m, \tag{2.5}$$

with the residue matrices defined by:

$$\mathbf{Z}_0^m = \begin{bmatrix} \frac{k}{\varepsilon} & 0 & -\frac{k}{\varepsilon} & 0 \\ 0 & \frac{1}{\varepsilon} & \mathfrak{k} & -\frac{\mathfrak{k}}{\varepsilon} \\ -\frac{k}{\varepsilon} & \mathfrak{k} & \left(\frac{k}{\varepsilon} + \mathfrak{k}\varepsilon\right) & -\mathfrak{k} \\ 0 & -\frac{\mathfrak{k}}{\varepsilon} & -\mathfrak{k} & \frac{1}{\varepsilon} \end{bmatrix}, \qquad \mathbf{Z}_\infty^m = \begin{bmatrix} 0 & 0 & 0 & 0 \\ 0 & \rho\varepsilon & 0 & 0 \\ 0 & 0 & \mathfrak{I}\,\varepsilon & 0 \\ 0 & 0 & 0 & 0 \end{bmatrix}.$$

In order to synthesize an analog circuit for the entire beam, it is sufficient to cascade connect a number of elementary analog networks of the beam element, thus assuring the compatibility of the displacement field and the equilibrium of the contact actions.

2.2. Synthesis. The synthesis problem that we tackle is to find a four port grounded network, the admittance matrix of which is equal to the impedance matrix $\mathbf{Z}^m$, given in (2.5), in the sense of the analogy (2.3).

Hence, we are looking for an electrical circuit (see Figure 3) whose admittance matrix $\mathbf{Y}(s)$ is

$$\mathbf{Y}(s) = \frac{1}{s}\mathbf{Y}_0 + s\mathbf{Y}_\infty$$

where s represents the Laplace variable and the residue matrices are:

$$\mathbf{Y}_0 = \frac{I^*}{V^*}\begin{bmatrix} \frac{\Omega^*}{M^*}\frac{k}{\varepsilon} & 0 & -\frac{\Omega^*}{M^*}\frac{k}{\varepsilon} & 0 \\ 0 & \frac{v^*}{T^*}\frac{\mathfrak{k}}{\varepsilon} & \frac{\Omega^*}{T^*}\mathfrak{k} & -\frac{v^*}{T^*}\frac{\mathfrak{k}}{\varepsilon} \\ -\frac{\Omega^*}{M^*}\frac{k}{\varepsilon} & \frac{v^*}{M^*}\mathfrak{k} & \frac{\Omega^*}{M^*}\left(\frac{k}{\varepsilon}+\mathfrak{k}\varepsilon\right) & -\frac{v^*}{M^*}\mathfrak{k} \\ 0 & -\frac{v^*}{T^*}\frac{\mathfrak{k}}{\varepsilon} & -\frac{\Omega^*}{T^*}\mathfrak{k} & \frac{v^*}{T^*}\frac{\mathfrak{k}}{\varepsilon} \end{bmatrix},$$

$$\mathbf{Y}_\infty = \frac{I^*}{V^*}\begin{bmatrix} 0 & 0 & 0 & 0 \\ 0 & \frac{v^*}{T^*}\rho\varepsilon & 0 & 0 \\ 0 & 0 & \frac{\Omega^*}{M^*}\mathfrak{I}\varepsilon & 0 \\ 0 & 0 & 0 & 0 \end{bmatrix}.$$

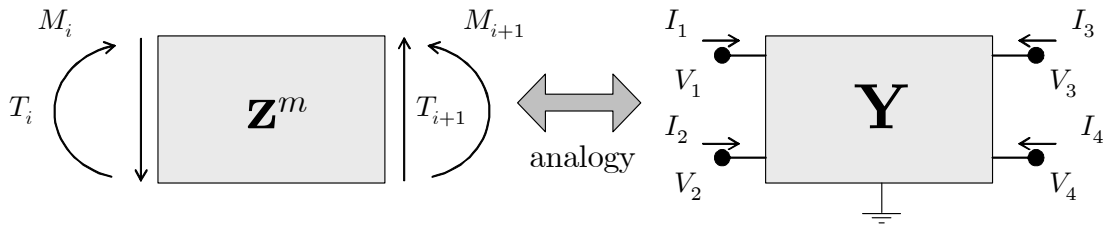

FIGURE 3. Analog circuit of a beam element utilizing the voltage-velocity analogy.

The strategy developed to solve the addressed synthesis problem consists of the following steps:

(1) synthesis of an inductive network whose admittance matrix is $\frac{1}{s}\mathbf{Y}_0$,
(2) synthesis of a capacitive network whose admittance matrix is $s\mathbf{Y}_\infty$,
(3) parallel connection of the aforementioned electrical networks (see Figure 4) for the design of the circuit, the admittance matrix of which is $\mathbf{Y}(s)$.

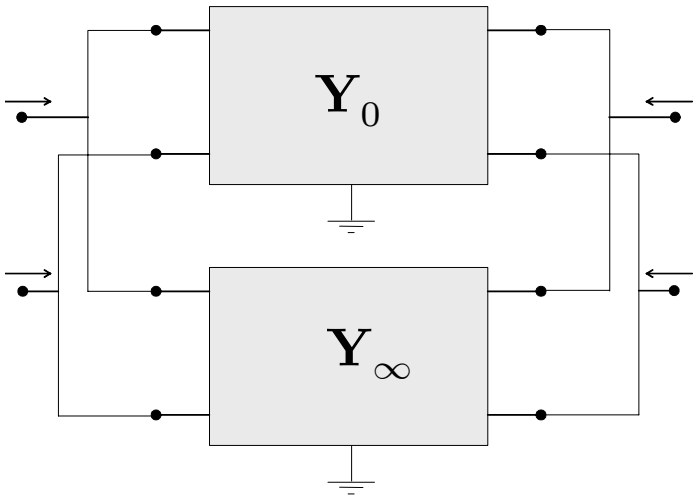

FIGURE 4. Realization of the analog circuit as the parallel connection of two elementary networks.

In order to guarantee that the analog network is reciprocal (see e.g. [**Newcomb (1966)**]), it is necessary to require the symmetry of the admittance matrix $\mathbf{Y}(s)$, which yields the following condition on the scaling parameters:

$$v^* T^* = \Omega^* M^*. \tag{2.6}$$

This condition, from a mechanical point of view, establishes that the power expended of the bending moment M^* on the angular velocity Ω^*, is equal to the power of the shear contact action T^* expended on the velocity v^*. Therefore, the scaling parameters cannot be chosen independently when one wants to design electric networks constituted only by reciprocal elements. Furthermore, introducing the parameters μ and κ, defined by:

$$\mu = \frac{\mathfrak{k}}{k}\frac{(v^*)^2}{(\Omega^*)^2}, \qquad \kappa = \frac{\mathfrak{k}\varepsilon^2}{k},$$

the residue at zero becomes:

$$\mathbf{Y}_0 = \frac{I^*\Omega^*}{V^*M^*}\frac{k}{\varepsilon}\begin{bmatrix} 1 & 0 & -1 & 0 \\ 0 & \mu & \sqrt{\mu\kappa} & -\mu \\ -1 & \sqrt{\mu\kappa} & 1+\kappa & -\sqrt{\mu\kappa} \\ 0 & -\mu & -\sqrt{\mu\kappa} & \mu \end{bmatrix}.$$

The capacitive network can be designed as two capacitors connected at the second and third terminals of the grounded network as shown in Figure 5; the capacitance of these two elements are given by:

$$C_1 = \frac{I^* v^*}{V^* T^*}\rho\varepsilon, \qquad C_2 = \frac{I^*\Omega^*}{V^* M^*}\mathfrak{I}\varepsilon.$$

Therefore, the ratio of the two capacitances is given by:

$$\frac{C_1}{C_2} = \frac{(v^*)^2}{(\Omega^*)^2}\frac{\rho}{\mathfrak{I}}.$$

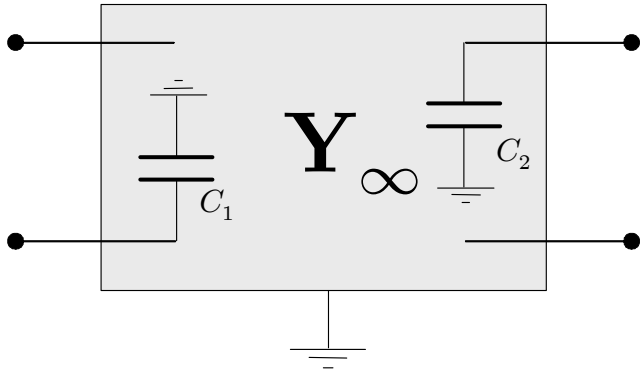

FIGURE 5. Realization of the network $s\mathbf{Y}_\infty$.

The design of the inductive circuit is much more involved, since the residue in zero is not diagonal. It is well known (see e.g. [**Slepian and Weinbeg (1958)**] and [**Panel (1962)**], regarding the synthesis of one-element type networks) that $\frac{1}{s}\mathbf{Y}_0$ is realizable as the admittance of an n-port network constituted only by inductors and containing only $n+1$ terminals, one of which is a common terminal for all the ports, if and only if the residue matrix $\mathbf{Y}_0$ is dominant[11] and each of the off-diagonal terms is non-positive[12]. One can easily verify that $\mathbf{Y}_0$ is not dominant and that some of the off-diagonal elements are positive. Therefore, even if the realization of $\frac{1}{s}\mathbf{Y}_0$ is not unique, it is impossible to synthesize it without using ideal transformers. In what follows, we synthesize the considered network with a single two-port transformer. Towards this goal, we decompose $\mathbf{Y}_0$ as the sum of the two following matrices:

$$\mathbf{Y}_0 = \frac{I^*\Omega^*}{V^*M^*}\frac{k}{\varepsilon}\begin{bmatrix} 1 & 0 & -1 & 0 \\ 0 & 0 & 0 & 0 \\ -1 & 0 & 1 & 0 \\ 0 & 0 & 0 & 0 \end{bmatrix} + \frac{\Omega^*}{M^*}\frac{k}{\varepsilon}\begin{bmatrix} 0 & 0 & 0 & 0 \\ 0 & \mu & \sqrt{\mu\kappa} & -\mu \\ 0 & \sqrt{\mu\kappa} & \kappa & -\sqrt{\mu\kappa} \\ 0 & -\mu & -\sqrt{\mu\kappa} & \mu \end{bmatrix}. \tag{2.7}$$

By means of this decomposition, the synthesis problem has been drastically reduced to the design of a three-port inductive grounded network, whose residue at zero matrix is:

$$\mathbf{Y}_0^{red} = \frac{I^*\Omega^*}{V^*M^*}\frac{k}{\varepsilon}\begin{bmatrix} \mu & \sqrt{\mu\kappa} & -\mu \\ \sqrt{\mu\kappa} & \kappa & -\sqrt{\mu\kappa} \\ -\mu & -\sqrt{\mu\kappa} & \mu \end{bmatrix}.$$

In fact, the first term on the RHS of (2.7) can be immediately synthesized as an inductor interconnecting the first and the third terminals (see Figure 6). The value of the inductance is equal to:

$$L_1 = \frac{V^*M^*}{I^*\Omega^*}\frac{\varepsilon}{k}.$$

[11]A real matrix is said to be dominant if each of its main-diagonal elements is not less than the sum of the absoulute values of all the other elements in the same row.

[12]If one is not restricting to $n+1$ terminals the following results are known: i) a dominant matrix, with any distribution of signs in the off-diagonal terms, may always be realized with only inductors; ii) paramountcy is a necessary (and sufficient, for the three-port case) condition for the matrix for its realizability without transformers.

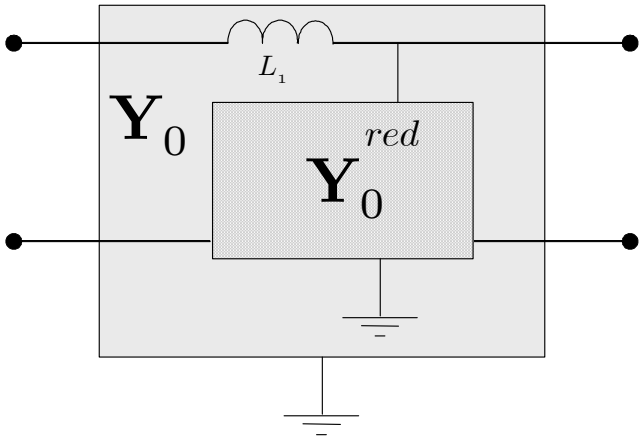

FIGURE 6. A first step towards the synthesis of $\frac{1}{s}\mathbf{Y}_0$.

Multiplying the inductance L_1 by the capacitance C_1 we get:

$$C_1 L_1 = \frac{(v^*)^2}{(\Omega^*)^2}\frac{\rho}{k}\varepsilon^2.$$

The synthesis of a network governed by $\mathbf{Y}_0^{red}$ is still very tricky. Nevertheless, by noticing that the rank of $\mathbf{Y}_0^{red}$ is equal to one, the following decomposition hold

$$\mathbf{Y}_0^{red} = \begin{bmatrix} 1 \\ \sqrt{\frac{\kappa}{\mu}} \\ -1 \end{bmatrix} \left(\frac{I^*\Omega^*}{V^*M^*}\frac{k}{\varepsilon}\mu\right) \begin{bmatrix} 1 & \sqrt{\frac{\kappa}{\mu}} & -1 \end{bmatrix};$$

and the circuit can be designed (see [**Newcomb (1966)**]) as shown in Figure 7, were the appearing inductance given by

$$L_{red} = \frac{V^*T^*}{I^*v^*}\frac{\varepsilon}{\ell}.$$

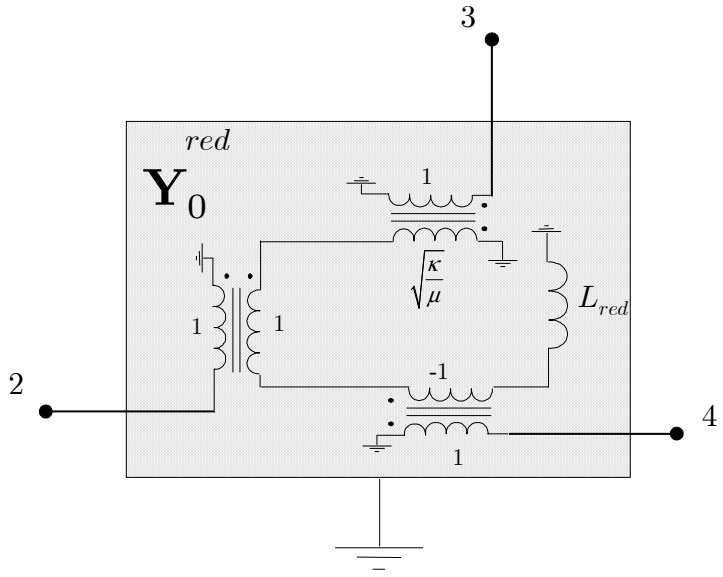

FIGURE 7. Direct design of $1/s\mathbf{Y}_0$.

The previous topology can be further simplified by noticing that the turns-ratio of the first and third transformers are equal in absolute value and opposite in sign, as shown in Figure 8.

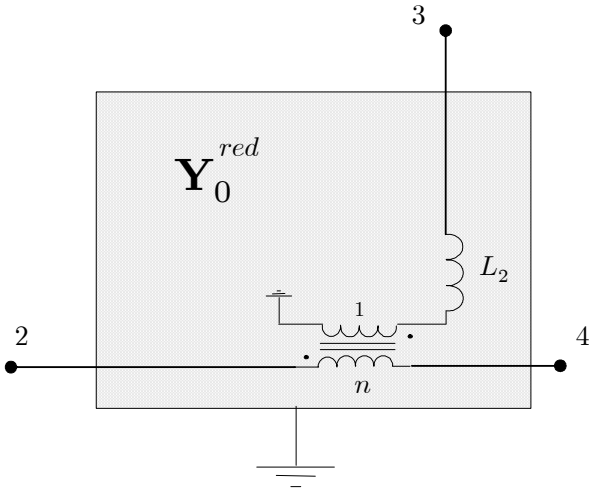

FIGURE 8. Minimal design of $1/s\mathbf{Y}_0^{red}$.

In order to find the turns-ratio of the used transformer and the value of the introduced inductance, let us find the admittance matrix of the network shown in Figure 8 and compare it to $\mathbf{Y}_0^{red}$. The constitutive equation of the inductor L_2 and of the ideal transformer yields:

$$\begin{gathered}\tilde{I}_2 = -\tilde{I}_4,\\ -\frac{\tilde{V}_2 - \tilde{V}_4}{n} + \tilde{V}_3 = sL_2\,\tilde{I}_3,\\ n\tilde{I}_4 = \tilde{I}_3.\end{gathered}$$

Therefore the admittance of the circuit in Figure 8 is

$$\frac{1}{sL_2}\begin{bmatrix} 1/n^2 & -1/n & -1/n^2 \\ -1/n & 1 & 1/n \\ -1/n^2 & 1/n & 1/n^2 \end{bmatrix},$$

which, when compared with $\mathbf{Y}_0^{red}$, gives

$$L_2 = \frac{V^* M^*}{I^* \Omega^*}\frac{1}{\mathfrak{k}_\varepsilon}, \qquad n = \frac{\Omega^*}{v^*}\varepsilon$$

Hence, the inductance L_{red} is related to L_2 by:

$$\frac{L_2}{L_{red}} = \frac{(v^*)^2}{(\Omega^*)^2}\frac{1}{\varepsilon^2} = \frac{1}{n^2}.$$

By inspection, one can immediately obtain the following set of relations between all the parameters so far introduced:

$$n^2 C_1 L_1 = \frac{\rho}{k}\varepsilon^4, \quad \frac{C_1}{C_2}n^2 = \frac{\rho}{\mathfrak{J}}\varepsilon^2, \quad \frac{L_1}{L_2} = \frac{\mathfrak{k}}{k}\varepsilon^2. \tag{2.8}$$

The previous set of equations provides a group of conditions to be imposed on the employed circuit elements, completely independent of the arbitrarily chosen scaling parameters. Hence, it is easily seen that for every possible choice of scaling parameters there are always three fixed constraints on the circuit elements, which depend only on the physical properties of the beam and on the sampling step of the grid.

In order to synthesize the analog circuit for the whole Timoshenko beam, it is sufficient to cascade connect a number of the found analog circuits for the generic beam element. Indeed, the electrical cascade connection corresponds exactly to the mechanical conditions of continuity of the contact actions and the kinematical descriptors over the length of the beam.

In order to synthesize the electric analog of an Euler-Bernoulli beam, it is sufficient to take the limit of (2.8) as the rotatory inertia goes to zero and the shear stiffness goes to infinity, thus:

$$L_2 \to 0, \quad C_2 \to 0.$$

Therefore, for the Euler-Bernoulli beam, the analog circuit becomes that one depicted in Figure 9, with

$$C_1 L_1 n^2 = \frac{\rho}{k}\varepsilon^4. \tag{2.9}$$

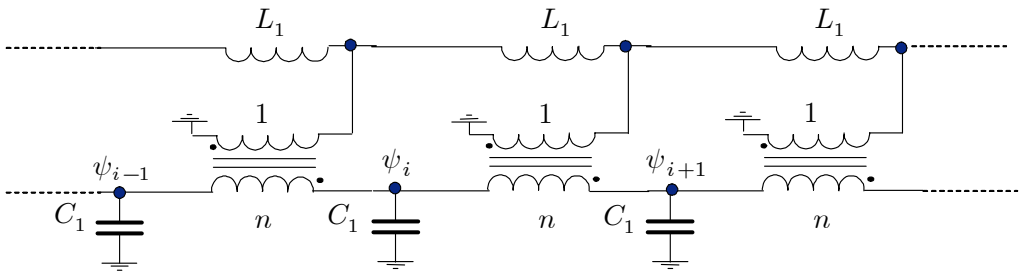

FIGURE 9. Circuit analog of an Euler beam corresponding to the voltage-velocity analogy.

We emphasize that once the transformers ratio n and the capacitance C_1 have been chosen, the inductance decreases with the fourth power of the grid size ε.

The equation of equilibrium of the analog circuit sketched in Figure 9 in terms of the flux-linkage ψ_i at the generic internal node i is

$$\frac{\psi_{i+2} - 4\psi_{i+1} + 6\psi_i - 4\psi_{i-1} + \psi_{i-2}}{L_1 C_1 n^2} + \ddot{\psi}_i = 0, \tag{2.10}$$

which represents a discrete form of the beam equation, once condition (2.9) is satisfied.

REMARK 9. *In order to synthesize the analog circuit for the Euler-Bernoulli beam using a finite difference approximation and exploiting the standard immittance matrices synthesis techniques, it is necessary to study initially the Timoshenko beam and then set the shear deformability and the rotatory inertia to zero. In fact, as the shear stiffness goes to infinity, the mechanical impedance matrix representation in (2.4) becomes impossible.*

2.3. Synthesis of the constraints. The external constraints applied at the beam ends impose electrical constraints on the analog circuit (representing e.g. the electric terminations of the circuit depicted in Figure 9), which can be easily synthesized. The obtained boundary circuits are cascade connected to the ending modules of the analog network.

For instance, for a simply supported beam, the electrical elements to simulate the hinged ends are respectively determined by the following set of equations:

$$\begin{cases} \text{Left hinge:} & V_2 = 0, \quad I_1 = 0 \\ \text{Right hinge:} & V_4 = 0, \quad I_3 = 0 \end{cases}.$$

The corresponding analog circuit is shown in Figure 10.

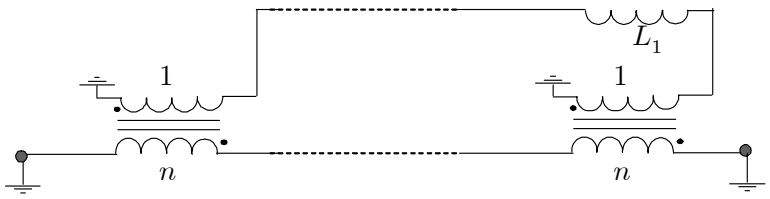

FIGURE 10. Boundary elements of the circuit analog to a simply supported Euler beam.

3. Synthesis of the analog circuit based on a variational formulation

In this Section we present an alternative method for synthesizing the analog circuit of the vibrating Timoshenko beam described in the previous Section. The proposed method exploits the basic version of the Euler finite difference method (employed for instance in numerical analysis as an alternative to the Finite Element Method, see e.g. [**Richards (1977)**]) and is articulated as follows:

(1) we recall the variational principle governing the free vibrations of Timoshenko beams,
(2) we define a mesh over the beam reference configuration and introduce- as a set of Lagrange coordinates- the sampled values of the fields describing the beam kinematics at the mesh nodes,

(3) we approximate the infinite dimensional Lagrangian for Timoshenko beam via a finite dimensional Lagrangian in terms of introduced Lagrange coordinates,
(4) with a well-known procedure (see e.g. [**Karplus and Soroka (1959)**], [**Crandall et al. (1968)**], [**Gantmacher (1980)**]) we synthesize a lumped electrical circuit, the evolution of which is governed by the so found finite dimensional Lagrangian.

3.1. Lagrangian of the lumped network. The Hamilton's principle is given as:

$$\delta \int_{t_0}^{t_1} \mathcal{L}\, dt = \delta \int_{t_0}^{t_1} \left(\mathcal{K} - \mathcal{E} - \mathcal{W}_{in}\right)\, dt = 0,$$

where is the $\mathcal{L}$ is the Lagrangian, $\mathcal{K}$ is the total kinetic energy, $\mathcal{E}$ is the total strain energy, $\mathcal{W}_{in}$ is the total input energy and t_0 and t_1 are two arbitrary instants in time.

For a Timoshenko beam excited only at its ends, the Lagrangian reads (see for instance [**Soedel (1993)**] and [**Meirovitch (2000)**]):

(3.1)
$$\mathcal{L} = \int_0^l \mathcal{K}^{(d)}\left(\dot{w}, \dot{\vartheta}\right)\, dx - \int_0^l \mathcal{E}^{(d)}\left(\vartheta, w', \vartheta'\right)\, dx - T_0 w\left(0,t\right) - T_l w\left(l,t\right) - M_0 \vartheta\left(0,t\right) - M_l \vartheta\left(l,t\right).$$

In equation (3.1), the density of kinetic energy $\mathcal{K}^{(d)}$ and the density of elastic strain energy $\mathcal{E}^{(d)}$ are given by:

$$\mathcal{K}^{(d)}\left(\dot{w}, \dot{\vartheta}\right) = \frac{1}{2}\left(\rho\, \dot{w}^2 + \mathfrak{I}\, \dot{\vartheta}^2\right), \tag{3.2a}$$

$$\mathcal{E}^{(d)}\left(\vartheta, w', \vartheta'\right) = \frac{1}{2}\left(\mathfrak{k}\, \left(w' - \vartheta\right)^2 + k\, \left(\vartheta'\right)^2\right), \tag{3.2b}$$

and T_0, T_l , M_0 , M_l represent in this case the transversal forces and bending moments applied at the edges of the beam.

The Euler-Lagrange equations associated to (3.1) and (3.2) are:

$$\begin{cases} \rho\, \ddot{w} - \mathfrak{k}\, \left(w' - \vartheta\right)' = 0 \\ \mathfrak{I}\, \ddot{\vartheta} - \mathfrak{k}\, \left(w' - \vartheta\right) - k\vartheta'' = 0 \end{cases}. \tag{3.3}$$

In order to approximate the infinite dimensional system governed by the Lagrangian (3.1) with a finite dimensional Lagrangian system we consider the following extended numerical formula for the integration of the Lagrangian spatial density $\mathcal{K}^{(d)} - \mathcal{E}^{(d)}$ appearing in (3.1):

$$\mathcal{L} \simeq \varepsilon \sum_{i=0}^{N} \mathcal{K}_i^{(d)}\left(\dot{w}_i, \dot{\vartheta}_i\right) - \varepsilon \sum_{i=1}^{N} \mathcal{E}_i^{(d)}\left(\vartheta_i, w_i', \vartheta_i'\right) - T_0 w_0 - T_l w_N - M_0 \vartheta_0 - M_l \vartheta_N,$$

where we have used the notation:

$$\left(\cdot\right)_i := \left(\cdot\right)\left(x_i, t\right), \qquad \left(\cdot\right)_i' := \frac{\left(\cdot\right)_i - \left(\cdot\right)_{i-1}}{\varepsilon}, \tag{3.4}$$

for the sampled values of the mechanical fields. We explicitly remark that for estimating spatial derivatives the backward finite differences rule has been chosen.

We can express $\mathcal{K}_i^{(d)}$ and $\mathcal{E}_i^{(d)}$, i.e. the kinetic and strain energy densities at x_i by:

$$\begin{aligned} \mathcal{E}_i^{(d)} &\simeq \frac{1}{2}\left(\mathfrak{k}\left(\frac{w_i - w_{i-1}}{\varepsilon} - \vartheta_i\right)^2 + k\left(\frac{\vartheta_i - \vartheta_{i-1}}{\varepsilon}\right)^2\right), \\ \mathcal{K}_i^{(d)} &= \frac{1}{2}\left(\rho\, \dot{w}_i^2 + \mathfrak{I}\, \dot{\vartheta}_i^2\right). \end{aligned}$$

Hence, the Lagrangian of the Timoshenko beam can be conveniently approximated by:

$$\mathcal{L} \simeq \frac{1}{2}\varepsilon \sum_{i=0}^{N} \left(\rho\, \dot{w}_i^2 + \mathfrak{I}\, \dot{\vartheta}_i^2 \right) + \tag{3.5}$$
$$- \frac{1}{2}\varepsilon \sum_{i=0}^{N-1} \left(\mathfrak{k} \left(\frac{w_{i+1} - w_i}{\varepsilon} - \vartheta_{i+1} \right)^2 + k \left(\frac{\vartheta_{i+1} - \vartheta_i}{\varepsilon} \right)^2 \right) +$$
$$- T_0 w_0 - T_l w_N - M_0 \vartheta_0 - M_l \vartheta_N =: \mathcal{L}^{fin}.$$

The Lagrangian $\mathcal{L}^{fin}$ in (3.5) can be regarded as the Euler finite difference approximation of the Timoshenko beam Lagrangian given by (3.1). Furthermore, it is easy to see that $\mathcal{L}^{fin}$ describes the mechanical system reported in Figure 11 in [**Roseau (1987)**], where the blocks are rigid bodies, and the bars are massless rigid links. The mass and rotatory inertia of the rigid blocks are related to the linear mass density ρ and to the cross section inertia $\mathfrak{I}$, respectively; the stiffness of the extensional springs is related to the bending stiffness k; the stiffness of the rotational springs depends on the shear stiffness $\mathfrak{k}$.

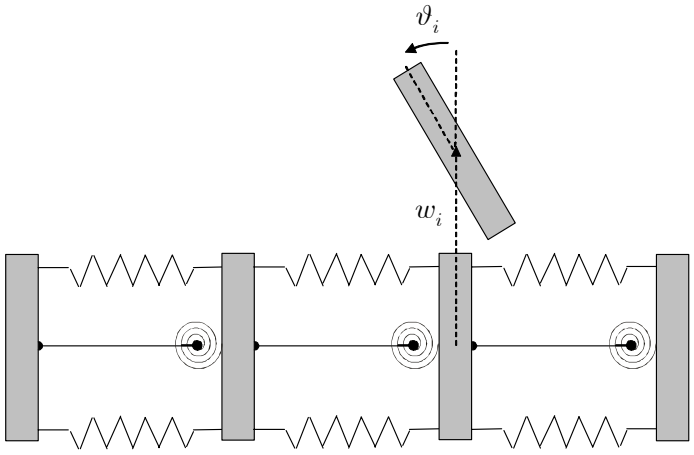

FIGURE 11. Sketch of a finite degrees of freedom mechanical system approximting the Timoshenko beam.

Similarly, the Euler-Lagrange equations obtained by (3.5) can be easily seen to govern the evolution of a completely passive lumped circuit, once an analogy between mechanical and electrical kinematical descriptors has been established. The standard procedure for determining physical analogies requires the introduction of suitable scaling factors for the kinematical descriptors to be recognized as analogs. In the considered instance we introduce the scaling factors w^*, ϑ^*, ψ^*, φ^* respectively for transverse displacement, section rotation, and the two flux linkages respectively.

Therefore the synthesis problem is to find a $2N+2$ degrees of freedom electrical circuit whose Lagrangian is given by:

$$\mathcal{L}^{el} = \frac{1}{2}\varepsilon \sum_{i=0}^{N} \left(\frac{\rho \left(w^*\right)^2}{\left(\psi^*\right)^2} \dot{\psi}_i^2 + \frac{\mathfrak{I} \left(\vartheta^*\right)^2}{\left(\varphi^*\right)^2} \dot{\varphi}_i^2 \right) + \tag{3.6}$$
$$- \frac{1}{2}\varepsilon \sum_{i=0}^{N-1} \left(\mathfrak{k} \left(\frac{w^*}{\psi^*} \frac{\psi_{i+1} - \psi_i}{\varepsilon} - \frac{\vartheta^*}{\varphi^*} \varphi_{i+1} \right)^2 + k \left(\frac{\vartheta^*}{\varphi^*} \frac{\varphi_{i+1} - \varphi_i}{\varepsilon} \right)^2 \right) +$$
$$- T_0 \frac{w^*}{\psi^*} \psi_0 - T_l \frac{w^*}{\psi^*} \psi_N - M_0 \frac{\vartheta^*}{\varphi^*} \varphi_0 - M_l \frac{\vartheta^*}{\varphi^*} \varphi_N,$$

where the ψ_i's and φ_i's represent the flux linkages of $2N+2$ nodes measured with respect of a common reference ground.

3.2. Synthesis. To each mechanical sampling node must correspond two electrical nodes in the analog circuit, as shown in Figure 12: ψ_i is the electrical analog of the mechanical deflection at node i, while φ_i is the electrical analog of the rotation also at node i. However the generalized variables of the electrical system are given by ψ_i and φ_i with i varying between 0 and N. In this way the flux linkages represent the analog variables of the displacements and rotations, while the currents are the electrical analogs of the bending moments and shear contact actions[13].

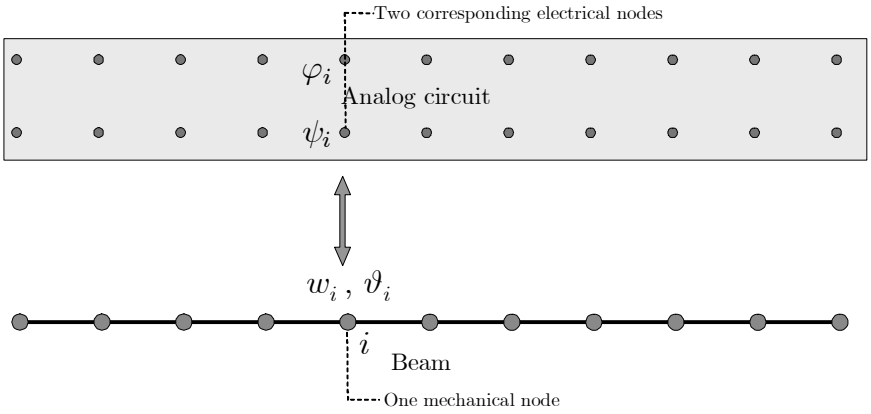

FIGURE 12. Schematic representation of the beam and its analog circuit.

The synthesis of the analog circuit is really straightforward, in fact we connect each node of the circuit to a grounded capacitor the value of which is

$$C_1 = \frac{\varepsilon\rho \left(w^*\right)^2}{\left(\psi^*\right)^2},$$

if the flux-linkage at that node is analog to the beam deflection, or

$$C_2 = \frac{\varepsilon\mathfrak{I} \left(\vartheta^*\right)^2}{\left(\varphi^*\right)^2},$$

[13]Nevertheless the problem may be solved also in a different way, looking for an analog circuit where the displacements are represented by stored charges and the contact actions by voltage drops.

if the flux-linkage at that node is analog to the beam rotation. Following the presented procedure we design a circuit the electric energy of which is given by the kinetic energy in (3.6): i.e. the mechanical kinetic energy finds its electrical analog in the electric (capacitive) energy.

By interconnecting a pair of adjacent nodes the flux linkages of which are φ_{i+1} and φ_i via an inductor of inductance

$$L_1 = \frac{\varepsilon\,(\varphi^*)^2}{k\vartheta_0^2},$$

it is immediate to obtain the strain energy term (3.6) in which the bending stiffness appears by means of magnetic (inductive) energy. Furthermore, in order to obtain the remaining term in the strain energy (3.6), again by means of magnetic energy, a set of auxiliary nodes α_i must be introduced (see Figure 13), the flux linkages of which we want to fix equal to

$$\alpha_{i+1} = \frac{\varphi^* w^*}{\vartheta^* \psi^*} \frac{\psi_{i+1} - \psi_i}{\varepsilon}.$$

This is done by means of an ideal transformer interconnected with a port between ψ_{i+1} and ψ_i and with the other port between ground and α_{i+1}; the turns-ratio is given by

$$n = \frac{\varepsilon \vartheta_0 \psi^*}{\varphi^* w^*}.$$

Finally the nodes α_i and φ_i must be interconnected by an inductor of inductance

$$L_2 = \frac{(\varphi^*)^2}{\varepsilon \mathfrak{k}\,(\vartheta^*)^2}.$$

The last four terms in (3.6), involving the input work of the concentrated external loads at the edges of the beam, have as electric analogs four current generators applied in parallel connections with the four capacitors at the boundary nodes of the circuit analog. For instance the current generator at the node ψ_0 imposes a current of value

$$I_1 = T_0 \frac{w^*}{\psi^*},$$

the current imposed by the other three sources are similarly determined (see equations (3.7) below).

Heretofore, we have designed a completely passive circuit the Lagrangian of which is given by:

$$\begin{aligned}\mathcal{L}^{el} = \frac{1}{2}\sum_{i=0}^{N}\left(C_1\,\dot{\psi}_i^2 + C_2\,\dot{\varphi}_i^2\right) + \\ - \frac{1}{2}\sum_{i=0}^{N-1}\left\{\frac{1}{L_2}\left(\frac{(\psi_{i+1}-\psi_i)}{n} - \varphi_{i+1}\right)^2 + \frac{1}{L_1}\left(\varphi_{i+1}-\varphi_i\right)^2\right\} + \\ - I_1\psi^* - I_2\psi_N - I_3\varphi_0 - I_4\varphi_N,\end{aligned}$$

with:

$$C_1 = \varepsilon\rho\frac{(w^*)^2}{(\psi^*)^2}, \quad C_2 = \varepsilon\mathfrak{I}\frac{(\vartheta^*)^2}{(\varphi^*)^2}, \tag{3.7a}$$

$$L_1 = \frac{\varepsilon}{k}\frac{(\varphi^*)^2}{(\vartheta^*)^2}, \quad L_2 = \frac{1}{\varepsilon\mathfrak{k}}\frac{(\varphi^*)^2}{(\vartheta^*)^2}, \quad n = \varepsilon\frac{\vartheta^*\psi^*}{\varphi^* w^*}, \tag{3.7b}$$

$$I_1 = T_0\frac{w^*}{\psi^*}, \quad I_2 = T_l\frac{w^*}{\psi^*}, \quad I_3 = M_0\frac{\vartheta^*}{\varphi^*}, \quad I_4 = M_l\frac{\vartheta^*}{\varphi^*}.. \tag{3.7c}$$

In Figure 13 (being equal to Figure 9 with the exception of the specific nodes labelling) the aforementioned analog circuit for the internal nodes of the Timoshenko beam is exhibited,

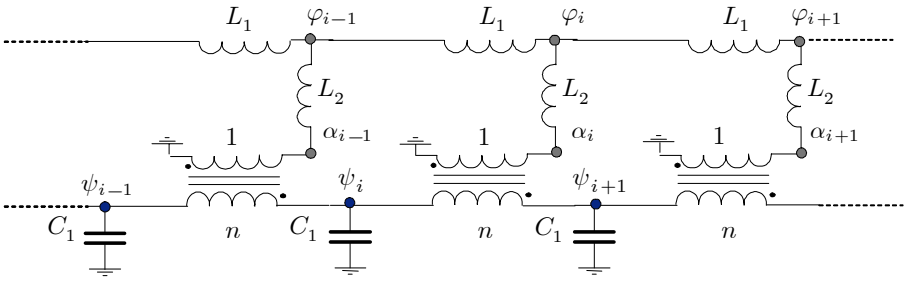

FIGURE 13. Internal modules of the electrical analog of the Timoshenko beam.

while Figure 14 explains the connection of the current sources simulating the external loads at the edges.

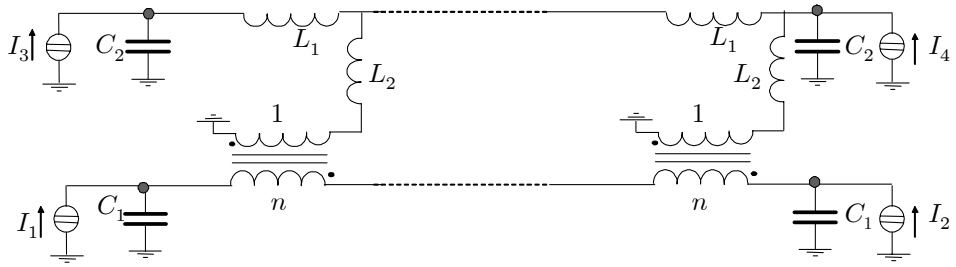

FIGURE 14. Boundary elements of the electrical analog.

Starting from relations (3.7) it is immediate to see that the conditions (2.8), independent of the adopted electromechanical scaling factors, hold.

Before concluding the Section we specify the approximation scheme in which the lumped circuit in Figure 13 verifies the Timoshenko equations. Indeed Euler-Lagrange equations for the internal nodes are:

$$\begin{cases} C_1\ddot{\psi}_i - \dfrac{1}{L_2 n^2}\left(\psi_{i+1} - 2\psi_i + \psi_{i-1}\right) + \dfrac{1}{L_2 n}\left(\varphi_i - \varphi_{i-1}\right) = 0 \\ C_2\,\ddot{\varphi}_i - \dfrac{1}{L_2}\left(\dfrac{\left(\psi_{i+1} - \psi_i\right)}{n} - \varphi_i\right) - \dfrac{1}{L_1}\left(\varphi_{i+1} - 2\varphi_i + \varphi_{i-1}\right) = 0 \end{cases},$$

and as we expected, the previous set of ordinary differential equations represents a finite difference approximation of the governing equations for the free vibrations of a Timoshenko beam given by equations (3.3). Similar considerations hold for the transversality conditions.

REMARK 10. *Within this variational framework, the problem of designing electrical circuits to simulate external constraints acting on the beam have not been addressed. Nevertheless the theory so far developed allows for an immediate solution of this problem. As an example consider a simply supported beam: the electrical analog of the simply supported beam can be trivially synthesized short-circuiting the nodes ψ_0 and ψ_N to ground and leaving open circuited φ_0 and φ_N, i.e. open-circuiting the two current generators I_3 and I_4.*

4. Analysis of the PEM beam

4.1. Synthesis of the dissipative circuit. For arbitrary boundary conditions the needed dissipative circuit is not represented by a differential operator. We limit our analysis to simply supported beams; in this case the square root of the fourth derivative is equal to the negative second derivative. For other boundary conditions it is possible to represent the square root of the fourth derivative as a transform of the negative second derivative (see [**Russell (1988)**]) and the small sensitivity of the system performance on the electric damping may allude that the negative second derivative is giving acceptable results for different boundary conditions.

The negative second derivative is easily synthesized by interconnecting each piezoelectric element to the adjacent one by means of a resistor, whose resistance is R.

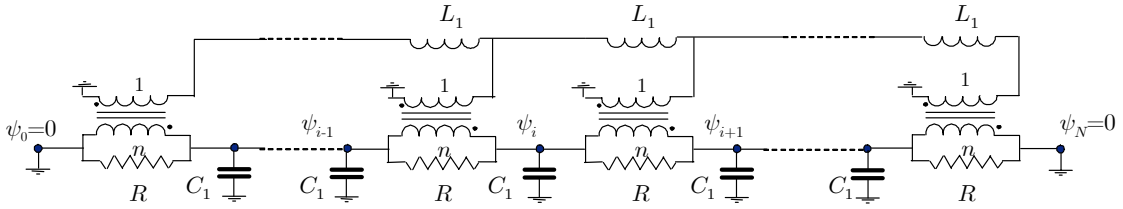

FIGURE 15. Analog circuit of a simply supported beam with square root damping.

In Figure 15 we report the circuit analog of a simply supported beam with square root damping. In this case the homogenized equations of the electric circuit is

$$c_{\text{hom}}\ddot{\psi} + a_{\text{hom}}\psi^{IV} - b_{\text{hom}}\dot{\psi}'' = 0,$$

with boundary conditions

$$\psi(0,t) = \psi(l,t) = 0, \quad \psi''(0,t) = \psi''(l,t) = 0,$$

and homogenized coefficients

$$c_{\text{hom}} = \frac{C_1}{\varepsilon}, \quad a_{\text{hom}} = \frac{\varepsilon^3}{L_1 n^2}, \quad b_{\text{hom}} = \frac{\varepsilon}{R}. \tag{4.1}$$

While the equations of the lumped circuit are

$$
\begin{aligned}
& C_1\ddot{\psi}_j + \frac{1}{L_1 n^2}\left(\psi_{i+2} - 4\psi_{i+1} + 6\psi_i - 4\psi_{i-1} + \psi_{i-2}\right) \\
& \qquad -\frac{1}{R}\left(\dot{\psi}_{i+1} - 2\dot{\psi}_i + \dot{\psi}_{i-1}\right) = 0, \quad i = 2, ..., N-2, \\
& C_1\ddot{\psi}_1 + \frac{1}{L_1 n^2}\left(5\psi_1 - 4\psi_2 + \psi_3\right) - \frac{1}{R}\left(\dot{\psi}_2 - 2\dot{\psi}_1\right) = 0, \\
& C_1\ddot{\psi}_{N-1} + \frac{1}{L_1 n^2}\left(5\psi_{N-1} - 4\psi_{N-2} + \psi_{N-3}\right) - \frac{1}{R}\left(-2\dot{\psi}_{N-1} + \dot{\psi}_{N-2}\right) = 0, \\
& \psi_0 = 0, \\
& \psi_N = 0,
\end{aligned}
\tag{4.2}
$$

4.2. Prototype design. We consider a simply supported aluminum beam fully covered by piezoelectric ceramics and interconnect the electric elements as the capacitors C_1 in Figure 15. The material properties of the beam and piezoelectric transducers are the reported in Table 2, while the geometry is reported in the second line of Table 1. Therefore the homogenized constitutive coefficients are:

$$
\begin{aligned}
k_{\text{hom}} &= k_P = 3.859\,\text{N}\,\text{m}^2, \\
c_{\text{hom}} &= \frac{C}{\varepsilon} = 3.633\ \mu\text{F}/\,\text{m}, \\
g_{\text{hom}} &= g = 1.006 \times 10^{-3}\,\text{N}\,\text{m}\,\text{V}^{-1}, \\
\rho_{\text{hom}} &= \rho_P = 0.2280\,\text{kg}/\,\text{m}.
\end{aligned}
$$

From equation (1.6), the modal coupling is

$$
\gamma = \frac{g_{\text{hom}}}{\sqrt{k_{\text{hom}} c_{\text{hom}}}} = 0.2687.
$$

From equation (1.6) together with (1.7) and (1.8) the optimal constitutive coefficients of the distributed network, a_{hom} and b_{hom}, are

$$
\begin{aligned}
a_{\text{hom}} &= \frac{k_{\text{hom}} c_{\text{hom}}}{\rho_{\text{hom}}} = 61.48 \times 10^{-6}\,\text{m}^3\,\text{H}^{-1}, \\
b_{\text{hom}} &= \sqrt{\frac{3}{2}}\sqrt{\frac{c_{\text{hom}}}{\rho_{\text{hom}}}}\, g_{\text{hom}} = 4.918 \times 10^{-6}\,\text{m}\,\Omega^{-1}.
\end{aligned}
$$

Hence, the optimal values of the inductance, transformer turn-ratio and resistance are:

$$
L_1 n^2 = 16264\ \varepsilon^3\,\text{H}\,\text{m}^{-3}, \quad R = 203330\ \varepsilon\ \ \Omega\,\text{m}^{-1}.
$$

These values may be expressed in terms of the number of used piezoelectric elements N_P, since $\varepsilon = \dfrac{l}{N_P}$:

$$
L_1 n^2 = 9807\frac{1}{(N_P)^3}\,\text{H}, \quad R = 40870\frac{1}{N_P}\,\Omega,
$$

which shows that by using 10 piezoelectric elements (see Figure 16) and unitary transformer the inductance becomes smaller than 10 H and the resistance is still greater than 4 kΩ.

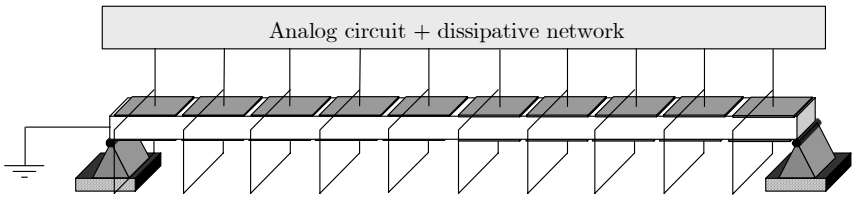

FIGURE 16. Sketch of a simply supported PEM beam with fourth order transmission line.

4.3. Analysis of the lumped circuit. In the present Section we sketch a method to analyze the modal properties of the lumped circuit described in Figure 15. The analysis of the synthesized lumped optimal circuit leads to (4.2) which upon introducing the matrix where the dimensionless $(N_P-2)\times(N_P-2)$ matrix

$$\mathring{\mathcal{N}} = \begin{bmatrix} 2 & -1 & 0 & ... & 0 \\ -1 & 2 & -1 & ... & ... \\ 0 & -1 & ... & ... & 0 \\ ... & ... & ... & 2 & -1 \\ 0 & ... & 0 & -1 & 2 \end{bmatrix},$$

may be written as

$$C_1\,\ddot{\boldsymbol{\psi}} + \frac{1}{L_1 n^2}\mathring{\mathcal{N}}^2\boldsymbol{\psi} + \frac{1}{R}\mathring{\mathcal{N}}\dot{\boldsymbol{\psi}} = 0.$$

Let us notice that the square root damping is inherited by the lumped circuit. As a consequence the analysis of the lumped interconnecting circuit is drastically simplified, because the modal properties of the considered circuit are completely known once the three-point boundary value difference problem associated to $\mathring{\mathcal{N}}$ has been solved.

The eigenvalues and eigenvectors of the tridiagonal matrix $\mathring{\mathcal{N}}$ are determined by the set of linear equations:

$$\begin{cases} -\mathring{v}_{i-1} + \left(2 - \mathring{\lambda}\right)\mathring{v}_i - \mathring{v}_{i+1} = 0, \quad 1 \le i \le N_P - 1, \\ \mathring{v}_0 = 0, \quad -\mathring{v}_{N_P} = 0. \end{cases} \tag{4.3}$$

By following the same procedure as in Section 2.3, the general solution to the given constant coefficients second order difference equation is

$$\mathring{v}_i = c_1 T_i(z) + c_2 U_{i-1}(z), \quad z = 1 - \frac{\mathring{\lambda}}{2}, \tag{4.4}$$

where c_1 and c_2 are arbitrary constants, and the Chebysev polynomials in (2.8a) and (2.8b) in Chapter 6 have been used.

The constants c_1 and c_2 are found by imposing the boundary conditions

$$\mathring{v}_0 = c_1 = 0, \quad \mathring{v}_{N_P} = c_2 U_{N_P-1}(z) = 0.$$

Since we are seeking a non-trivial solution to (4.3), $c_2 \neq 0$, we have the condition

$$U_{N_P-1}(z) = 0, \tag{4.5}$$

which determines the solution in the form

$$v_i = c_2 U_{i-1}(z).$$

The roots of the polynomial equation (4.5) are found by the use of (2.9b) in Chapter 6

$$z = \cos\left[\frac{k\pi}{N_P+1}\right], \quad k = 1, ..., N_P.$$

Therefore, the eigenvalues become

$$\mathring{\lambda}^{(j)} = 2\left(1 - \cos\left[\frac{j\pi}{N_P+1}\right]\right) = 4\sin^2\left[\frac{j\pi}{2\,(N_P+1)}\right], \qquad k = 1, ..., N_P. \tag{4.6}$$

The eigenvectors are

$$\mathring{v}_i^{(j)} = \frac{\sqrt{2}}{\sqrt{N_P+1}}\sin\left[i\frac{j\pi}{N_P+1}\right], \quad i, j = 1, ..., N_P. \tag{4.7}$$

where the constant c_2 has been chosen in order to have an orthonormal set.

Comments similar to those made in Section 2.3 of Chapter 6 may be addressed.

CHAPTER 8

Concluding remarks and recommendations

This work was focused on investigating the vibration control of beams via piezoelectric transducers and passive electric networks. The objectives were to:

- Present the basic tools for modeling stepped piezoelectric beams, i.e. beams hosting piezoelectric transducers;
- Develop different and reliable algorithms for computing the modal characteristics of a stepped piezoelectric beam;
- Develop a homogenized model suitable for distributed control applications;
- Develop some identification methods for estimating the key modal parameters of a stepped piezoelectric beam;
- Present the basic concepts of the piezoelectric shunting technique;
- Demonstrate the use of RL distributed circuits for damping narrow-band structural vibrations;
- Analyze the effects of uncertainties of the electric parameters on the passive damping performances;
- Prove the effectiveness of the concept of electric analogs in the design of distributed passive controllers.

Each of these objectives has been addressed.

1. Conclusions

In Chapter 2, a one-dimensional model for stepped piezoelectric beams has been presented. Each segment of the stepped piezoelectric beam has been modelled as a standard Euler-Bernoulli beam. The bending moment in a piezocomposite segment depends on the beam curvature and on the voltage applied at the piezoelectric transducer terminals. On the other hand, the charge stored in a piezoelectric transducer depends on the applied voltage and on the relative rotation of the end cross sections of the piezocomposite segment. In the technical literature many research efforts have been devoted to derive accurate estimations of the constitutive electromechanical coefficients of the considered 1D model from linear 3D piezoelectricity. In the present work simple formulas for estimating these constitutive coefficients have been derived and their range of applicability has been questioned. The model has been validated through an experimental setup consisting of a cantilever beam hosting two bimorph pairs of piezoceramic transducers. The estimation of the mechanical coefficients of the 1D model seems to be accurate and reliable as it is shown in Table 3 of Chapter 3 where the experimental natural frequencies are compared with the theoretical predictions. The simple Euler-Bernoulli beam model guarantees precise forecasts of the resonance frequencies of the slender stepped beam over a wide frequency range (lowest four natural frequencies).

In Chapter 3, the effects of piezoelectric transducers on the beam modal properties have been investigated. The eigenvalue problem related to a system consisting of several one-dimensional continuous substructures has been tackled. Two main strategies have been considered:

i) to retain the continuous nature of the system and solve the exact trascendental eigenvalue problem for the infinite-dimensional system;
ii) to project the stepped beam deflection on a finite dimensional space with a standard Galerkin method, and solve the eigenvalue problem for the resulting finite-dimensional system.

The solution of the trascendental eigenvalue problem has required the exploitation of special techniques, since native treatments may generally lead to numerical problems which become quickly unsolvable as the number of segments increase. The Last Energy Norm technique has been applied to the considered problem, and the eigenvalues and the corresponding mode shapes are found without any matrix inversion. The accuracy of the approximate solutions based on the Galerkin approximation depend strongly on the choice of the basis functions. We have examined three diverse alternatives for the basis functions: the popular Assumed Modes method, the Finite-Element method, and an enhanced version of the assumed modes method that we have named Enhanced Assumed Modes method. From the comparison among the different methods reported in Table 4 of Chapter 3 one can conclude that

- the assumed modes, even if it is the most widespread, does not provide satisfactory determinations of the modal properties. This is due to the excessive smoothness of the basis functions which forbids to capture the curvature jumps at the material discontinuities;
- the enhanced assumed modes method provides very good estimates of the natural frequencies and of the mode shapes. Its implementation is very easy and it seems to be directly applicable to 2D problems, i.e. plates and shells hosting piezoelectric transducers;
- the finite-element method provides accurate predictions only of the lowest natural frequencies. Furthermore, the computation of the mode shapes is generally not satisfactory, due to the lack of continuity of their curvatures at the element junctions. Its implementation is very easy and may be handled with standard commercial codes;
- the least energy norm method guarantees the highest precision in the computation of the beam modal properties. Furthermore, its precision may be easily controlled when tuning the tolerance of the root-finding algorithm for the natural frequencies. Its implementation is very straightforward, but its extension to 2D problems seems difficult.

In Chapter 4, the derivation of a homogenized model for stepped periodic piezoelectric beams has been presented. Within the homogenized model the stepped piezoelectric beam may be treated as a homogeneous beam, whose constitutive coefficients are determined by the solution of a unit-cell problem. The finite set of piezoelectric voltages is replaced by a unique voltage field defined on the entire beam span. The homogenized model is extremely valuable in distributed control applications when one is refraining from discretizing the continuous plant. In this way, it is possible to treat the plant together with its controller by coupled partial differential equations and achieve deep insights into the system behavior. When designing piezo-electromechanical structures it is generally advisable to start from a coarse homogenized model for understanding the qualitative system behavior and dimensioning the needed electric elements, and then later to refine the model and improve the design's parameters by accounting for the discrete nature of the electric controller. In Chapter 4, the static deflection of a beam clamped at both ends has been considered as a sample problem. The two-scale convergence has been exploited

and the homogenized equation together with the convergence proof have been achieved. The homogenized model has been validated through some numerical tests. The performed numerical test assess that even with few piezoelectric elements (five) the predictions of the homogenized model are acceptable for dimensioning purposes.

In Chapter 5 the performances of the resonant piezoelectric shunting has been investigated. The model presented in Chapter 2 together with the modal analysis techniques developed in Chapter 3 have been exploited to derive a 2 d.o.f. model of the vibrating electromechanical system. The key parameters of the reduced-order model are the electric tuning parameter β, the electric modal damping δ and the gyroscopic modal coupling γ. The inductance determines only the value of the tuning parameter, and the resistance determines only the value of the electric damping, and none of them influence the modal coupling. This model has been used throughout this work, to describe the dynamics of resonantly coupled systems, and the results stemming from its analysis and optimization have been applied to the design of other electric networks. The tuning parameter and the electric damping have been optimized in order to minimize the ∞-norm of the transfer function of the reduced-order model. The existence of fixed points in the graph of the absolute value of the system transfer function, has lead to closed-form formulas for the optimal parameters. As a consequence, optimal values of the inductance and resistance have been established. It has been shown that the insertion of additional capacitance in the shunting circuit lowers the value of the optimal inductance, but simultaneously decreases the damping effectiveness. The effects of variations of the electric parameters on the system norm have been investigated by the use of two distinct approaches. The first approach transforms the problem of computing the transfer function ∞-norm into the simpler problem of bounding the eigenvalues of a certain Hamiltonian; it does not provide closed-form formulas but its implementation is simple, and it can handle arbitrary large variations of the system parameters. The second approach relies on the sensitivity analysis of the transfer function; it provides simple closed-form formulas whose validity is limited to small parameters variations. Comparisons between the two different methods have been drawn for a sample case. The results from the sensitivity analysis are very accurate for small variations of the electric parameters and, since the reduced-order model is reliable only when the coupling between the considered electromechanical degrees and the discarded modes is negligible, it is generally satisfactory to refer simply to the sensitivity analysis formulas. These formulas have been used to estimate the effects of uncertainties of the electric elements on the system performances. Closed-form formulas have been presented and validated through numerical Monte Carlo tests. Small uncertainties of the tuning parameter (inductance) leads to huge variances of the system ∞-norm, while the variance of the damping parameter (resistance) is not influencing the system performances. Therefore, it is mandatory to use self-adjusting inductances in real engineering applications. An identification technique based on the piezoelectric shunting has been presented. It is capable of accurately estimating at once the piezoelectric capacitance and the modal coupling coefficient. The proposed technique has been compared with a standard technique based on the measurements of the mechanical mode frequencies when either short or open-circuiting the piezoelectric elements. From the comparison shown in Table 2 of Chapter 5 one can conclude that the present technique, besides some implementation difficulties related to the need of an adjustable inductor, represents a more accurate and complete tool for identification. The same experimental setup used for assessing the stepped beam modeling has been exploited for proving the piezoelectric shunting damping effectiveness, and testing the proposed identification method. The adjustable inductor been simulated by exploiting a two operational amplifiers RC-circuit.

From the comparison of the identified piezoelectric capacitances and the predicted one, see Table 3 of Chapter 5, the need of more reliable electrical models of piezocomposite beams has been outlined and possible ameliorations, from the technical literature, has been indicated.

In Chapter 6 the performances of the second order transmission line have been investigated. The homogenized model developed in Chapter 4 together with the results from the $\mathcal{H}_\infty$ control problem in Chapter 5 have been used to derive a procedure for optimizing the electric boundary conditions, line inductance and line resistance for narrow-band vibration suppression. The presented methodology has been applied to the vibration suppression of the first mode of a cantilever beam. It has been shown that the optimal electric boundary conditions consist of open-circuiting the transducer at the clamped end and to short-circuiting the transducer at the free end. Furthermore it has been proved that small grounded impedances at the piezoelectric element at the free end do not alter significantly the modal coupling. Closed form expressions for the optimal line inductance and line resistance have been found. The inductance per unit length depends only on the piezoelectric capacitance per unit length and on the resonance frequency; therefore, once the amount of piezoelectric material on the host beam has been selected, the value of the needed line inductances decreases linearly with the number of available transducers. The predictions of the homogenized model have been verified by regarding the electric circuit as a finite d.o.f. system. Closed-form expressions for the eigenproperties of the electric network have been derived, by transforming the matrix eigenvalue problem into a three-point boundary value difference problem. The effects of independent variations of the inductances, with respect to their optimal value, on the electrical eigenproperties have been studied and valuable closed-form results have been derived. These expressions together with the results in Chapter 5 have been used to compute the sensitivity of the damping effectiveness with respect to the inductances' deviations. In the piezoelectric shunting, the inductance's deviation influences only the tuning parameter, while in the second order transmission line the inductances' deviations influences both the tuning and the modal coupling parameters. The effects of uncertainties of the inductances on the system performances have been treated, by regarding the inductances' deviations as independent random variables with zero mean value and equal variance. Closed-form expressions for the mean value and variance of the system ∞-norm have been presented. The second order transmission line reduces the effects of electric uncertainties on the damping effectiveness with respect to the simple piezoelectric shunting. By increasing the number of piezoelectric transducers the uncertainties' effects are drastically reduced. An experimental setup has been realized to prove the effectiveness of the second order transmission line in suppressing narrow-band structural vibrations. Six equal piezoceramics have been positioned on a host beam, five of them have been equally distributed on one beam surface and used for control purposes and the remaining one has been located on the other surface, close to the clamped end, and used for exciting the beam on its first mode. The floating inductances have been realized by the use of three operational amplifiers RC-circuits and the internal resonance in between the electrical and the mechanical system have been achieved by the use of a variable grounded inductor located at the beam free end. The piezoelectric capacitances and the modal coupling used in the circuit design have been identified through the technique presented in Chapter 5.

In Chapter 7 the performances of the fourth order transmission line have been investigated. The eigenvalue problem for the fourth derivative operator with natural boundary conditions has been reviewed. It has been shown that given a beam with perfect mechanical constraints, it is possible to uniquely define a dual set of perfect mechanical

constraints such that the dual problem has the same modal frequencies of the original one and has the original modal curvatures as mode shapes. The PEM beam has been studied by the use of the homogenized model in Chapter 4. It has been demonstrated that whence the electric circuit is governed by the fourth derivative operator, the electric boundary conditions are the dual of the mechanical ones, and the electric damping is proportional to the square root of the fourth derivative, it is possible to damp simultaneously all the structural vibration modes with the same optimal efficiency. The main properties of the square root of the fourth derivative operator with natural boundary conditions have been recalled and it has been shown that it is, in general, a nonlocal operator, which only in few cases is equal to the negative second derivative (e.g. simply supported beams). The modal frequencies and electromechanical mode shapes of the optimized non dissipative PEM beam have been found in terms of the original mode frequencies and mode shapes of the host beam. Two distinct synthesis strategies have been exploited in order to realize the same electric circuit analog of the Euler-Bernoulli beam. The circuit is constituted only by inductors, capacitors and elementary two-port transformers. Both the approaches has relied on the finite-difference discretization of the Timoshenko beam model. Within the former approach, the multiport synthesis of a circuit whose admittance matrix is the electric version of the finite-difference approximation of the beam element mechanical impedance has been tackled. It has been demonstrated that the transformerless realization of the beam element analog circuit is impossible, indicating the optimality of the proposed synthesis based on a single two-port transformer. The analog circuit of an entire Timoshenko beam has been obtained by cascade connecting the analog circuits of the beam elements discretizing the beam. The analog circuit of the Euler-Bernoulli beam has been derived as the limit of the Timoshenko beam analog circuit as the rotatory inertia and shear compliance go to zero. Within the latter approach, the Lagrangian of the lumped network has been derived by finite-difference approximating that of the continuous Timoshenko beam and by paralleling mechanical displacements with flux-linkages. The lumped electric analog has been directly assembled by the discrete Lagrangian by following standard techniques. This Lagrangian based approach can be easily generalized to the synthesis of electric circuits analog to more complicated structures, e.g. plates, but, in this framework, conditions for transformerless synthesis are not available. For simply supported beams, the electric circuit analog to the Euler-Bernoulli beam with structural damping has been derived. A PEM beam prototype has been designed and its multimodal damping performances has been discussed. It has been proved that the product of the optimal inductance per unit length and the square of the transformers turns-ratio per unit length depends only on the beam constitutive properties and on the piezoelectric capacitance per unit length. Therefore, once the amount of piezoelectric material on the host beam together with the he transformers turns-ratio have been selected, the value of the needed line inductances decreases linearly with the cube of the number of available transducers. The predictions of the homogenized model have been verified by regarding the electric circuit as a finite d.o.f. system and by studying its modal properties.

2. Recommendations for future works

The work presented in the dissertation may be expanded to include the following tasks:

- To study the influence of the discarded modes on the experimental identification of the piezoelectric capacitance and modal coupling;
- To apply the developed modal properties algorithms to more complicated structures, in order to rank their effectiveness in real engineering structures;

- To analyze the effects of uncertainties of the inductances and transformers turns-ratios on the damping effectiveness of the fourth order transmission line for the simply supported case. It is reasonable to state that the technique used for treating the second order transmission line is applicable;
- To modify the discretization technique used in the synthesis of the analog circuit in order to completely dispense with the use of transformers;
- To realize an experimental setup for proving the multimodal damping effectiveness of the fourth order transmission line.

Bibliography

[Alessandroni et al. (2002)] Alessandroni S, dell'Isola F, Porfiri M., 2002. A revival of electric analogs for vibrating mechanical systems aimed to their efficient control by PZT actuators, Int. J. Sol. Struct. 39(20), 5295-5324.

[Alessandroni et al. (2004)] Alessandroni A., Andreaus U., dell'Isola F., Porfiri M., 2004. Piezo-ElectroMechanical (PEM) Kirchhoff-Love plates, European J. of Mechanics A/Solids 23, 689-702.

[Alessandroni et al. (2005)] Alessandroni A., Andreaus U., dell'Isola F., Porfiri M..A passive electric controller for multimodal vibrations of thin plates, Computers and Structures available online since 26/2/2005.

[Allaire (1992)] Allaire G., 1992. Homogenization and two-scale convergence, SIAM J. Math. Anal., 23(6), 1482-1518.

[Andreaus et al. (2004)] Andreaus U., dell'Isola F., Porfiri M., 2004. Piezoelectric Passive Distributed Controllers for Beam Flexural Vibrations, J. of Vibration and Control 10(5), 625-659.

[Barboni et al. (2000)] Barboni R., Mannini A., Fantini E., Gaudenzi P., 2000. Optimal placement of PZT actuators for the control of beam dynamics, Smart Mater. Struct. 9, 110-120.

[Batra et al. (2004)] Batra, R. C., Porfiri, M., Spinello, D., 2004. Treatment of Material Discontinuity in Two Meshless Local Petrov-Galerkin (MLPG) Formulations of Axisymmetric Transient Heat Conduction, Int. J. Num. Meth. Engr. 61(14), 2461-2479.

[Beckert and Pfundtner (2002)] Beckert W., Pfundtner G., 2002. Analysis of the deformational behaviour of a bimorph configuration with piezoelectric actuation, Smart Mater. Struct. 11, 599-609.

[Benjeddou (2000)] Benjeddou A., 2000. Advances in piezoelectric finite element modeling of adaptive structural elements: a survey, Computers and Structures 76, 347-363.

[Bernadou and Haenel (2000)] Bernadou M., Haenel C. Modelization and numerical analysis of active thin shell structures, Proc. European Congress on Computational Methods in Applied Sciences and Engineering ECCOMAS 2000, Barcelona, 2000.

[Boller (1998)] Boller C., 1998. State of the art and trends in using smart materials and systems in transportation vehicles, Proc. Instn. Mech. Engrs. 212, Part 1, 149-158.

[Botkin (1999)] Botkin N.D., 1999. Homogenization of an equation describing linear thin plates excited by piezopatches, Commun. Appl. Anal. 3(2), 271-281.

[Breiman (1969)] Breiman L., 1969. Probability and Stochastic Processes, with a view towards applications, Houghton Mifflin Company, Boston.

[Bruton (1980)] Bruton L.T., 1980. RC-active circuits: theory and design, Prentice-Hall.

[Buslenko et al. (1966)] Buslenko N.P., Golemko D.I., Shreider Y.A., Sobol' I.M., Sragovich V.G., 1966. The Monte Carlo method, Pergamon Press, Oxford.

[Canon and Lenczner (1999)] Canon E., Lenczner M., 1999. Modelling of Thin Elastic Plates with Small Piezoelectric Inclusions and Distributed Electronic Circuit. Models for Inclusion that Are Small with Respect to the Thickness of the Plate, J. Elasticity 55, 111-141.

[Caruso (2001)] Caruso G., 2001. A critical analysis of electric shunt circuits employed in piezoelectric passive vibration damping, Smart Mater. Struct. 10, 1059–1068.

[Chandrasekharan (1996)] Chandrasekharan P.C., 1996. Robust Control of Linear Dynamical Systems, Academic press, London.

[Chen and Russell (1982)] Chen G., Russell D.L., 1982. A mathematical model for linear elastic systems with structural damping, Quart. appl. math. 39, 433-454.

[Chopra (2002)] Chopra I., 2002. Review of State of Art of Smart Structures and Integrated Systems, AIAA J. 40(11), 2145-2187.

[Corr and Clark (2002)] Corr L.R., Clark W.W., 2002. Comparison of low-frequency piezoelectric switching techniques for structural damping, Smart Mater. Struct. 11, 370-376.

[Crandall et al. (1968)] Crandall S. H., Karnopp D. C., Kurtz E. F. Jr., Pridmore-Brown F. C., 1968. Dynamics of Mechanical and Electromechanical systems, McGraw-Hill, New York.

[Crawley and de Luis (1987)] Crawley E.F., de Luis J., 1987. Use of Piezoelectric actuators as Elements of Intelligent Structures, AIAA J. 25(10), 1373-1385.

[Curtain and Zwart (1995)] Curtain R.F., Zwart H.J., 1995. An introduction to infinite-dimensional linear systems theory, Springer-Verlag, Berlin.

[Deboo (1967)] Deboo G., 1967. Application of a Gyrator-Type Circuit to Realize Ungrounded Inductors, IEEE Trans. Circuit Theory March 101-102

[de Faria (2003)] de Faria A.R., 2003. The impact of finite-stiffness bonding on the sensing effectiveness of piezoelectric patches, Smart Mater. Struct. 12, N5–N8.

[dell'Isola and Vidoli (1998, 1)] dell'Isola F., Vidoli S., 1998. Continuum modelling of Piezo-ElectroMechanical truss beams: an application to vibration damping, Arch. Appl. Mechanics 68, 1-19.

[dell'Isola and Vidoli (1998, 2)] dell'Isola F. and Vidoli S., 1998. Bending-waves damping in truss beams by electrical transmission line with PZT actuators, Arch. Appl. Mechanics 68, 626-636.

[dell'Isola et al. (2001)] dell'Isola F., Henneke E. G., Porfiri, M., 2001. Synthesis of electrical networks interconnecting PZT actuators to damp mechanical vibrations, Int. J. Appl. Electr. Mech. 14(1-4/2001/2002), 417-424.

[dell'Isola et al. (2003, 1)] dell'Isola F., Porfiri, M., Vidoli, S., 2003. Piezo-ElectroMechanical (PEM) structures: passive vibration control using distributed piezoelectric transducers, Comptes Rendus de l'Académie des Sciences - Series IIB - Mechanics 331(1), 69-76.

[dell'Isola et al. (2003, 2)] dell'Isola F., Henneke E.G, Porfiri M. Piezoelectromechanical structures: a survey of basic concepts and methodologies, Proc. SPIE Smart Structures and Materials, Smart Structures and Integrated Systems, San Diego, 2003, Volume 5052, 392-402.

[dell'Isola et al. (2004)] dell'Isola F., Maurini C., Porfiri M., 2004. Passive damping of beam vibrations through distributed electric networks and piezoelectric transducers: prototype design and experimental validation, Smart Mater. Struct. 13(2), 299-308.

[Den Hartog (1934)] Den Hartog J., 1934. Mechanical Vibrations, McGraw-Hill, New York.

[Doyle et al. (1989)] Doyle J.C., Glover K., Khargonekar P.P., Francis B.A., 1989. State-Space Solutions to Standard $\mathcal{H}_2$ and $\mathcal{H}_\infty$ Control Problems, IEEE Tran. on Automatic Control 34(8), 831-846.

[El-Kady and Al-Ohaly (1997)] El-Kady M.A., Al-Ohaly A.A., 1997. Fast eigenvalue sensitivity calculations for special structures of system matrix derivatives, J. Sound Vib. 199(3), 463-471.

[Fleming et al. (2000)] Fleming A.J., Behrens S., Moheimani S.O.R., 2000. Synthetic impedance for implementation of piezoelectric shunt-damping circuits, Electronic Letters 36, 1525-6.

[Fleming et al. (2002)] Fleming A.J, Behrens S., Moheimani S.O.R., 2002. Optimization and Implementation of Multimode Piezoelectric Shunt Damping Systems, IEEE/ASME Trans. on Mechatronics 7(1), 87-94.

[Fleming et al. (2003)] Fleming A.J., Behrens S. and Moheimani S.O.R, 2003. Reducing the inductance requirements of piezoelectric shunt damping systems, Smart Mater. Struct. 12, 57-65.

[Forward and Swigert (1981)] Forward R.L., Swigert G J., 1981. Electronic Damping of Orthogonal Bending Modes in a Cylindrical Mast– Theory, J. of Spacecraft and Rockets 18, 5-10.

[Gantmacher (1980)] Gantmacher F. R., 1980, Lezioni di meccanica analitica, Edizioni Mir, Mosca, (In Italian).

[Gaudenzi and Bathe (1995)] Gaudenzi P., Bathe K.J., 1995. An iterative finite element procedure for the analysis of piezoelectric continua, J. Intell. Mater. Syst. Struct. 6, 266-273.

[Gopinathan et al. (2000)] Gopinathan S.V., Varadan V.V., Varadan V.K., 2000. A review and critique of theories for piezoelectric laminates, Smart Mater. Struct. 9, 24-48.

[Hagood and von Flotow (1991)] Hagood N.W., von Flotow A.H, 1991. Damping of structural vibrations with piezoelectric materials and passive electrical networks. J. Sound Vib. 146(2), 243-368.

[Hanagud (1985)] Hanagud S., Obal M.W., Meyyappa M. Electronic Damping Techniques and Active Vibration Control. Proc. of the 26th AIAA/ASME/ASCE/AHS Structures, Structural Dynamics and Materials Conference April 1985, AIAA Paper 85-0752.

[Hanagud et al. (1992)] Hanagud S., Obal M.W., Calise A.J., 1992. Optimal Vibration Control by the use of Piezoceramic Sensors and Actuators, J. Guid. Contr. Dyn. 15(5) 1199-1206.

[Hoffman and Botkin (1998)] Hoffman K.-H., Botkin N.D., 1998. Oscillations of Nonlinear Thin Plates Excited by Piezoelectric Patches, ZAMM 78(7), 495-503.

[Hoffman and Botkin (2000)] Hoffman K.-H., Botkin N.D., 2000. Homogenization of von Karman Pllates Excited by Piezoelectric Patches, ZAMM 80(9), 579-590.

[Hollkamp (1994)] Hollkamp J.J., 1994. Multimodal Passive Vibration Suppression with Piezoelectric Materials and Resonant Shunts, J. Intell. Mater. Syst. Struct. 5, 49-57.

[Hollkamp (1994)] Hollkamp J.J., 1996. An experimental comparison of piezoelectric and constrained layer damping, Smart Mater. Struct. 5, 715–722.

[Ikeda (1990)] Ikeda T., 1990. Fundamentals of Piezoelectricity, Oxford University Press, Oxford.

[Jordan and Ounaies (2001)] Jordan T L, Ounaies Z. Piezoelectric Ceramics Characterization. NASA/CR-2001-211225, CASE Report No. 2001-28.

[Juang (1984)] Juang J.-N., 1984. Optimal Design of a Passive Vibration Absorber for a Truss Beam, J. Guid. Contr. Dyn. 7(5), 733-739.

[Juang and Phan (2001)] Juang J.-N., Phan M.Q., 2001. Identification and control of mechanical systems, Cambridge University Press, Cambridge, UK.

[Kader (2001)] Kader M., Lenczner M., Mrcarica Z., 2001. Distributed control based on distributed electronic circuits: application to vibration control, Microelectronics Reliability 41, 1857-1866.

[Karplus and Soroka (1959)] Karplus W. J., Soroka W. W., 1959. Analog Methods: computation and simulation, McGraw-Hill, New York.

[Kalamkarov and Georgiades (2002)] Kalamkarov A.L., Georgiades, A.V., 2002. Micromechanical modeling of smart composite structures, Smart Mater. Struct. 11, 424-434.

[Kapuria et al. (2003)] Kapuria S., Dumir P.C., Ahmed A., 2003. An efficient coupled layerwise theory for dynamic analysis of piezoelectric composite beams, J. Sound Vib. 261, 927-944.

[Kato (1966)] Kato T., 1966. Perturbation Theory of Linear Operators, Springer-Verlag, Berlin.

[Keun-Ho and In (2001)] Keun-Ho R, In L., 2001. Adaptive Shunting for Vibration Control of Frequency-Varying Structures, J. Guid. Contr. Dyn. 24(6), 1223-1225.

[Kim et al. (2000)] Kim J., Ryu Y.-H., Choi S.B., 2000. New shunting parameter tuning method for piezoelectric damping based on measured electrical impedance, Smart Mater. Struct. 9, 868-877.

[Krommer (2001)] Krommer K., 2001. On the correction of the Bernoulli–Euler beam theory for smart piezoelectric beams, Smart Mater. Struct. 10, 668-680.

[Krongauz and Belytschko (1998)] Krongauz Y., Belytschko T., 1998. EFG approximation with discontinuous derivatives. Int. J. Num. Meth. Engr. 41, 1215-1233.

[Kusculuoglu et al. (2004)] Kusculuoglu Z.K., Fallahi B., Royston T.J., 2004. Finite element model of a beam with a piezoceramic patch actuator, J. Sound Vib. 276, 27-44.

[IEEE (1987)] IEEE Std 176-1987 IEEE Standard on Piezoelectricity, The Institute of Electrical and Electronic Engineers.

[Lebedev and Vorovich (2002)] Lebedev L.P., Vorovich I.I., 2002. Functional Analysis in Mechanics, Springer, New-York.

[Lenczner and Mercier (2004)] Lenczner M., Mercier D., 2004. Homogenization of Periodic Electrical Networks including voltage to current amplifiers, Multiscale Model. Simul. 2(3), 359-397.

[Lesieutre (1998)] Lesieutre G.A., 1998. Vibration damping and control using shunted piezoelectric materials, The Shock Vibr. Digest 30(3), 187-195.

[Lutes and, Sarkani (2004)] Lutes L.D., Sarkani S., 2004. Random vibrations, analysis of structural and mechanical systems, Elsevier Butterworth-Neinemann, Burlington, USA.

[Maurini et al. (2004, 1)] Maurini C., dell'Isola F., Del Vescovo D., 2004. Comparison of Piezoelectronic networks acting as distributed vibration absorbers, Mech. Syst. Signal Processing 18(5), 1243-1271.

[Maurini et al. (2004, 2)] Maurini C., Pouget J., dell'Isola F., 2004. On a model of layered piezoelectric beams including transverse stress effect, Int. J. Sol. Struct., Int. J. Sol. Struct. 41, 4473-4502.

[Maurini et al. (submitted)] Maurini C., Porfiri M., Pouget J.. Experimental and numerical methods for modal analysis of stepped piezoelectric beams, submitted for pubblication.

[Maxwell and Asokanthan (2004)] Maxwell N.D., Asokanthan S.F., 2004. Modal characteristics of a flexible beam with multiple distributed actuators, J. Sound Vib. 269, 19-31.

[Mackerle (1998)] Mackerle J., 1998. Smart materials and structures—a finite-element approach: a bibliography (1986–1997), Modelling Simul. Mater. Sci. Eng. 6(3), 293–334.

[Mackerle (2003)] Mackerle J., 2003. Smart materials and structures—a finite-element approach—an addendum: a bibliography (1997-2002), Modelling Simul. Mater. Sci. Eng. 11(5), 707–744.

[Meirovitch (2000)] Meirovitch L., 2000. Fundamentals of vibrations, McGraw-Hill, Boston.

[Molloy (1958)] Molloy C.T. Four Pole Parameters in Vibration Analysis in Mechanical impedance Methods for Mechanical Vibrations. Colloquium on Mechanical Impedance Methods for Mechanical Vibrations presented at the ASME Annual Meeting 1958, New York, N.Y., December 2, sponsored by Shock And Vibrating Committee Applied Mechanics Division, The American Society of Mechanical Engineers, New York, edited by R.Plunkett.

[Newcomb (1966)] Newcomb R.W, 1966. Linear Multiport Synthesis, McGraw-Hill, New York.

[Niezreski et al. (2001)] Niezreski C., Brei D., Balakrishnam S., Moskalik A., 2001. Piezoelectric Actuation: State of the Art, The Shock Vibr. Digest 33(4), 269-280.

[Olsen (1956)] Olsen H. F., 1956. Electronic control of noise, vibration and reverberation, J. Acoust. Soc. 28, 976-972.

[Panel (1962)] Panel, 1962. The realization of n-port networks without transformers: a panel discussion, Trans.IRE Circuit Theory CT-9(3), 202-214.

[Park and Inman (2003)] Park C.H., Inman D.J., 2003. Enhanced piezoelectric shunt design, Shock and Vibr. 10, 127-133

[Park (2003)] Park C.H., 2003. Dynamics modelling of beams with shunted piezoelectric elements, J. Sound Vib. 268, 115-129.

[Parton and Kudryavtev (1988)] Parton V.Z., Kudryavtev B.A., 1988. Electromagnetoelasticity Piezoelectrics and Electrically Conductive Solids, Gordon and Breach Science Publishers, New York.

[Porfiri et al. (2004)] Porfiri M., dell'Isola F., Frattale Mascioli F.M., 2004. Circuit analog of a beam and its application to multimodal vibration damping, using piezoelectric transducers, Int. J. Circuit Theory Appl. 32, 167-198.

[Porfiri et al. (accepted)] Porfiri M., dell'Isola F., Santini E. Modeling and design of passive electric networks interconnecting piezoelectric transducers for distributed vibration control, accepted for pubblication in Int. J. Appl. Electr. Mech..

[Press (1992)] Press W.H., Flannery B.P., Teukolsky S.A., Vetterling W.T., 1992. Numerical Recipes in Fortran, Cambridge University Press, Cambridge.

[Richards (1977)] Richards T. H., 1977. Energy methods in stress analysis: with an introduction to finite element techniques, Halsted Press, New York.

[Roseau (1987)] Roseau M., 1987. Vibrations in Mechanical Systems. Analytical Methods and Applications, Springer-Verlag, Berlin.

[Russell (1988)] Russell D.L., 1988. On the positive square root of the fourth derivative operator, Quart. appl. math. 46, 751-773.

[Samarskii and Nikolaev (1989)] Samarskii A.A., Nikolaev E.S., 1989. Numerical Methods for Grid Equations, Birkhauser Verlag, Basel.

[Sanchez-Hubert and Sanchez-Palencia (1989)] Sanchez-Hubert J., Sanchez.Palencia E., 1989. Vibration and coupling of continuous systems - Asymptotic methods, Springer-Verlag, Berlin.

[Sanchez-Palencia (1980)] Sanchez-Palencia E., 1980. Non-Homogeneous Media and Vibration Theory, Lecture Notes in Phys. 127, Springer Verlag, New-York.

[Saravanos and Heyliger (1999)] Saravanos D.A., Heyliger P.R., 1999. Mechanics and computational models for laminated piezoelectric beams, plates, and shells, Applied Mechanics Reviews 52, 305-320.

[Senani (1996)] Senani R., 1996. Alternative modification of the classical GIC structure, Electronic Letters 32, 1329.

[Slepian and Weinbeg (1958)] Slepian P., Weinbeg L., 1958. Synthesis. Synthesis applications of paramount and dominant matrices. Proc. of the National Electronics Conference 14, 611 630.

[Soedel (1993)] Soedel W.,1993. Vibrations of shells and plates, 2nd edition, Marcel Dekker, New York.

[Soong and Bogdanoff (1963)] Soong T.T., Bogdanoff J.L., 1963. On the natural frquencies of a disordered linear chain of N degrees of freedom, Int. J. Mech. Sciences 5, 237-265.

[Strambi et al. (1995)] Strambi G., Barboni R., Gaudenzi P., 1995. Pin-Force and Euler-Bernoulli Models for Analysis of Intelligent Structures, AIAA J. 33(9), 1746-1749.

[Sze et al. (2004)] Sze K.Y., Yang X.-M., Fan H., 2004. Electric assumptions for piezoelectric laminate analysis, Int. J. Sol. Struct. 41 (9-10), 2363-2382.

[Tang and Wang (2001)] Tang J., Wang K.W., 2001. Active-passive hybrid piezoelectric networks for vibration control: comparisons and improvement, Smart Mater. Struct. 10, 794-806.

[Tiersten (1969)] Tiersten H.F., 1969. Linear Piezoelectric Plate Vibrations, Plenum Press, New-York.

[Tsai1 and Wang (2002)] Tsai1 M.S., Wang K.W., 2002. A coupled robust control/optimization approach for active–passive hybrid piezoelectric networks, Smart Mater. Struct. 11, 389–395.

[Valis et al. (1991)] Valis T., von Flotow A.H., Hagood N.W. An acousto-electromagnetic piezoelectric waveguide-couple. Active Materials and Adaptive Structures Proc. of the ADPA/AIAA/ASME/SPIE Conference Nov.1991 Alexandria Virginia Gareth J Knowles Ed. Inst. of Physics Publishing Bristol and Philadelphia, 383-394.

[Veiga (1995)] Veiga M.F., 1995. Asymptotic approximation of an elastic beam with a rotating cross section, Asymptotic Analysis 11, 73-105.

[Vidoli and dell'Isola (2000)] Vidoli S., dell'Isola F., 2000. Modal coupling in one-dimensional electromechanical structured continua, Acta Mechanica 141, 37-50.

[Wang (2001)] Wang K.W., 2001. Vibration suppression utilizing piezoelectric networks The mechanical system design handbook: modeling, measurement and control, edited by Nwokah O.D.I. and Hurmuzlu Y. CRC press, Chapter 15

[Williams and Wittrick (1970)] Williams F.W., Wittrick W.H., 1970. An automatic computational procedure for calculating natural frequencies of skeletal structures, Int. J. Mech. Sciences 12, 781-791.

[Wittrick and Williams (1971)] Wittrick W.H., Williams F.W. 1971. A general algorithm for computing natural frequencies of elastic structures, Quart. J. Mech. Appl. Math. 24 (3), 263-284.

[Wu (1996)] Wu, S. Y. Piezoelectric Shunts with a Parallel R-L Circuit for Structural Dampingand Vibration Control. Smart Structures andMaterials 1996: Passive Damping, edited by C. D. Johnson, Proc. of the SPIE 2720, Society of Photo-Optical Instrumentation Engineers—The International Society of Optical Engineering, Bellingham, WA, 1996, pp. 259–269.

[Yang (1991)] Yang B., 1991. Eigenvalue Inclusion Principles for Distributed Gyroscopic Systems, Vibration Analysis - Analytical and Computational, ASME, DE-37, 7-12.

[Yang and Lee (1994, 1)] Yang S.M., Lee Y.J. ,1994. Modal analysis of stepped beams with piezoelectric materials, J. Sound Vib. 176, 289–300.

[Yang and Lee (1994, 2)] Yang S.M., Lee Y.J. ,1994. Interaction of structure vibration and piezoelectric actuation, Smart Mater. Struct. 3, 494-500.

[Zhang and Kirpitchenko (2002)] Zhang N., Kirpitchenko I., 2002. Modelling the dynamics of a continuous structure with a piezoelectric sensor/actuator for passive structural control, J. Sound Vib. 249(2), 251-261.

[Zhaohui et al. (2004)] Zhaohui Q., Kennedy D., Williams F.W., 2004. An accurate method for transcendental eigenproblems with a new criterion for eigenfrequencies, Int. J. Sol. Struct. 41 (11-12), 3225-3242.

[Zhou et al. (1996)] Zhou K., Doyle J., and Glover K., 1996. Robust and Optimal Control, Prentice-Hall.